Development and Implementation of a Tactile Feedback System Using End-to-end Tactile Sensor Data Projections for Wearable Human-Robot Interaction

---

触覚データのエンドツーエンド射影に 基づく装着型触覚フィードバックシステムの開発

Andreas GEIER
ガイアー アンドレアス

February, 2021

Development and Implementation of a Tactile Feedback System Using End-to-end Tactile Sensor Data Projections for Wearable Human-Robot Interaction

触覚データのエンドツーエンド射影に 基づく装着型触覚フィードバックシステムの開発

A thesis submitted in fulfillment of the requirements
for the degree of Doctor of Engineering.

Waseda University

Graduate School of Creative Science and Engineering
Department of Modern Mechanical Engineering
Research on Intelligent Machines

February, 2021

Author

Andreas GEIER
ガイアー アンドレアス

Supervisor

Prof. Shigeki SUGANO
菅野重樹

Abstract

Andreas GEIER

Development and Implementation of a Tactile Feedback System Using End-to-end Tactile Sensor Data Projections for Wearable Human-Robot Interaction

The proliferation of distributed tactile sensing technologies and the large-scale implementation of soft, distributed tactile sensor skins into robots has been widely adopted for tactile recognition, tactile exploration, and autonomous control. However, in human-centred applications like teleoperation, the complex sensory input data generated by a multitude of distributed tactile sensors must be projected to the skin of a human operator to generate effective, yet efficient tactile feedback during remote operation of a robotic agent.

Till to date, tactile displays suffer from a high energy consumption and a large form factor. Moreover, most tactile displays are restricted to simplified application scenarios, such as virtual reality, and previous research has not considered the end-to-end transformation from tactile sensor input data to tactile actuator driving signal for the realization of a vastly applicable tactile feedback system to establish the tactile sensory information flow between robots and humans.

The objective of this thesis was the development and implementation of a tactile feedback system that integrates distributed tactile skin sensors originally developed for the large-scale implementation into robots with ultra-compact tactile displays that deploy sparse actuator arrays to provide direct tactile feedback in unstructured environments in an energy- and space-saving way.

The data-driven tactile feedback system features a set of novel capabilities: **(1)** it deploys tactile illusory phenomena to mitigate energy and space restrictions for compact tactile display designs, **(2)** a rigorous end-to-end design from raw tactile sensor data to tactile display output, and

(3) a modular design paradigm to ensure the tactile feedback system is scalable, extendable, and generalizes to a plurality of applications.

Tactile feedback is the conveyance of information on the location of contacts and the physical properties at these contact locations: The proposed algorithm termed **Sequential Tactile Data Clustering for Tactile Image Compression** performs a dynamic compression of the tactile sensor data into a number of desired contact locations and stimulus intensities; thereby, enables the generation of tactile illusions with sparse actuator arrays. The complementary algorithm termed **End-to-end Tactile Texture Projection with Psychophysically-meaningful Latent Space Encodings** enables the implicit representation of tactile sensor data in psycho-physically meaningful latent space coordinates and allows for conveying generic textural surface properties in accordance with the tactile sensor input data.

Several prototypes of a **tactile display fingertip module** were developed for the experimental evaluation of the proposed tactile feedback system. The experiments showed that the presented algorithms for the implicit or compressed representation of tactile sensor data enable the transformation from tactile sensor data to tactile display driving signal and allow for the generation of precise spatio-temporal actuation patterns for the conveyance of macro-geometric and micro-geometric contact information. The final prototype (size 2.7x2.3x1.2cm) implemented a sparse 3D actuator array of eight shape memory alloy-based micro-vibrators and a driver module with a power consumption of only 180mW per actuator with a total weight of only 16.74g, including a WiFi-enabled driver unit with current amplifiers.

In conclusion, the proposed tactile feedback system utilizes algorithms for the end-to-end projection of tactile sensor data and adheres to psycho-physiological paradigms for the generation of tactile illusions, which enables the efficient real-time transmission of tactile feedback from tactile sensor skin to the human user by deploying only sparse actuator arrays of shape memory alloy-based micro-vibrators. The experimental results suggest that the developed tactile feedback system constitutes an effective and efficient technical framework for real-time end-to-end tactile feedback during active tactile object exploration in teleoperation and human-robot interaction applications.

Acknowledgements

This dissertation was written during my time as doctoral researcher at the Department of Modern Mechanical Engineering (Sugano Laboratory, Prof. Shigeki Sugano) in cooperation with the Department of Applied Physics (Prof. Hideyuki Sawada) at the Faculty of Science and Engineering of Waseda University, Tokyo. I am thankful for their continuous support that has enabled the research of this thesis.

In addition, I would like to thank Dr. Sophon Somlor and Dr. Tito Pradhono Tomo for their support and open ear, which were one important contributor to the success of this dissertation. Furthermore, I would like to thank all my co-authors for the fruitful and pleasant cooperation and especially the study participants for their patience and sacrificed time.

In addition, I would like to thank my colleagues Prathamesh Sathe and Rawleigh Tucker, who provided stimulating discussions and a great source of optimism, both of which have been indispensable to accomplish this thesis.

My special thanks go to my parents Heike and Frank as well as my grandparents Margrit and Hans, who always supported me throughout my studies and beyond.

Tokyo, February, 2021
Andreas Geier

Contents

List of Figures

List of Tables

Some people see things that are and ask, Why?
Some people dream of things that never were and
ask, Why not? Some people have to go to work
and don't have time for all that.

George Carlin

Chapter 1

Introduction

1.1 Motivation: The Importance of Tactile Feedback

Tactual perception is a combination of kinesthetic and cutaneous feedback that enables humans to perform a great variety of exploration and manipulation tasks in physical, unstructured environments [1] [2] [3] [4] [5]. In contrast to kinesthetic feedback, cutaneous feedback is mediated by sets of distributed mechanoreceptors in the skin and allows humans for sensing local object properties. In analogy to tactile skin sensors for robots, this type of feedback is also referred to as tactile feedback, i.e., extrinsic feedback that enables the sensing of distributed contacts and contact properties at the site of physical interaction [6] [7].

In addition to visual perception, tactile sensing is paramount for the direct perception of unstructured environments. Solely direct physical contact enables the direct transmission of forces, vibrations, and heat fluxes, which inform us not only about macro-geometric object and micro-geometric surface properties but also about important physical quantities, e.g. weight distributions, that cannot be perceived otherwise. Without tactile feedback, humans would not be able of robustly grasping and dexterously manipulating objects, as it has been demonstrated in experiments that investigated influencing factors of the force control during precision grip under local anesthesia [8].

In this context, it has been shown that autonomous robot operation tremendously benefits from tactile sensing as it provides extrinsic feedback that facilitates safe operation and robust, dexterous object manipulation [9] [6] [10] [7]. Thus, tactile sensor skin has been widely adopted in robot design and control. Especially, the integration of distributed tactile sensors

enables information-rich feedback from the robot's environment and makes robot manipulators increasingly capable of dexterous object manipulation and even active (tactile) exploration [6] [7]. Not only modern industrial robots but also emerging robot applications like social and service robots benefit from the combined deployment of anthropomorphic, dexterous robot hands with compliant skin that carries distributed arrays of tactile sensors, because of their higher manipulation capabilities, higher deployment flexibility, and in turn, a tremendous potential for versatile, human-like interaction with the physical world [6] [10] [7].

The recreation of tactual perception is the goal of so-called haptic devices. A sub-category to haptic devices are so-called tactile displays, which, by analogy to tactile sensors, implement distributed sets of actuators to stimulate the mechanoreceptors in the human skin and therefore seek to provide direct, distributed feedback to resemble the physical interaction with the environment [1] [11] [2].

The realization of a wearable tactile feedback system that possesses the capability of transmitting tactile sensor data from robots to humans in a meaningful manner establishes the tactile sensory information flow between robots and humans, thus, yields the potential for powerful and immersive human-machine interaction. Depending on the application scenario, this tactile information must be artificially recreated, e.g. in virtual reality, or transmitted, e.g. in robot teleoperation, in a manner that produces the salient features of touch needed to enhance realism and enable human-like performance [2].

Apart from well-known applications in interactive computing and virtual reality, tactile feedback has therefore important implications for human-robot interaction and robot-teleoperation [12] [1] [4] [5]. For example, robot-assisted surgery seeks to enhance delicate procedures at a level that is beyond the capabilities of the human hand. In such teleoperation scenarios, the human operator requires an accurate sense of *telepresence* [13] such that the tactile feedback resembles the physics of directly manipulating the environment, rather than being indirectly mediated, e.g. by visual cues [1] [2] [4].

While there has been research on the importance of tactile, i.e. cutaneous, feedback during teleoperation [1], e.g. McMahan *et al.* [14] and more recently by Quek *et al.* [15] and Abiri *et al.* [16], or the deployment of tactile skin sensors for haptic device calibration [17], there have been very

few examples of the combination of distributed tactile skin sensors with tactile displays [18] [19]; the most popular example being the *Tactile-Telerobot* from *HaptX*[1] [12]. This might be attributed to the proliferation of tactile sensors being limited to the robotic community and, certainly, the enormous technical challenges to integrate distributed tactile sensing and tactile feedback into technical systems [1] [16] [4].

Thus, the objective of this thesis is the development and implementation of a tactile feedback system that integrates distributed tactile skin sensors originally developed for the large-scale implementation into robots or robotic manipulators with ultra-compact tactile displays that deploy sparse actuator arrays to provide direct tactile, i.e., cutaneous feedback in unstructured environments in an energy- and space-saving way.

The following sections review the theory behind the psycho-physiology of human mechanoreceptors and the state-of-the-art in tactile technologies, i.e. tactile sensors and tactile displays, that aspire to create an artificial tactile feedback for the use in robot control, human-robot interaction, or robot teleoperation.

1.2 Background

1.2.1 Tactile Feedback in Humans

The development of a tactile display relies heavily on the fundamentals of human mechanoreceptor physiology. This section therefore briefly reviews fundamentals and relevant literature on mechanoreceptor physiology and tactile perception in response to spatio-temporal stimulation patterns.

Spatio-temporal stimulation patterns that act in accordance with the psycho-physiological paradigms of the brain allow for conveying tactile information to a human user in more meaningful and more effective ways [20] [2] [21]. Understanding the underpinning mechanisms of human tactile sensing and tactile perception is thus especially important as it may allow for the optimization of the tactile display design and its working principle. The physiology fundamentals are adopted from [9] [22] [23] [24] [3] to which the reader is referred to for a more comprehensive review on human tactile sensing and perception.

[1] https://haptx.com/robotics/

1.2.1.1 Human Mechanoreceptors from a Technical Perspective

In contrast to the other human sensing modalities (vision, audio, etc.), the sense of touch is distributed across the entire body in the skin, joints, muscles, and tendons. Tactual perception is therefore a combination of feedback from proprioceptive (internal) and cutaneous (external) receptors.

Proprioception, also termed kinesthesia, is the sensory channel that gives feedback on the position, velocity, and load of our extremities. In contrast, cutaneous receptors are sets of distributed sensors that are directly located in the glabrous, hairless skin and perceive pressure, vibration, and temperature due to direct physical contact with the environment, Fig. 1.1. Tactile displays are devices that implement sets of distributed actuators that stimulate the cutaneous receptors. This thesis focuses on cutaneous mechanoreceptors in terms of tactile sensing and tactile stimulation.

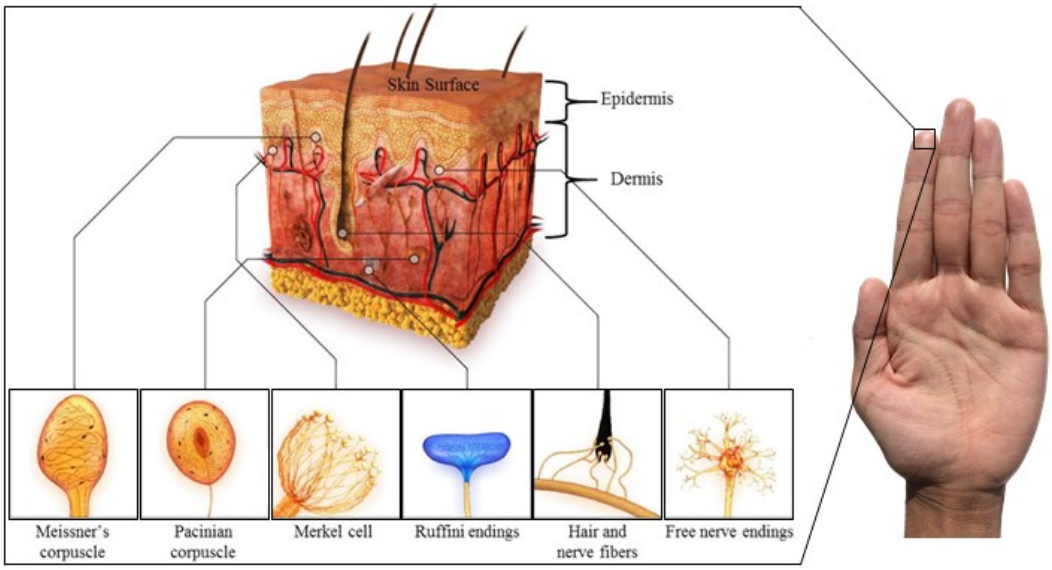

FIGURE 1.1: Cutaneous receptors are sets of distributed sensors directly located in the glabrous, hairless skin and perceive pressure, vibration, and temperature. Tactile displays are devices that stimulate these cutaneous receptors. Picture adopted from Park *et al.* [3], modified.

Embedded in the dermis, the glabrous skin includes four main types of cutaneous mechanoreceptors, which are located in different depths: namely *Merkel* disks ($\varnothing \approx 10mm$) and *Ruffini* nerve (L≈0.5-2mm) endings as well as *Meissner* corpuscles (L≈30-140mm, $\varnothing \approx 40$-60mm) and *Pacinian* corpuscles (L≈0.5-2mm, $\varnothing \approx 0.7mm$).

These mechanoreceptors have specific stimuli responses depending on the mechanical loading and stimulation frequency. They are divided according to their adaptation rate yielding two categories: fast adapting (FA) units sensing transient stimuli and slow adapting (SA) units sensing (quasi)-static stimuli. SA-type receptors are sensitive to sustained static stimuli, thus, generate a time-invariant signal output. FA-type receptors, on the other hand, are sensitive to dynamic stimuli. Each category furthermore comprises type-I and type-II receptors depending on the respective size of their receptive fields and their density, as depicted in Figure 1.1 and summarized in Table 1.1. Type-I receptors are located in the superficial layer of the skin and have small receptive fields. Type-II receptors are located in the deeper layers of the dermis and have comparatively larger receptive fields.

TABLE 1.1: Characteristics of the mechanoreceptors in the human skin [23] [24] [3].

	Meissner	Pacinian	Merkel	Ruffini
Receptor type	FA-I	FA-II	SA-I	SA-II
Adaption	Fast	Fast	Slow	Slow
Skin Layer	Upper	Lower	Upper	Lower
Density $[units/cm^2]$	140	20	70	10
Resolution $[mm]$	3-4	$>$10	0.5	$>$7
Receptive Field $[mm]$	3-5	$>$20	2-3	10-15
Frequency $[Hz]$	10-200	70-1000	0.4-10	0.4-10
Mechanical Response	Slip, Texture	Vibrations	Static Forces	Shear

Merkel endings are SA-I receptors that provide information on macro-geometric properties, namely position, shape, and orientation; as they respond to sustained skin deformation and the static pressure distribution between the skin and the asperities of the contact surface. Even though this information is rather quasi-static, it is reported that *Merkel* disks (SA-I) have their optimal frequency response at 0.4 to 15Hz and are able of detecting skin deflections of as less as 1mm. *Ruffini* nerve endings (SA-II) generate a slowly adapting static response to sustained pressure and, moreover, to skin stretch due to shear forces; i.e., they are capable of detecting slip at the fingertips.

Meissner (FA-I) and *Pacinian* corpuscles (FA-II), on the other hand, respond to temporal or vibratory information that occurs by relative movement of the skin to the contact surface, such as shape and textural

changes along a timely trajectory. *Meissner* corpuscles exhibit the highest sensitivity at 30-50Hz, but respond to stimuli up to 200Hz. They encode light touch, grip control, and texture discrimination [24] [3]. *Pacinian* corpuscles respond to frequencies from 50Hz-1kHz with their peak sensitivity to frequencies at around 250Hz. Vibrations of up to a maximum of 1kHz could occur, e.g., during very rapid explorative motion of the finger on very fine surfaces [24]. *Pacinian* corpuscles play therefore a crucial role in the perception of micro-geometric surface properties [24] [3].

1.2.1.2 Vibro-tactile Actuation Patterns for Spatio-temporal Stimulation

Vibration is an information-rich signal that is inherently produced during physical interactions with the environment. The human sense of touch excels at sensing and interpreting these vibrations to gather information about interactions with the physical world [25] [26].

In fact, in addition to displaying static sensations at discrete locations on the body, previous research [27] [20] [28] [29] [30] [31] [32] on the psycho-physiological aspects of the human sense of touch investigated the impact of vibro-tactile stimulation patterns by single or multiple, independently driven actuators. The creation of meaningful higher-order tactile percepts as the result of spatio-temporal actuation patterns from only few actuators enables the transmission of complex tactile information on, e.g., textures, directions, or shapes, thus constitutes an interesting solution to alleviate limitations of tactile actuator technology inherent to any technical tactile feedback loop.

It has been shown that by controlling the timing and intensity of tactile stimuli patterns, information can be communicated in a compact and efficient manner by so-called tactile illusions [33] [34] [35]. Hence, vibro-tactile actuation patterns for spatio-temporal stimulation that create meaningful tactile illusions bear the potential of mitigating the problem of space and energy consumption of large arrays of tactile actuators. The following paragraphs elaborate on important psycho-physical tactile phenomena, namely the apparent tactile motion and the phantom tactile sensation, as a major design tool to achieve a compact and wearable tactile feedback system, Fig. 1.2.

Apparent tactile motion (AM) [33] [20] [2] is observed, when the projection of two vibro-tactile stimuli is spatio-temporally controlled so that their stimuli on the skin are in close proximity to each other and their stimuli times overlap. Then, humans do not perceive two separated

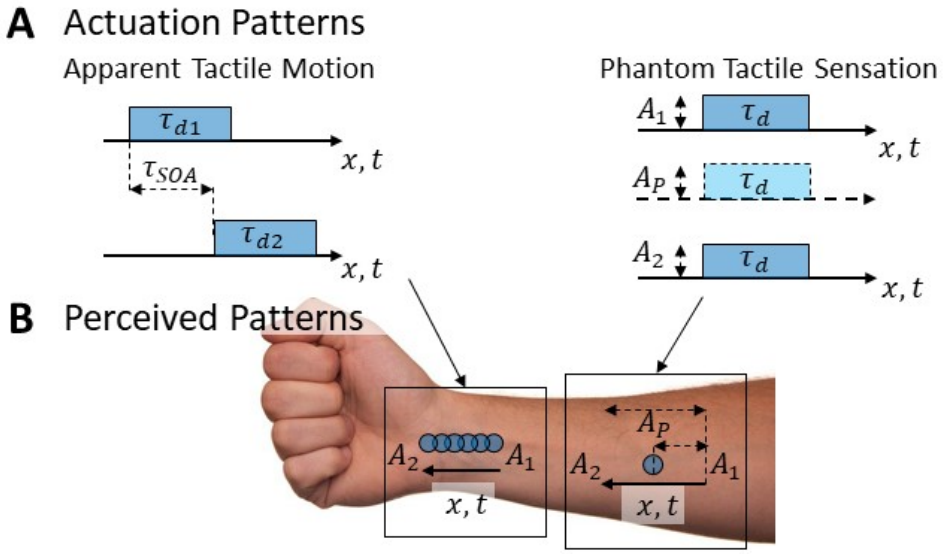

FIGURE 1.2: Illusory tactual percepts due to vibro-tactile stimulation: Apparent tactile motion (A) and phantom tactile sensation (B) may allow to mitigate limitations in tactile information transmission due to a limited actuator grid density.

actuators, but merely a single actuator that appears to be moving between the two points of the actual stimulation [33]. Neuhaus *et al.* demonstrated that the variables allowing for a robust generation of AM were (1) stimuli duration τ_d and (2) inter-stimulus onset asynchrony (SOA) τ_{SOA}. SOA is defined as the time interval between the onsets of subsequent actuation stimuli [36] [37] [25], Fig. 1.2-A. The optimal values for τ_{SOA} are a function of the stimuli duration τ_d [36] [37] [25]. The stimuli duration is inversely proportional to the perceived velocity of the illusory movement. Due to their inter-dependency, τ_d and τ_{SOA} require careful adjustment to preserve the illusion.

Phantom tactile sensation (PS) [34] [20] [2] is observed, when the intensity of two simultaneous vibro-tactile stimuli is controlled so that their stimuli on the skin are in close proximity to each other, however, the stimulus intensities differ. Then, humans do not perceive two separated actuators, but merely an illusory vibrating actuator located between the physical actuators, Fig. 1.2-B. Unlike AM, the PS is perceived as static [35]. Hence, the resulting location and intensity are controlled by the relative intensities of the two vibro-tactile stimuli [34]. For example, if two vibro-tactile stimuli intensities are equal, the resulting sensation is perceived at the center between these two actuators. Alles [35] found that the logarithmic relation of stimuli intensities maintains a constant PS intensity

over the entire range of locations. Different relations between the stimuli intensities have been proposed to control the resulting PS localization and intensity [20] [38] [28] [21].

Israr and Poupyrev [20] proposed an algorithm called the *Tactile Brush* that combined AM and PS to create tactile illusions of 2D tactile strokes by controlling a sparse 4×3 array of C-2 tactors inside a sheet of foam glued to the back of a wooden chair. Park *et al.* [28] presented an extension to the *Tactile Brush* algorithm that controls a set of three actuators to create smoother, non-linear PS and was deployed to render moving tactile sensations on the palm by means of a sparse 2D-array of piezo-electric vibrators. In [39] and [21] these efforts have been extended towards the haptic interaction with a 3D virtual object by means of tactile illusions generated by a sparse 3D-array of piezo-electric vibrators. These algorithms enabled the sensation of continuous tactile motion with sparsely, grid-like arranged actuators.

Given this previous research, AM and PS are important design elements of tactile displays, since they may allow for the creation of tactile stimuli to convey locations of contact and textural properties [27] [20] [21], yet with only a small number of physical actuators. Up-to-date, however, it is a major challenge to design tactile displays based on tactile illusions, as the knowledge of the control parameters that enable tactile illusions depend on the individual user, the body site and the deployed hardware for stimulus generation [40] [31] [41].

1.2.2 State of the Art in Tactile Technology

1.2.2.1 Tactile Sensors and their Large-scale Implementation into Robots

Recently, the development of tactile sensors and the demonstration of their potential in robotic applications promoted the technical development of a large diversity of transduction principles and design criteria to further facilitate their application in robotics [9] [6] [7], Fig. 1.3.

The biomimetic sensor from *BioTac* [48] is a multi-modal sensor module that integrates three transduction principles, Fig. 1.3-A. Normal forces can be measured by an arrangement of 24 electrodes and with a resolution of $0.01N$ at up to $100Hz$. Given the knowledge on the sensor geometry, tri-axial forces can be computed [49]. Furthermore, due to an integral pressure sensor that senses the oscillations of a fluid inside the fingertip

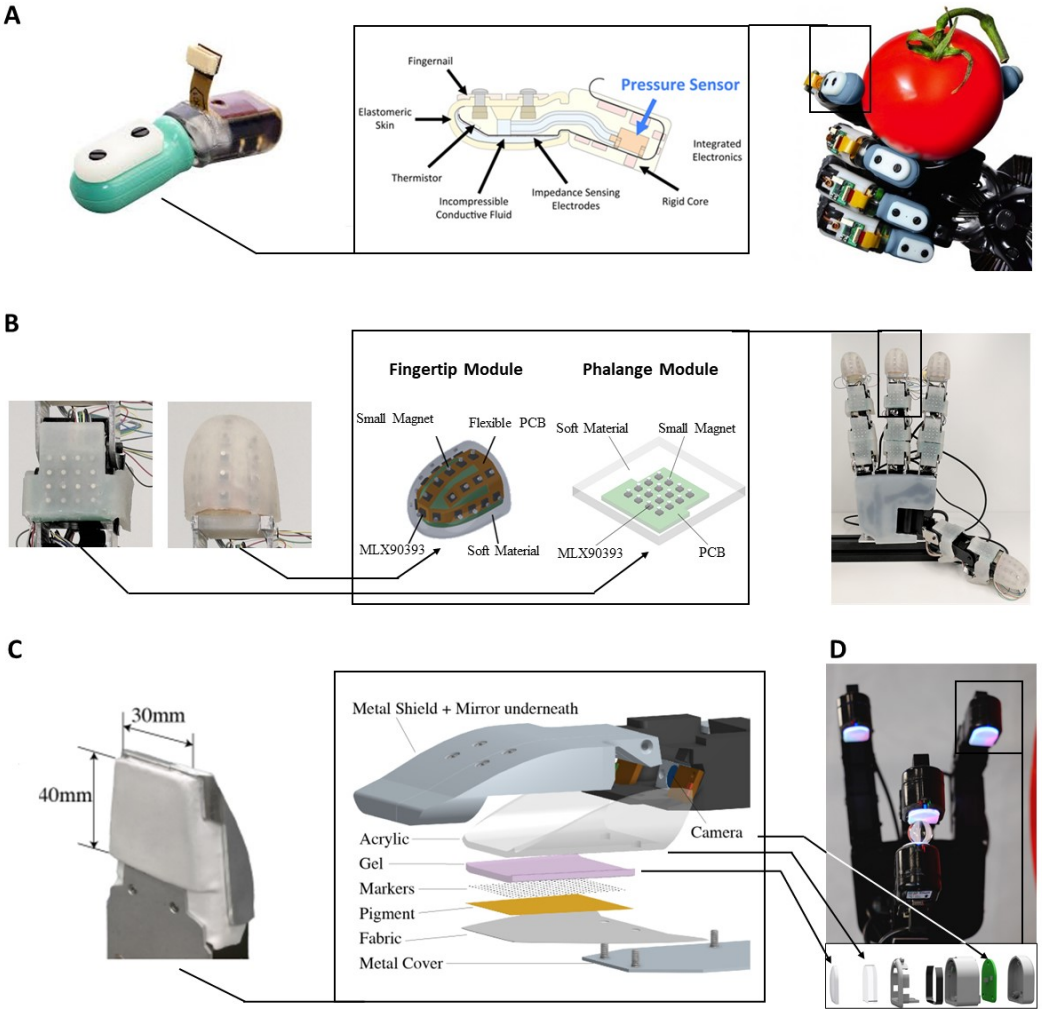

FIGURE 1.3: Representative selection of robot hands with tactile sensors: Fishel *et al.* [42] [43] (A), Tomo *et al.* [44], [45] (B), Daolin *et al.* [46] (C), and Lambeta *et al.* [47] (D).

compartment, vibrations from 10-1040Hz can be measured. The *BioTac* has been deployed to many anthropomorphic robot hands, e.g. the *Shadow Hand* [43] [50], the *BarretHand* [51] as well as the *Allegro* hand [52]. The *BioTac* sensor is also, to the author's best knowledge, the only modern tactile skin sensor that has been utilized in academic research on tactile feedback by means of tactile displays: Pacchierotti [18] [12] and co-workers used the *BioTac* to provide a human operator with tactile feedback in terms of fingertip contact deformations and vibrations for robotic surgery-applications, however, only by directly mapping the tactile data to input commands for the tactile display.

In this context, our lab has been developing the tactile sensor module *uSkin*, which is a soft 3-axis skin sensor [53] in a compact form factor. It was

developed for the implementation into the *Allegro* hand [54], Fig. 1.3-B. Each sensor element inside the module contains a small permanent magnet that is suspended above a tri-axial *Hall*-effect sensing microchip which allows for sensing of tri-axial force vectors upon external deformation of the silicon. A flat *uSkin* sensor module accommodates 16 sensor elements in a grid-like array of the size $24 \times 28 \times 5.5\ mm$.

Another example is the *GelSlim* [55] [46], a high-resolving tactile sensor module that enables tactile sensing by monitoring the deformations of a soft elastomer matrix with a small camera, Fig. 1.3-C. In detail, a camera system captures highly detailed images of an illuminated, clear elastomer that is covered with a reflective coating and deforms under load. While the *GelSlim* has a very high resolution and can sense fine micro-geometric surface features, it has a comparatively low frequency response due to the required signal processing of the huge amounts of data. The *GelSlim* module is comparatively large, but has been deployed to robotic grippers, e.g. [46].

Adapting the operational principle of *GelSlim*, Lambeta *et al.* [47] developed a low-cost tactile sensor that was termed *DIGIT*. *DIGIT* has a smaller form factor compared to *GelSlim* and has been implemented into a multi-fingered *Allegro* hand, Fig. 1.3-D.

Recently, Padmanabha *et al.* [56] developed *OmniTact*, which deploys a vision-based operational principle comparable to *GelSlim*, but combines high-resolution with multi-directional tactile sensing. The group around Padmanabha *et al.* reported that these features of tactile sensors are crucial for robot manipulation as it allows for higher accuracy in the state estimation task.

A summary of the technical specifications of most of the here mentioned sensors is given in Tab. 1.2. Note that the sampling frequency must be regarded with respect to the mechanical design and the technical transduction principle of the sensor. It does therefore not necessarily reflect the maximum achievable frequency response of the sensor. Additionally, extensive signal processing might be necessary to calculate physical quantities like force vectors, e.g. in the *BioTac* [49] or in the *GelSlim* [55].

Evidently, tactile sensors for the implementation into robots are designed to be (1) distributed and high-resolving, (2) compliant, and (3) compact. The intrinsic compliance mimics the human skin and adds passive safety, which is important, since active control schemes that involve feedback loops from joint encoders are typically not sufficient, neither to provide direct feedback

TABLE 1.2: Technical specifications of representative tactile sensors.

	BioTac [42]	GelSlim [55] [46]	uSkin [53]	DIGIT [47]
Sensor type	Impedance, Thermistor, Hydrophone	Camera	Hall-Effect	Camera
Size [mm]	$(15x28x18)^2$	$50x205x20$	$24x28x5.5$	$20x27x18$
Sensing Field [mm]	NA	$30x40$	$17.6x17.6$	$19x16$
Sensing Points[1]	19 Electrodes $(4x5)^3$ 1 Thermistor 1 Hyrdroph.	$640x480$	$4x4x3$	$640x480$
Frequency*	$10\text{-}1040Hz$	60FPS	$100Hz^4$	60FPS
Remarks	multi-modal, soft	soft	tri-axial, soft	soft

*Does not reflect the overall frequency response.
[1]Direct readout without extensive signal processing.
[2]Estimated from pictures, datasheets, etc.
[3]Non-linear pattern.
[4]For $4x4$-module with one microcontroller unit.

from the environment in terms of distributed sensing modalities nor precise contact localization. Furthermore, compliance of joints and sensors have been shown to facilitate robot tactile servoing [57] as well as grasp stability and in-hand manipulation [58] [59] [60] [61] [62]. Large-scale implementations of tactile sensors into humanoid robots are depicted in Fig. 1.4.

For example, the *TWENDY-ONE* robot [58] is entirely covered with a tactile sensor skin that contains distributed force sensors implemented into the hands (2×241), into the arms (2×54), and into the torso, Fig. 1.4-A. The fingers and hand are covered with silicone-like materials, which was reported to enhance the stability of grasping and manipulating objects with complicated shapes.

The *NAO* robot is equipped with 116 multi-modal skin sensors, termed *Hex-O-Skin*[65]: These sensor cells have been implemented into the chest (32), each hand (14), fore arm (12), and upper arm (16), Fig. 1.4-B. In total, the seven body segments of *NAO* were providing 348 normal-force, 116 *x,y,z*-axis accelerometer, 116 proximity, and 116 temperature sensor readouts.

Other examples are the small humanoid *iCub* with 2000 force sensors

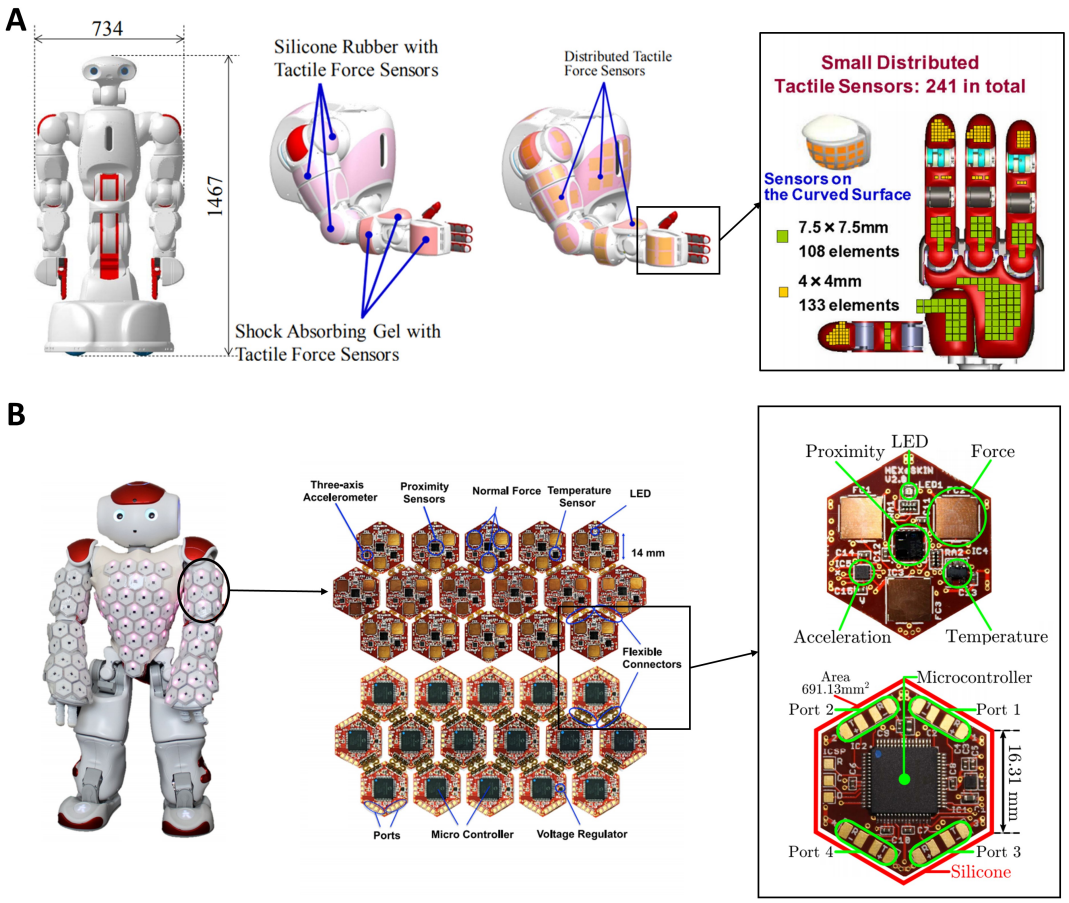

FIGURE 1.4: Representative selection of robots with large-scale tactile sensor implementations: Iwata *et al.* [58] (A), and Cheng *et al.* [63] and Kaboli *et al.* [64] (B).

[66] or the H1 robot, i.e. the REEM-C bipedal humanoid from *PAL Robotics* [2], whose entire body is covered with 1260 *Hex-O-Skin* [67]. The large-scale implementation of tactile sensor skin and associated challenges are an interesting and ongoing field of research, a very good overview is given by Cheng *et al.* [63].

1.2.2.2 Active Tactile Recognition and Compression of Tactile Data

Active tactile (texture) recognition is the active engagement of robot manipulators with objects in unstructured environments to retrieve information on physical object properties, e.g. contact locations and surface properties transmitted at these locations. An extensive overview is given by Li and co-workers in [7].

[2] https://robots.ieee.org/robots/reemc/

Commonly, the sensing of micro-geometric textural surface features necessitates sensors that can sample high frequency signals [68] [69] [70]: Fishel *et al.* published a study in which they described the algorithm called *Bayesian exploration*, which allowed for the recognition of 117 different textures by means of the *BioTac* sensor module that provided a combination of reaction forces and comparatively high-frequency vibration signals as input data.

Kaboli and Cheng [64] constructed a set of so-called tactile descriptors that were adopted from *Hjorth* parameters, i.e. a set of time-domain parameters for the signal analysis in real-time electroencephalography. This approach was used in the tactile signal analysis of the vibro-tactile signals measured during human-like exploration of 120 different materials by robots carrying a variety of multi-modal tactile sensors. In this regard, Chathuranga *et al.* [71] combined statistical descriptors for the signal analysis with artificial neural networks to distinguish seven wooden textures with a biomimetic fingertip sensor with soft material properties.

Takahashi and Tan [72] used a convolutional autoencoder approach to associate the tactile data to the corresponding images of the surfaces of 25 material probes enabling the perception of tactile properties indirectly via vision. Polic *et al.* [73] used a convolutional autoencoder to identify a universal set of tactile features from tactile sensor data, i.e. an unsupervised feature extraction, and investigated the usefulness of these features for different robot manipulation tasks.

Albeit many applications regard data compression as a key technique for image processing, or in general, for information retrieval [74] [75], the task-specific compression of tactile data, in particular for the control of tactile displays, has rarely been investigated [12] [1] [17].

Compressed learning has been used in the classification of tactile signals by performing the recognition directly on compressed, low-dimensional sensor data obtained from embedded tactile skin sensor arrays [76] [77]. Another recent approach suggests to encode sub-sequences of the tactile input data using a linear dynamic system approach and the application of fuzzy c-means to cluster the obtained representation [78]. Liu *et al.* [79] investigated the direct recognition of the shape of objects that are in contact with a robotic finger by deploying a novel feature extractor, which uses the tactile pressure map to construct a feature vector for finite contact shape classification. This is in contrast to purely analytic approaches [80] [7].

In this context, the interpretation of tactile information is one of the trending challenges in computational learning [81] and could be potentially useful for the control of tactile displays in the context of large-scale implementation of tactile sensors.

1.2.2.3 Tactile Displays

Due to a major shift towards wearable devices, haptic systems have started to be designed with wearability in mind [11] [82]. Arguably, wearability and, in particular, the portability of haptic systems are important factors for the ubiquitous communication between humans and machines. Thus, stationary, handheld, or invasive devices, e.g. the *Tactile-Telerobot* from *HaptX*[3], are not considered further. These type of devices naturally exhibit restrictions that impede their uncomplicated use for manipulation tasks, e.g., free finger motion and natural hand-eye coordination for multi-fingered teleoperation. However, comprehensive reviews on haptic devices in general can be found in [24] [11] [2] [82].

In fact, cutaneous feedback has been reported to play a crucial role in enhancing the performance and effectiveness of teleoperation [83] [84] [15] [4] [5]. Tactile displays are therefore gaining increasing interest, as they are generally easier and safer to integrate into teleoperation systems, because they do not introduce instability into the control loop of the manipulators [1] [4].

Wearable systems are typically tactile, i.e. cutaneous, devices [11] [2] [82]. By analogy to tactile sensors, tactile displays are arrays of typically very small actuators that stimulate the cutaneous mechanoreceptors to resemble the extrinsic sense of touch by the projection of forces, pressure, vibration or temperatures onto the human skin [5]. In this sense, tactile displays yield the potential of immersive and direct tactile feedback in the form of wearable and portable devices [82]. Their technical realization, however, imposes severe demands on the actuator technology.

The following section reviews wearable tactile displays according to their mode of stimulation, as adopted from Biggs & Srinivasan [85]: normal skin indentation, skin shear, and vibration. Additionally, electro-tactile displays are shortly reviewed, Fig. 1.5.

[3]https://haptx.com/robotics/

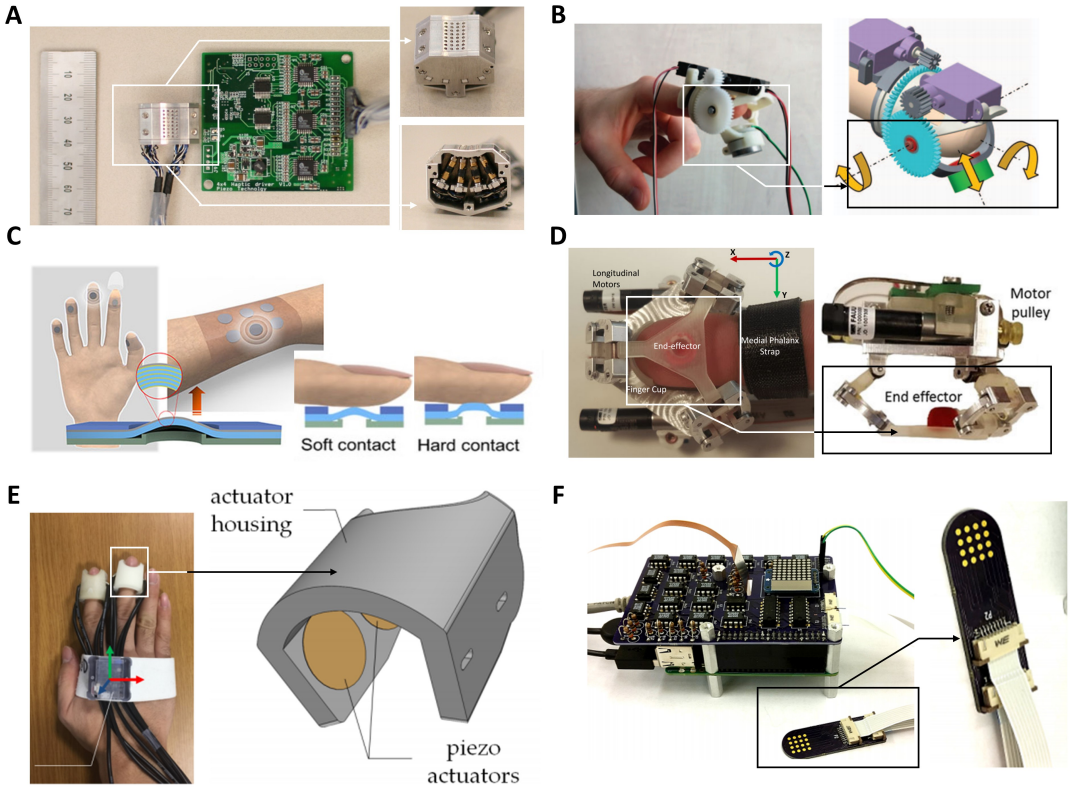

FIGURE 1.5: Representative selection of wearable tactile displays: Kim *et al.* [86] (A), Gabardi *et al.* [87] (B), Mun *et al.* [88] (C), Schorr *et al.* [89] (D), Kim *et al.* [39] (E), Rahimi *et al.* [90] (F).

Normal indentation displays transmit tactile stimuli via indentation of the skin by one or multiple moving tactors, which enables spatially distributed tactile information transmission into the skin. Contact, pressure, curvature, and soft-/hardness displays belong to this category. For example, Kim *et al.* [86] presented a piezoelectric ultrasonic actuator-based tactile display that drove a 8×4 array of pins with a spatial resolution of $1.5mm$ and a temporal resolution of $20Hz$, Fig. 1.5-A. Despite the mechanical embodiment as pin array, they achieved a rather lightweight and wearable design with an overall dimension of $1.7 \times 3.4 \times 3.2cm$. The authors managed to implement three of these modules into a glove, making them able to provide a human user with cutaneous stimuli to the thumb, index, and middle fingers. The controller hardware was rather bulky and the system was attached to the back of the user to enable free finger motion. Gabardi *et al.* [87] presented a haptic device called *Haptic Thimble* for surface exploration in virtual environments, Fig. 1.5-B. It uses a serial kinematics

chain to combine the rendering of surface orientation with fast transient and wide frequency bandwidth tactile cues of up to $300Hz$. It combines a compact servo motor for orienting a plate that is in contact with the finger pad and a voice coil actuator that actuates the plate. The total weight of *Haptic Thimble* was reported to $30g$ and the overall size to $6.6 \times 3.5 \times 3.8cm$. Mun *et al.* [88] developed a flexible tactile display using an electro-active polymer that activates with an external electrical voltage and protrudes vertically to cause normal skin indentations, Fig. 1.5-C. Mun *et al.* reported that the maximum protrusion is $650\mu m$ with a maximum force of $255mN$. One actuator has a diameter of around $15mm$ and can be worn on the finger phalanges and the forearm.

In contrast, **skin shear** devices exert shear forces which stimulate the cutaneous mechanoreceptors efficiently, due to their high sensitivity to tangential stretch. These devices can transmit directional cues, which can be even further enhanced by combining stretch and tangential motion stimuli, e.g. to generate perceptions of slippage. Friction, indentation, push-button, proprioception, and large-radius surface curvature display fall under this category [11]. Schorr & Okamura [89] presented a 3-degree-of-freedom (DOF) wearable device of this category, which is able to engage and disengage with the finger pad skin surface as well as to resemble shear and normal skin deformations at the finger pad, Fig. 1.5-D. The device deploys a delta parallel-link mechanism, which has three translational DOFs that enable normal as well as lateral and longitudinal skin deformations. This device weighs $32g$ with a size of $2.1 \times 4.9 \times 4.0cm$, has an operational workspace of $1 \times 1 \times 1cm$, and maximum achievable forces of $2N$ (normal) and $7.5N$ (shear). Young & Kuchenbecker [91] presented a 6-DOF parallel manipulator capable of controlling the position and orientation of a single end-effector platform, such that any combination of normal and shear force can be delivered. Even-though this device is technically wearable and can display normal and shear forces at any location on a fingertip, the immense size of the mechanical construction severely limits the applicability and makes teleoperation almost impossible.

In addition to the above-mentioned types of tactile displays, there is also a growing interest in **vibro-tactile stimuli**. Due to the small form factor and low mass of vibro-tactile actuators, highly-wearable interfaces can be more easily achieved [11], which makes these type of actuators most applicable in terms of unobstructed human-robot interactions and dexterous

teleoperation. Murray *et al.* [92] presented a wearable, vibro-tactile glove containing miniature voice coils that enabled the display to convey continuous, proportional force information to the user's fingertips. In psychophysical experiments, Murray and co-workers could show that vibro-tactile feedback allowed the users to control the grip forces more effectively during pick-and-place manipulation tasks. They concluded that correlated amplitude and frequency signals of vibro-tactile feedback substantially improved teleoperation.

Recently, Kim *et al.* [39] developed an adaptive vibro-tactile fingertip module that implemented four piezoelectric actuators (four $9mm$ ceramic disks concentrically mounted on $12mm$ metal disk) on the sides of the user's finger around an opening at the bottom for touch screen interaction, Fig. 1.5-E. In conjunction with a rendering algorithm that made use of the AM-theory by modulating τ_{SOA} and τ_d, the module was able to create a vibration flow and virtually resemble 2.5D surface features on a touch screen when using multiple fingertip interfaces.

Electro-tactile displays elicit tactile sensation by artificially stimulating the mechanoreceptors, i.e., by directly inducing electrical current from surface electrodes into nerve fibers within the skin. Despite the high variability and the somewhat unnatural perception, electro-tactile displays can be designed to be thin, light, and flexible, thus, highly wearable. In this regard, Kajimoto *et al.* [93] presented a compact ($7.5 \times 5cm$) electro-tactile display with 512 electrodes for the display of tactile images based on camera data of a smartphone. Recently, Rahimi *et al.* [90] investigated the feasibility of projecting identifiable moving patterns using electro-tactile stimulations by means of a 4×4 array of fingertip contacting electrodes ($\varnothing 1.5mm$) using varying voltages and frequencies, Fig. 1.5-F. Within an experimental session, only 39.6% of the participants could exactly identify the variously moving patterns induced by electrical signals. Further drawbacks of electro-tactile displays are the varying electrical impedance of the skin and effects of receptor fatigue due to electrical stimulation. However, solutions for the automated online-estimation of optimal electric stimulation to mitigate these effects are discussed in [94].

1.2.2.4 Shape Memory Alloy-based Tactile Displays

The use of SMAs for the construction of tactile displays goes back to the research of Howe *et al.* [95] and Wellman *et al.* [96] in the late 1990s,

Fig. 1.6-A. Howe and co-workers device consisted of an array of SMA-driven pin elements that were raised against the finger pad to approximate the desired surface shape on the skin of a human operator. It was pneumatically cooled and closed-loop position controlled. They achieved a maximum frequency bandwidth between $6Hz$ to $7Hz$ (-$3dB$ attenuation). In this regard, Wellman and co-workers investigated SMA-driven ($Ø75\mu m$, L$30mm$) multi-pin matrix arrays with active thermal liquid cooling (water and ethylene glycol), which increased the frequency bandwidth to up to $40Hz$ (-$3dB$). Both the devices were limited in their frequency response, thus directed towards static shape representation, and at that point only stationary prototypes. The power consumption of these devices was not reported. However, the groups around Howe and Wellman established important groundwork for SMA-based actuators for the use in tactile displays.

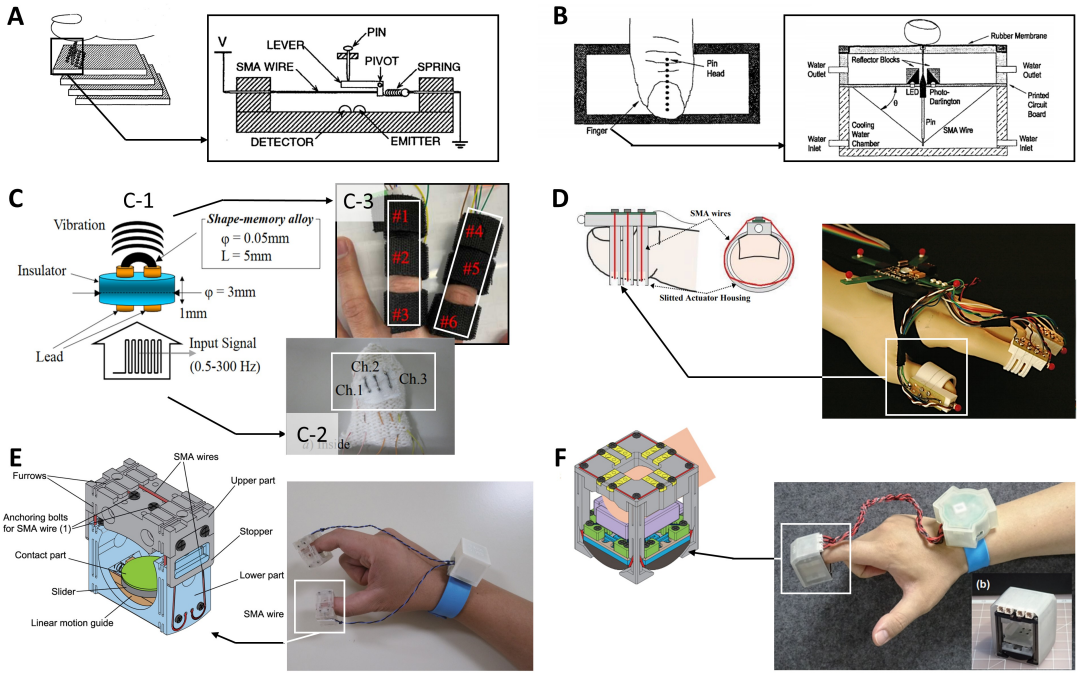

FIGURE 1.6: Shape memory ally-based tactile displays: Howe *et al.* [95] (A), Wellman *et al.* [96] (B), Fukuyama *et al.* [27] (C1), Okumoto *et al.* [97] (C2), Aiemsetthee *et al.* [98] (C3), Scheibe *et al.* [99] (D), Hwang *et al.* [100] (E), Lim *et al.* [101] (F).

Firstly in 2006 by Mizukami *et al.* [102] and later in 2009 by Fukuyama *et al.* [27], SMA-based micro-vibrators for the transmission of tactile stimuli were investigated, Fig. 1.6-C1, and the control of short and thin SMA wires ($Ø50\mu m$, L$5mm$) by pulse width modulation (PWM) was established.

Mizukami *et al.* reported that by deploying pulsed current signals to thin SMA wires, frequencies of up to $300Hz$ could be generated in synchronization with the control signal.

Fukuyama *et al.* [27] constructed a stationary planar array of roughly $5.5 \times 5.0cm$ with up to eight SMA-wire actuators to transmit sensations of surface properties by means of vibration signals with a frequency bandwidth of $50Hz$ to $100Hz$. This prototype used static actuation patterns to generate AM and the SMA actuator itself consisted of an SMA wire ($Ø50\mu m$, L$5mm$, R3Ω) sitting inside an insulator embedded into the display matrix.

From 2012, several versions of SMA-based, glove-type devices were suggested: Okumoto *et al.* [97] presented *TactoGlove* having three SMA wires ($Ø50\mu m$, L$5mm$, R3Ω) sewed into a cloth spanning linearly across the center of the thumb's finger pad in an attempt to transmit distinguishable sensations of sliding or initial contact for virtual reality applications, Fig. 1.6-C2. *TactoGlove* was operated at $3.0V$ and had a maximum of nine independently controlled SMA actuators running at approx. 4% duty cycle.

In 2020, Aiemsetthee *et al.* presented a prototype of an *Braille* information display with up to six independently driven SMA actuators ($Ø100\mu m$, L$5mm$, R1.4Ω) similar to the ones used in Okumoto *et al.* [97], however with a pin-like design comparable to the early designs of Howe [95] and Wellman [96]. These actuators were sewed into six *VELCRO*® straps, each for every segment of index and middle finger, and were meant to act as refresh-able *Braille* display, Fig. 1.6-C3.

Scheibe *et al.* [99] presented an ergonomic SMA-based fingertip module that was designed for improving tactile interaction in virtual reality applications for the car industry, Fig. 1.6-D. Each fingertip module had a size of approx. $17 \times 28mm$ and implemented a maximum of three SMA wire ($Ø80\mu m$, L$50mm$, R11Ω) loops that wrapped around the finger pads and were fixed on top of the fingertip module using M2 screws with a head diameter of $3.8mm$. The spacing between the loops was approx. $6mm$. Due to the loop-like design, the SMA wires were much longer then in the above designs (cf. L$5mm$ in Okumoto *et al.* to L$50mm$ in Scheibe *et al.*) and implemented completely different tactile stimulus modalities. Scheibe and co-workers module was able to generate the sensation of vibratory contractions, which were intended to resemble typical tactile interactions inside a car interior, e.g. touching the steering wheel, operating various knobs and buttons. However, due to the control board, the maximum

number of SMA actuators was limited to eight actuators: three actuators were implemented into index and middle finger module, and two into the thumb module, respectively. The system was reported to operate at $12.6V$ input voltage with a rather high power consumption of $1.81W$ per actuator, because the internal SMA actuator resistance (R11Ω) is proportional to the length of the SMA wire loop, which was rather high.

Hwang *et al.* [100] proposed a haptic ring that displayed normal and shear forces to the fingertips by implementing three SMA wires (Ø100μm) that move a platform with a slider upon which the finger pad rests, Fig. 1.6-E. For the display of pressure, one SMA wire compresses the platform with the slider pressing against the fingertip. For the display of shear forces, two additional SMA wires move the slider alongside a linear motion guide. Hwang and co-workers reported achievable displacements of $0.5mm$ (normal direction) and $\pm 1mm$ (shear direction), and achievable force outputs of $3N$ (normal direction) and $3N$ (shear direction). However, due to the passive cooling of the SMA, these specifications depended heavily on the desired frequency response, which were reported to be up to only $2.6Hz$ (normal direction) and $3Hz$ (shear direction). The final prototypes had an overall size of $25 \times 14 \times 30mm$, a total weight of approx. $7.1g$, and it was operated at $8.5V$ supply voltage together with a desktop PC as part of a virtual reality environment.

Recently, Lim *et al.* [101] proposed *HaptiCube*, a cube-shaped 5-DOF finger-wearable tactile device that uses various SMA wires/helices (Ø150μm) to displace and tilt inner platforms against the finger pad, Fig. 1.6-F. This device was designed to display 3-DOF pressures and 2-DOF shear forces to the finger pad, i.e. force feedback. The motion trajectories were generated by PWM-control at high duty cycles of up to 30%, thus, the frequency response was limited to $4.1Hz$ to allow for sufficient passive cooling of the SMA actuators. However, a maximum shear force of approx. $2.1N$ and normal force of approx. $12N$ were achieved. The total weight and the overall size of *HaptiCube* were reported to $26g$ and $2.9 \times 2.9 \times 3$ cm, respectively. The operating voltage and power consumption were not reported.

1.2.2.5 Summary

Clearly, tactile sensing is an indispensable ability for the interaction with and the manipulation of unstructured environments; both for humans and

robots [1] [2] [3] [4] [5]. The complementation of robotic manipulators with tactile sensors has therefore demonstrated great potential, as physical feedback during dynamic interaction with unstructured environment greatly enhances automation and manipulation capabilities of robots [58] [9] [6][59] [60] [10] [61] [62] [7]. The vast majority of modern tactile sensors for the large-scale implementation into robots or robot manipulators are: soft, densely distributed, and often multi-modal [48] [53] [55] [46] [47] [56].

Despite decades of development of wearable tactile displays that seek to enable the emulation of natural tactile feedback, till to date the manufacturing of high-density tactile displays is challenging [1] [11] [2] [82]. Tactile displays are arrays of distributed actuators and inherently suffer from high energy consumption, large form factors, and a limited output range. For this reason, they are always restricted to a certain application, e.g. virtual reality, and only few modes of tactile stimulation, e.g. lateral skin deformation, because the integration of various actuators for the emulation of multi-modal tactile perception is challenging, especially in a compact form factor for, e.g., the application in telerobotics [103].

In this regard, the signal processing of tactile sensor data for the use in tactile displays has been rarely investigated [18] [17]. In particular, the generation of tactile feedback across the skin of a human user from a remotely operating robot or robot end effector that is equipped with soft, distributed tactile sensor skin and thus capable of sensing physical information in unstructured environments is a major technical challenge. The efficient yet meaningful end-to-end projection of arbitrary tactile sensor data for the generation of tactile stimuli by means of wearable tactile displays that provide information on the location of physical contacts and the conveyance of physical contact information, such as micro-geometric surface properties, is the objective of this thesis.

1.3 Objectives

The above limitations motivated the following outline of research objectives. They target the development of a data-driven tactile feedback system deploying end-to-end tactile sensor data projections for a compact and scalable tactile feedback solution and its implementation into a wearable human-machine interface for human-robot interaction and robot-teleoperation.

1. **Generalizability**: The presented research and the proposed solutions should possess external validity, i.e., should establish a framework rather than a particular solution for the specific hardware deployed throughout this thesis. For this reason, a major part of this thesis deals with the development of software algorithms that establish the tactile information flow regardless of the tactile technology deployed. The presented research rather adheres to a design concept of tactile feedback systems that is applicable beyond the hardware on which it is necessarily tested within this thesis.

2. **End-to-end Design**: A large majority of the in sections 1.2.2.3 and 1.2.2.4 presented tactile displays are designed for or verified in virtual reality applications or other strictly defined settings, e.g. *Braille* information displays. In fact, this is a dramatic limitation: Tactile sensors are ultimately designed to allow robots to explore, understand, and interact with new, unstructured environments. Similarly, tactile displays should enable human operators to perceive unstructured, raw tactile sensor data in a meaningful way. While this is a great challenge, since electro-mechanical design and technical transduction principles of both the deployed tactile sensor and the tactile actuator clearly affect the tactile information flow, algorithms must overcome or at least alleviate this issue and enable an end-to-end tactile information projection.

3. **Scalability**: The developed tactile feedback framework as a whole should scale in accordance with the desired application and the associated tactile sensor and tactile actuator technology. In terms of software, this means that the end-to-end projection of the tactile sensor data into a control signal that drives the tactile display must work with little as well as with immense amounts of sensor data. Likewise, the hardware design must be modular to be applicable across a wider range of application scenarios, e.g. a varying number of associated tactile sensor and display modules for differently designed robot manipulators, while keeping the form factor as compact as possible.

4. **Extensibility**: In contrast to sole scalability, an extensible system design allows the addition of new capabilities or functionality. The need for extensibility arises from the fact that tactile perception is multi-modal, since the set of cutaneous receptors includes

mechanoreceptors with different sensing modalities from static shear to dynamic micro-vibration to heat flux, compare section 1.2.1. The mechanical module and the electrical circuit driver design should allow for an easy complementation of the tactile display module by SMA-actuators of different embodiment or completely different actuators to generate a broader range of tactile stimuli. Likewise, the associated software must not impede those extensions.

5. **Wearability**: Even though any tangible addition to the human fingertip admittedly decreases the naturality of motion and tactile interaction, the hardware design must be compact enough to be worn comfortably and must not be connected to the ground. Furthermore, the manufacturing process of the complete module should be efficient and customizable to the individual finger size and shape.

1.4 Novel Contributions

There has been extensive research on tactile sensors, their large-scale implementation for robotic applications (section 1.2.2.1) and on algorithms that use tactile data to enhance tasks, e.g. tactile recognition or manipulation by robotic manipulators (section 1.2.2.2). Likewise, wearable tactile displays (section 1.2.2.3) have been researched for decades.

Just recently, however, the knowledge on tactile perception (section 1.2.1) is becoming sufficient to robustly control tactile illusory phenomena and integrate them as an integral part of the control of vibro-tactile displays. In this context, the development of a wearable tactile feedback system for human-robot interaction that uses end-to-end tactile sensor data projections to enable the creation of psychophysical tactile illusions from densely distributed tactile skin sensors and thereby enables the generation of high-resolution tactile stimuli using low-resolution vibro-tactile actuator grids has not been investigated before.

The choice of ultra-compact, energy-dense SMA-based micro-vibrators enables a compact and wearable mechanical design with comparably low energy consumption of approx. $180mW$ (cf. [27] [99]). These micro-vibrators have a frequency bandwidth of typically up to $300Hz$ [102] to stimulate the *Meissner* and *Pacinian* corpuscles, are sparsely distributed inside the

fingertip module, and thus enable the generation of tactile illusory stimuli onto the skin of the finger pad.

Moreover, the tactile feedback system implements algorithms that solve the unknown transformation from massive amounts of tactile sensor data to the driving signals of sparsely distributed actuators and enable the efficient end-to-end projection of contact locations and textural surface properties by means of tactile illusions. The use of tactile illusory stimuli to convey the locations of contact and textural surface properties with only a low-resolution actuator grid reduces the energy and space requirements compared to traditional tactile displays.

Due to the very high force-volume ratio of SMA-actuators and the data projection algorithms, the tactile display module can be complemented with more SMA-actuators without increasing the energy consumption. Owing to this compactness, the tactile display modules can also serve as an extension for the integration into tactile displays targeting other mechanoreceptors for multi-modal feedback or haptic devices for kinesthetic feedback.

Ultimately, the custom-made driver board of the tactile display module deploys a WiFi-enabled microcontroller unit that can connect with several compact I^2C-capable driver circuit units each of which can independently drive up to eight SMA-actuators; sufficient to cover the complete hand of a human operator.

The throughout this thesis developed prototype implements the in section 1.3 outlined objectives and yields the potential for a highly efficient tactile display module. To the author's best knowledge, no other tactile feedback system implements these features in a compact and complete tactile feedback system.

Thus, the presented research on hard- & software establishes a novel data-driven tactile feedback framework that deploys end-to-end tactile sensor data projections for the application as a wearable human-machine interface for robot-teleoperation and human-robot interaction.

1.5 Thesis Outline

1.5.1 Chapter 2: System Architecture and Design Concept of the Tactile Feedback System

Chapter 2 establishes the system architecture for the experimental studies on the design and evaluation of the proposed data-driven tactile feedback system. The system architecture adheres to the outlined research objectives. Concretely, the system architecture involves an anthropomorphic robot hand that is covered with a soft, distributed tactile sensor skin, a host PC running resource-intensive algorithms on the tactile sensor data, a compact WiFi-enabled microcontroller unit that can control the actuation of multiple I^2C-enabled custom-made tactile display driver circuits that, in turn, can generate pulsed driving currents for the actuation of tactile display modules consisting of arrays of energy-dense and ultra-compact SMA-based actuators to create vibro-mechanical stimuli on the human skin. Chapter 2 thoroughly analyzes made design choices and functional aspects in the light of human tactile perception and robot tactile sensing technology as reviewed in section 1.2.2.

1.5.2 Chapter 3: End-to-end Tactile Texture Projection with Psychophysically-meaningful Latent Space Encodings

Chapter 3 introduces the concept and associated algorithm of *End-to-end Tactile Texture Projection with Psychophysically-meaningful Latent Space Encodings*, which takes inspiration from human material perception by representing physical surface properties in low-dimensional latent space. Thus, the presented algorithm investigates the auto-compression of tactile sensor data into psycho-physically meaningful latent space coordinates by deploying a deep gated recurrent unit-based autoencoder. It is investigated how this auto-compression of tactile sensor data allows to identify the generally unknown end-to-end mapping from tactile sensor data to tactile actuator driving signal, i.e., the end-to-end generation of illusory tactile stimuli that convey generic information on micro-geometric surface properties in accordance with the tactile sensor input data. The proposed algorithm was experimentally verified by deployment to the custom-made

tactile display prototype from chapter 2 and the evaluation of the emulated tactile feedback within user studies.

1.5.3 Chapter 4: Sequential Tactile Data Clustering for Tactile Image Compression to Enable Direct Adaptive Feedback

Chapter 4 introduces a to chapter 3 complementary algorithm termed *Sequential Tactile Data Clustering for Tactile Image Compression*. This algorithm resolves the dimensional mismatch between tactile sensor space and tactile display space by performing two data compression stages on the raw tactile sensor data at each time instant. This dynamic compression addresses the technological yet fundamental mismatch between the technical specifications of tactile sensor array and tactile actuator array by discretizing the tactile sensor data into a number of desired contact locations and stimuli intensities to match the tactile display capabilities. The algorithm allows for the generation of direct feedback from massive tactile sensor data for a broad variety of tactile sensors and tactile displays, thereby, enables the compressed yet intuitive representation of massive tactile sensor information for real-time applications. The algorithm is experimentally verified within several parameter studies.

1.5.4 Chapter 5: System Integration into a Wearable Tactile Display Fingertip Module

Chapter 5 achieves the system integration of the initially in section 2.1 introduced system architecture into a compact and wearable human-machine interface. Chapter 5 is therefore application-oriented and describes the mechanical (wearable fingertip module) and electronic (compact PCB of the I^2C-enabled driver circuit) implementation of the system components with optimized wiring into a compact, ergonomic fingertip module. As a result, chapter 5 arrives at a novel, scalable tactile display fingertip module that implements the in section 1.3 initially outlined objectives. The proposed tactile feedback system solves the unknown transformation from tactile sensor space to tactile actuator space and utilizes tactile illusions to mitigate limitations of tactile display actuators in terms of energy consumption and actuator density.

1.5.5 Chapter 6: Conclusion

Finally, chapter 6 draws conclusion on the presented research by summarizing the key achievements and critical limitations of the developed data-driven tactile feedback system that deploys end-to-end tactile sensor data projections for the application as a wearable human-machine interface for robot-teleoperation. Chapter 6 also concretizes future work that needs, firstly, to investigate and implement solutions for the more robust generation of tactile illusions for the more effective and more efficient generation of illusory tactile feedback and, secondly, to address design and implementational challenges for the integration into robot-teleoperation applications.

Chapter 2

System Architecture and Design Concept of the Tactile Feedback System

This chapter introduces the system architecture and the comprising components for the development and experimental evaluation of the tactile feedback system. Additionally, the operational principles of the deployed SMA-based actuators are explained and important design principles that come with the SMA-based actuator are outlined. Moreover, the inherent benefits and limitations of the SMA-based tactile display module are elaborated on. Note, the tactile display module went through several stages of development: The first tactile display module prototype is introduced in this chapter. The associated software algorithms are explained separately in chapters 3 and 4. Finally, chapter 5 presents the latest tactile display module prototype and its implementation as a compact wearable tactile feedback system.

2.1 System Architecture and Experimental Setup

The system architecture included the low-cost anthropomorphic *Allegro* robot hand [54] (Wonik Robotics[1]), the *uSkin* tactile sensor module [53] with a microcontroller unit (MCU) (*MTB3* [104]), a host PC (Intel® Core(TM) i7-8700K CPU @ 3.70GHz and 32.0GB RAM) with GPU (NVIDIA® GeForce GTX 1080 Ti with 11 GB frame buffer), a second MCU (Adafruit® Feather M0 WiFi), an I^2C-enabled pulse width modulation (PWM)-driver (Adafruit® 16-Channel 12-bit PWM Driver Board), a custom-made current

[1] http://www.simlab.co.kr/

amplifying driver circuit, and several generations of SMA-based tactile display module prototypes for the generation of vibro-mechanical stimuli.

Figure 2.1 shows the complete system architecture as a block diagram and depicts the flow of information between the system components.

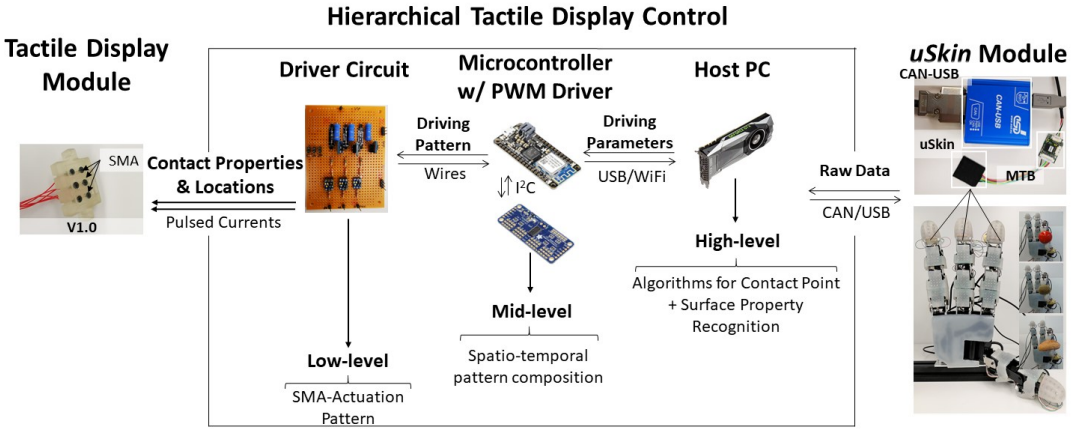

FIGURE 2.1: System architecture of the data-driven tactile feedback system. Pictures adopted from [45] [105].

Briefly, the *MTB3* of the *uSkin* tactile sensor module governed the collection of uncalibrated, raw tactile sensor readings using I^2C (Inter-Integrated Circuit)-communication and sent the tactile data via CAN (Controlled Area Network) bus and CAN/USB (Universal Serial Bus) converter[2] to the host PC. The host PC executed the algorithms for the driving signal computation. The algorithms were implemented in Python[3] (v3.7.6) and the neural networks were modelled in the high-level neural networks API KERAS[4] (v2.2.4) with Tensorflow[5] (v1.15.0) backend.

With the goal of wearability in mind, the host PC sent the computed driving parameters via WiFi to the WiFi-enabled MCU, which controlled the time-critical actuation of the SMA-based micro-vibrators for the generation of spatio-temporal actuation patterns that elicited illusory tactile sensations. To do so, the MCU controlled the PWM-driver, which triggered amplified, pulsed current signals flowing through each individual SMA-actuator. Note, an external power supply (Kikusui PWR800L, Regulated Power Supply) was used during the experimental studies (not depicted for the sake of simplicity).

[2]https://esd.eu/en
[3]https://www.python.org/
[4]https://keras.io/
[5]https://www.tensorflow.org/

2.1.1 Allegro Robot Hand with uSkin Tactile Sensor Modules

The *Allegro* robot hand is a low-cost anthropomorphic robot hand, which was equipped with *uSkin* tactile sensor modules [53] for research on in-hand manipulation [106] and active tactile (object) exploration [107] [54], Fig. 2.2. Important details on the operational principle and tactile features of *uSkin* are explained in the next section 2.1.2.

The *Allegro* robot hand setup was used as a testbed to experimentally verify the algorithm *Sequential Tactile Data Clustering for Tactile Image Compression* (chapter 4) under realistic conditions.

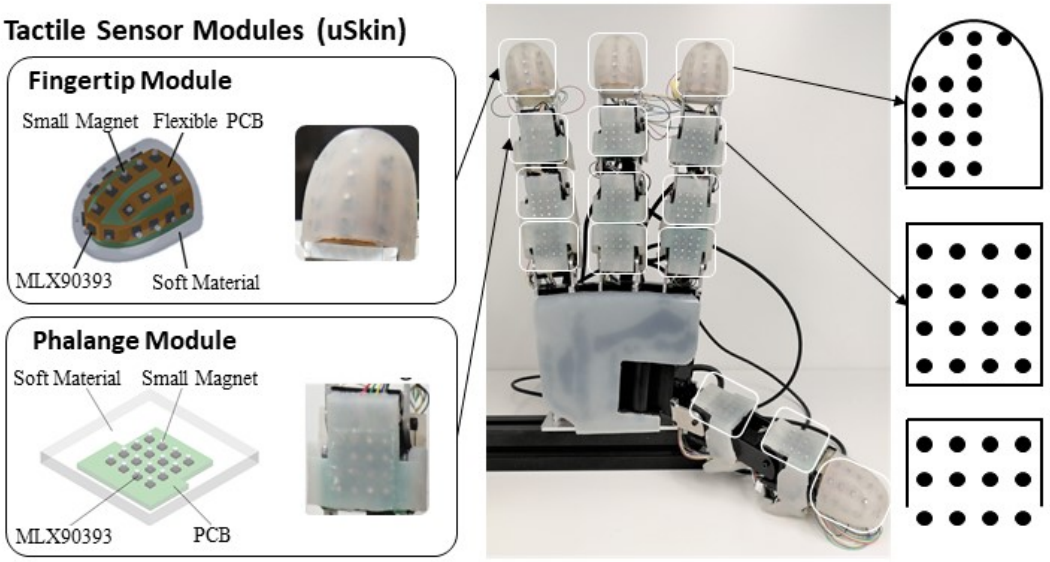

FIGURE 2.2: Allegro robot hand with uSkin sensor modules (left) and the arrangement of the active taxels within the uSkin modules (right).

The *Allegro* robot hand implemented two versions of the *uSkin* tactile sensor modules: a flat module for phalanges with 4×4 taxels [108] and a curved module for fingertips with 4×6 taxels [44]. In total, there were eleven flat modules mounted on the phalanges and four curved modules mounted on the fingertips. An *MTB3* reads up to 16 taxels, thus several *MTB3*s were daisy-chained via CAN bus to allow for proper transmission of all the tactile sensor data to the *Windows* machine.

The *Allegro* robot hand was connected via a PEAK[6] CAN/USB converter to a *Linux* machine, on which the motion controller was implemented using

[6]https://www.peak-system.com/

ROS (Robot Operating System[7]). Since the *uSkin* requires the *Windows* ESD-CAN library for CAN/USB conversion, the *uSkin* tactile data was bypassed to the *Linux* machine via LAN (local area network) using TCP/IP (Transmission Control Protocol/Internet Protocol) communication.

This enabled the simultaneous recording of the *uSkin* sensor and *Allegro* robot hand joint angle data at a maximum sampling rate of approx. $30Hz$. In the current implementation, the *Allegro* robot hand delivered $240\times$ 3-axis readings tactile sensor readouts in total.

2.1.2 uSkin Tactile Sensor Module

The *uSkin* is a soft, distributed 3-axis tactile sensor module with a magnetic sensing principle [44] and a dynamic range of $1gf$-$1800gf$, Fig. 2.3. The *uSkin*'s silicone structure suspends a grid-like array of 16 magnets over 16 *Hall* effect-based magnetometers, which detect changes in the magnetic field upon contact and deformation of the silicon structure.

The package size is $24 \times 28 \times 5.5\ mm$ and the sensor module provides digital readouts in three axes across the module's surface (x- and y-direction, shear forces) and along the surface normal (z-direction, normal forces) with a 16-bit resolution. The approximate sensor density is therefore 6.72 $taxels/cm^2$.

The skin sensor module [44] used throughout this thesis was similar to the previously presented compact, soft, and distributed 3-axis *uSkin* module for the deployment to robotic manipulators [53] and is of similar type to the sensor modules that covered the fingers of the *Allegro* robot hand [54] [106] for tactile sensing during object manipulation.

In the experiments, a flat 4×4 *uSkin* module with a maximum sampling frequency of approx. 100 Hz was used. The comparatively low frequency response arises due to the I^2C-communication bottleneck that requires to ping each sensor readout axis consecutively. Aiming for an end-to-end design, exclusively uncalibrated raw sensor readings were used throughout all the experiments described in chapters 3, 4, and 5.

Since the *uSkin* sensor module was designed for the implementation onto robot hands, a major design element of *uSkin* is the grid-like silicone structure made of *Dragon Skin 30*[8] providing the sensor with passive compliance. This

[7] https://www.ros.org/
[8] https://www.smooth-on.com/products/dragon-skin-30/

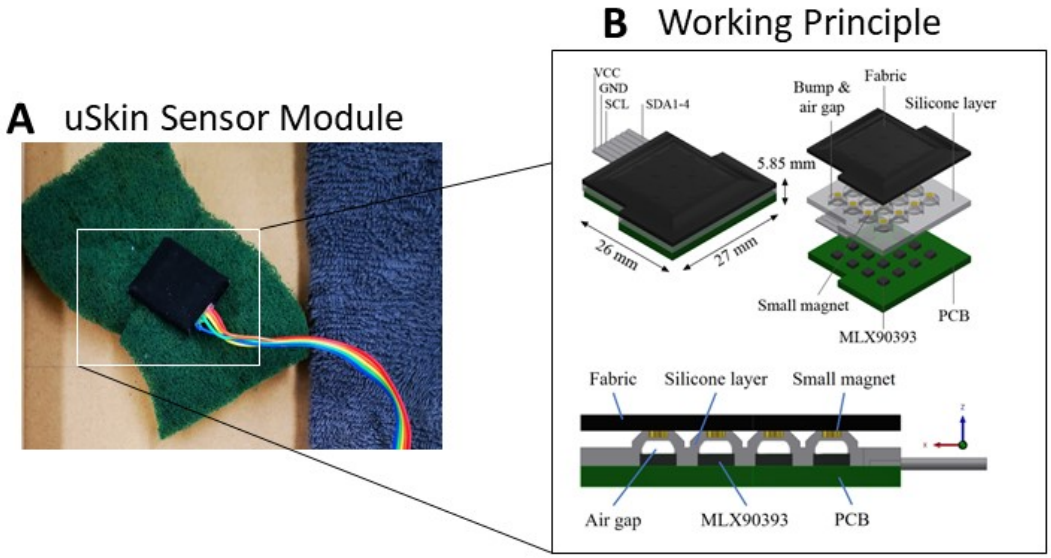

FIGURE 2.3: *uSkin* tactile sensor module deployed during the experiments (A) and the working principle (B). Note that there exist several versions of *uSkin* for which reason dimensions differ slightly. Pictures adopted from [105] (A) and [109] (B).

passive compliance is desirable for in-hand object manipulation, but causes the *uSkin* to act as a lowpass filter and thus limits the frequency response during tactile (object) exploration.

For durability reasons, the top layer of the *uSkin* consists of a flexible gripping fabric GM400[9] that prevents the silicone structure and magnets from direct contact with objects and increases the grasping stability and shear force detection by elevating the friction coefficient. These design choices were made to facilitate in-hand manipulation, but introduce additional bias when compared to the physiology of the human skin and mechanoreceptors.

As explained in chapter 1, the autonomous operation of robots requires tactile sensors to adhere to the paradigms of safe and robust manipulation of unknown objects in unstructured environments[6], for which reason the properties that *uSkin* and comparable tactile sensors [55] exhibit are often desired in anthropomorphic robot manipulators. Hence, these properties must be considered during the development of a tactile feedback system for teleoperation or human-robot interaction with anthropomorphic robot hands.

[9]https://www.3m.com/

2.2 Development of a Shape Memory Alloy-based Tactile Display Prototype

Chapter 1 reviewed design concepts of SMA-based tactile displays. This section elaborates on the choice of SMA wires as actuators, introduces the first generation of the tactile display module for the experimental testing of the algorithm *end-to-end tactile texture projection* (chapter 3), and discusses mechano-physiological implications of the SMA-based micro-vibrator design.

2.2.1 Design Choice: Shape Memory Alloy-based Actuator

Shape memory alloy (SMA)-based actuators were chosen, because they exhibit the following advantages for a space- and energy-conserving, yet efficient tactile display design:

1. **Space and energy density** Due to the fact that thin SMA wires can be controlled in an open-loop manner using pulsed currents, it is possible to design a compact circuitry with minimal wiring, i.e. only two wires per actuator for establishing the current flow. SMAs provide very high force-to-volume ratios [95], which is necessary for clear stimuli transmission under variable conditions when wearing the device. This enables ergonomic and space-saving design of the wearable device with comparably low weight ($\leq 10g$ per module) and high force-to-weight ratio ($\geq 0.3N/g$) [100], [101]. Noteworthy, when the SMA wire's diameter is doubled, the force output capacity increases by approx. four times while leaving the actuator weight almost unchanged [100] [101].

2. **Durability** Another major advantage is the enormous mechanical durability of SMA-actuators. In fact, nickel-titanium SMA wires can be cycled at approx. 4.8% strain with a $2N$ load for tens of thousands of cycles with no appreciable loss in performance, as reported by Wellman *et al.* [96]. SMAs made of nickel-titanium are regularly deployed in biomedical device development, since this type of alloy is inert. While this particular feature makes them difficult to solder [99], it prevents corrosion and material wear due to mechanical stress, debris, and saline liquids.

3. **Energy consumption** Yet, compared to other micro-actuator technologies, e.g. piezoelectric or magnetostrictive actuators, SMA-based actuators exhibit a low-power consumption while providing much larger displacements for perceptible skin deformation. Mizukami *et al.* [102] claimed that SMA wires could consume as little as $20mW$. Moreover, the usually reported voltage supply that is necessary to drive SMA wire actuators, although dependent on SMA type and dimensions, was between $0.8V$ [102] and $12.6V$ [99].

4. **Frequency bandwidth** Given an electrical current driving circuit, SMAs can generate micro-vibrations from $1Hz$ up to $300Hz$ [102], [99], [100] and therefore cover the most dominant frequency range for human tactile perception [24]. Moreover, SMA vibrators do usually not generate noise due to moving parts, which is a problem with electromagnetic actuators [101].

2.2.2 Concept of the Shape Memory Alloy-based Tactile Display Module

The conceptual idea and the first prototype of the tactile display module are depicted in Fig. 2.4. The WiFi-enabled MCU received the computed driving parameters and the I^2C-address of the targeted PWM driver. Each PWM driver board had an unique I^2C-address and was connected via four connection points to the MCU for I^2C-communication (V_{CC}, SDA, SCL & GND). Since each PWM signal output was associated with one current amplifier and one SMA actuator, all the SMA actuators were independently controlled by only one MCU. Hence, the MCU was operated at low currents and triggered high driving currents from an external power source in accordance with the desired driving patterns. Owing to an internal oscillator in each of the PWM driver boards, the MCU can loop through all the PWM outputs within one control cycle; i.e. the MCU can define synchronized actuation patterns that take effect in subsequent control cycles.

As a result, the tactile display module is highly scalable and modular. One control cycle can be executed at a rate up to $1.6kHz$ with 12-bit resolution, i.e. at a timely resolution of $1.6\mu s$, which is sufficient to cover the frequency range of the cutaneous mechanoreceptors and adheres to the

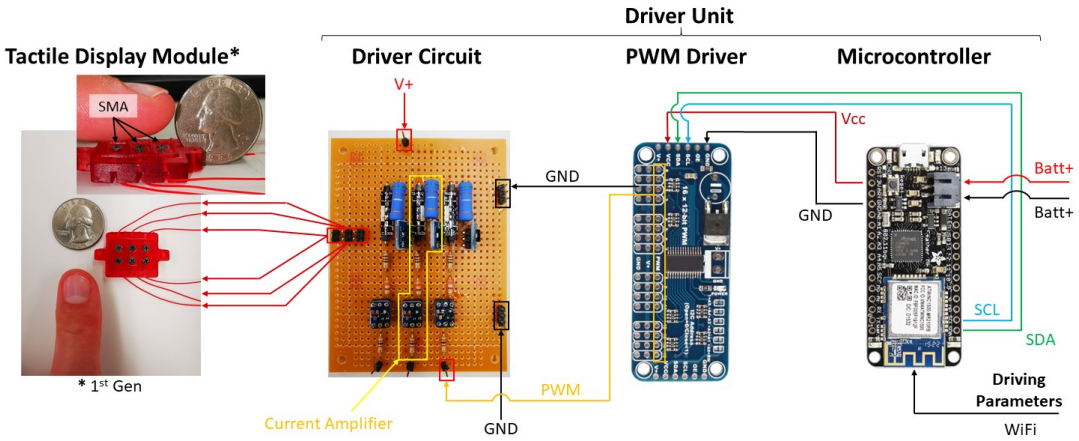

FIGURE 2.4: Concept of the SMA-based tactile display module.

timing specifications that are necessary to generate tactile illusions [33] [34], [35]. Note that the thermal properties of the SMA wire pose a limitation on the maximum achievable actuation frequency.

2.2.3 First Prototype of the Shape Memory Alloy-based Tactile Display Fingertip Module

The tactile display module prototype utilized bare SMA wires to generate micro-vibrations and to project tactile stimuli directly onto the skin [102] [27] [110], Fig. 2.5-A, B. The first prototype implemented three thin SMA wires ($Ø100\mu m$, $L5mm$, $R1.4\Omega$) into a small 3D-printed package and could deflect the skin by up to $10\mu m$ [110].

Connecting the SMA wires to the power supply is challenging and is commonly done by a proprietary soldering equipment. In fact, improper soldering can cause the SMA to lose its shape memory effect. Therefore, the first prototype used threaded steel inserts and M2 screws to fix the SMA wires inside the module and to electrically connect them by soldering AWG28 copper wires to the thread and the connectors of the current driver board.

As mentioned in chapter 1, the two-point-orientation discrimination threshold of the fingertips is around $5mm$ [22]. Accordingly, the actuator array was designed to have a linear alignment with distances of $6.5mm$ between actuators, which was larger than this discrimination limit and enables discretely perceivable signals for the generation of illusory tactile stimuli [33] [34], [35].

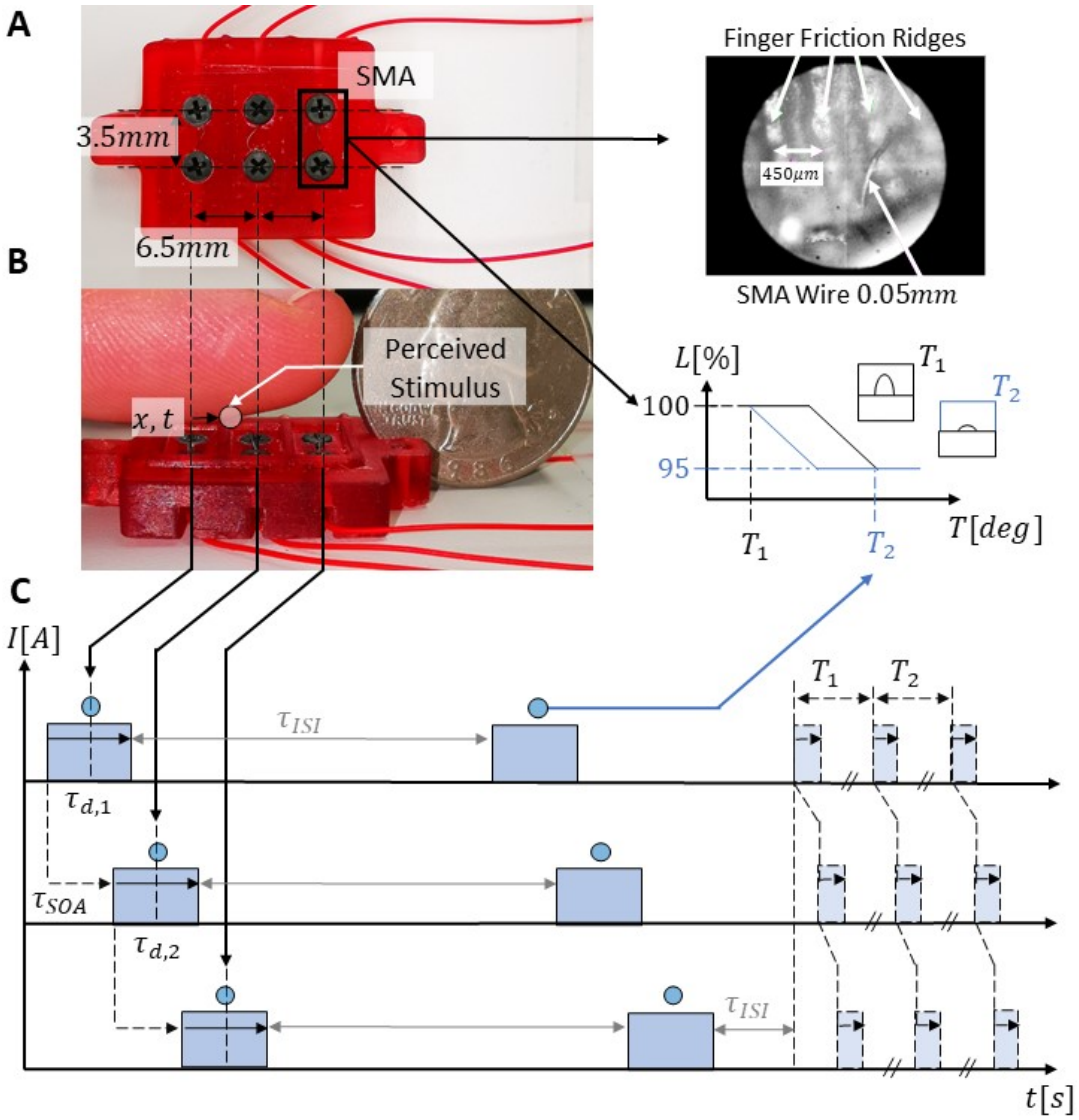

FIGURE 2.5: First generation prototype of the SMA-based tactile display module (A,B) and the PWM signal timing for the generation of tactile illusions (C). Microscopic image adopted from Sawada *et al.* [110].

The alloy composition of the utilized SMA caused the entire wire to shorten around 5% lengthwise when undergoing a temperature-induced phase transition from the Martensite to the Austenite phase. Due to the electrically induced temperature changes, periodic micro-vibrations of up to $300Hz$ could be generated [102] [27] [110]. Thus, the SMA wires could be electrically controlled by periodic current pulses for the presentation of tactile sensations using a PWM control scheme, Fig. 2.5-C.

One pulse had an amplitude of $I[A]$ and a width of $\tau_{d,i}[ms]$. The duty ratio D was calculated by $\tau_{d,i}/T_i$, where T_i was the period of the PWM signal.

The duty ratio controlled the strength of the vibrations and was a critical parameter for the heating/ cooling times of the SMA. Note that no active cooling was implemented, as the skin of the finger pad served as passive heat sink. The electrical power transmitted into a single SMA is equivalent to $I^2[A] \times R[\Omega] \times D$, considering a squared PWM-wave form.

The generation of tactile stimuli strongly depends on the spatio-temporal design of the vibro-tactile actuation patterns (cf. section 1.2.1.1). According to literature studies on the generation of illusory tactile stimuli [20] [38] [28] [21], the control parameters are: stimuli duration $\tau_{d,i}$, the inter-stimulus onset asynchrony (SOA) $\tau_{SOA,i}$ [37], i.e. the time interval between onsets of subsequent actuations, and the inter-stimulus interval (ISI) $\tau_{IOI,i}$ [36], i.e. the time interval between the offset and the onset of subsequent actuations.

2.2.4 Mechano-physiological Considerations on the Design of the Shape Memory Alloy-based Tactile Display Module

Given the design of the SMA-based micro-vibrator, mechanical micro-vibrations up to $300Hz$ [102] [27] [110] can theoretically be generated. Nevertheless, the maximum achievable frequency depends on the wire dimensions and the duration of the pulsed currents (cf. [99] and [101]). Mechanical micro-vibrations of the frequency range between 10 to $300Hz$ are predominantly perceived by the fast-adapting *Meissner* and *Pacinian* corpuscles, as described in section 1.2.1.1.

During the interaction with physical objects, *Meissner* corpuscles sense the rate of skin deformation caused by the slipping of a grasped object or by surface discontinuities and edges moving under the finger [1] [24] [3]. On the other hand, *Pacinian* corpuscles sense high-frequency vibrations caused by transient contacts with an object, as in collisions or during dragging of tools across a textured surface [1] [24] [3]. As the density of *Pacinian* and *Meissner* corpuscles in the finger pad is comparatively high [1] [24] [3], these mechanoreceptors are optimal for the generation of vibro-tactile illusions [2].

Hence, the underlying principle of the presented tactile display module is to resemble the occurrence of different moving textures under the resting finger. In this manner, the location of an object's contact on the finger pad is transmitted by conveying micro-geometric information on the textural properties at specified contact locations. This is majorly important

information for human-machine interaction and teleoperation applications [92] [1] [4].

Static or sustained deflection of the skin, however, are not easily achievable using the current design, because of the required on/off timing to allow for sufficient heat dissipation from the SMA wire into the skin. In this regard, it must be noted that mechanical interaction also includes macro-geometric information perceived by *Merkel* and *Ruffini* nerve endings through mechanical pressure or shear of the finger pad. Even though micro-vibrations carry information on the (moving) contact location and the controlled stimuli generation allows for transmitting this information via repetitive activation of *Meissner* and *Pacinian* mechanoreceptors at the desired location by orchestrating stimuli duration $\tau_{d,i}$ and inter-stimulus onset asynchrony $\tau_{SOA,i}$, the transmission is limited to information that can be encoded by *Meissner* and *Pacinian* corpuscles, which does not cover the entirety of modalities of the human sense of touch [23] [24] [3].

Moreover, *Pacinian* corpuscles have a comparably large receptive field ($\approx 20mm$) and low spatial resolution ($\approx 10mm$), for which reason the perception of the tactile stimulus and its localization might be less precise compared to the other mechanoreceptors (cf. section 1.2.1.1). This issue of discriminability is further compounded by the propagation of vibrations through the skin [32].

The generation of vibro-tactile illusions is an ongoing field of research, because the tactile perception also depends on the higher-level processing of the human brain, which is difficult to account for and might even be modified by experience or by injury [24]. As reviewed in chapter 1, it has been shown that by using effects of human higher-level perception, it is possible to generate more complex tactile sensations by orchestrating the temporal order (AM, [34]) and the relative intensities (PS, [35]) of several spatially distributed tactile stimuli. The knowledge of higher-level perception paradigms might partially alleviate the aforementioned SMA actuator limitations, however, this is still an open research question [20] [38] [28] [31] [41] [21].

An important *a priori* limitation in using SMA-based micro-vibrators is the restriction to a subset of tactile stimuli in accordance with the frequency/ stimuli response of the cutaneous mechanoreceptors. The absence of proprioceptive feedback, i.e. stimuli that inform the brain on dynamic positioning/loading of articulated body segments, is another

limitation that demands the integration of haptic feedback devices into the feedback loop, but is beyond the scope of this thesis [1] [11] [2].

In conclusion, the presented SMA-based tactile display module can stimulate the fast-adapting mechanoreceptors *Meissner* and *Pacini* for tactile feedback, yet does not cover the full range of the *Pacinian* frequency bandwidth of up to $1kHz$. Moreover, due to the mechanical embodiment of the SMA actuator, in which the SMA wire is directly in contact with the skin, long continuous pulses for the generation of shear or sustained pressure are not possible and would cause overheating of the SMA wire. The projection of shear forces due to lateral skin stretch or the conveyance of softness-hardness would require a complementation with other actuators [11] [2] [103] or a different embodiment of the SMA actuator (cf. [100] and [101]).

2.3 Chapter Summary

Chapter 2 presented the system architecture for the experimental design and evaluation of the proposed tactile feedback system: The system architecture involved the anthropomorphic *Allegro* robot hand covered with *uSkin* tactile sensor modules, a host PC running resource-intensive algorithms on the tactile data, a compact WiFi-enabled MCU that controls the computed spatio-temporal actuation patterns, an I^2C-enabled custom-made tactile display driver circuit, and the first generation of a SMA-based tactile display fingertip module.

Additionally, chapter 2 reviewed important design and operational principles to characterize the potential applications and limitations of the tactile feedback system, due to both the tactile skin sensor *uSkin* and the proposed tactile display module. The presented prototype implements three SMA-based micro-vibrators ($Ø100\mu m$, $L5mm$, $R1.4\Omega$) into a 3D-printed package with equidistant linear alignment ($6.5mm$). The SMA actuator has a frequency bandwidth of roughly $10Hz$ to $300Hz$ [102] [27] [110], which covers the full frequency bandwidth of the *Meissner* and the most sensitive frequency range of the *Pacinian* mechanoreceptors [24] [3]. The distances between the micro-vibrators are larger than the two-point-orientation discrimination threshold in the index finger [22] and enables the module to generate micro-vibrations for the realization of illusory tactile stimuli at intermediate finger pad locations [20] [38] [28] [2] [21].

Thus, the employed design concept of the SMA actuator module, in conjunction with the variable PWM-control scheme, relies on the generation of variable spatio-temporal pulse patterns to stimulate the fast-adapting mechanoreceptors and to convey tactile stimuli of textural surface properties at desired contact locations by micro-vibrations. Since the stimuli patterns involve higher-level perceptual effects, thus, partially allow for alleviating the SMA-based actuators' limitations in terms of actuator density and frequency bandwidth, the following chapters must investigate the resulting integrity of the perceived tactile sensations.

Due to the mechanical embodiment of the SMA actuator, in which the SMA wire is directly in contact with the skin, long continuous current pulses are not suitable. The projection of static, macro-geometric information on the skin, which is perceived by the mechanoreceptors *Merkel* and *Ruffini* nerve endings, is therefore not possible. The current SMA actuator design is not capable of projecting the full variety of mechanical tactile stimuli onto the skin. In fact, the projection of softness-hardness due to sustained pressure or the projection of shear due to lateral skin stretch require the complementation with other actuators [11] [2] [103] or a different embodiment of the SMA wire [100] [101]. This is assumed feasible, due to the extremely compact form factor and low energy consumption of SMA materials.

Chapter 3

End-to-end Tactile Texture Projection with Psychophysically-meaningful Latent Space Encodings

3.1 Problem Formulation and Solution Concept

3.1.1 Problem Formulation

As described in section 1.2.2.1, tactile sensor modules for the implementation into robots are designed to carry a large number of distributed sensing points for high-resolving tactile feedback and to be compliant for increased stability during manipulation tasks and safety reasons [6] [48] [46] [44] [47]. The tactile feedback from tactile sensor data that projects micro-geometric surface properties or generally micro-vibrations during the operation of a robot that actively engages with arbitrary contact surfaces carries important information about the robot's interaction with its environment [92] [72] [4] [5].

As this feedback on the contact state is a physical information modality inherent to the human sense of touch, its transmission is required during human-robot interaction and robot teleoperation. The transformation of the tactile sensor data from soft, distributed tactile sensor modules to a tactile display control signal that generates physiologically meaningful tactile stimulation for the transmission of this feedback by a tactile display with only few tactile actuators is, however, an open technical challenge.

3.1.2 Solution Concept

This chapter addresses the implementation of an end-to-end transformation from tactile sensor data to tactile display control signals to enable the generation of convincing tactile stimuli in accordance with the tactile input data for emulating micro-geometric surface properties by means of micro-vibrations. As outlined in section 1.3, the actuator control is defined such that it allows for the generation of illusory tactile sensations by means of the tactile display module prototype from chapter 2 with sparsely distributed SMA-based micro-vibrators. The algorithm *end-to-end tactile texture projection* deploys an auto-encoder approach, specifically a deep gated recurrent unit-based autoencoder (GRU-AE), to encode the perceptual dimensions of tactile textures in latent space coordinates that coincide with the psychophysical layer of human material perception.

This compact auto-compression of raw tactile sensor data enables an end-to-end projection from tactile sensor data to tactile actuator control signal by modulating the free parameters of a control signal in accordance with the latent space encodings of the tactile sensor raw data. The algorithm does not depend on any specific hardware: Since the retrieved tactile sensor data is encoded into perceptual coordinates of a psychophysically meaningful latent space, it allows for the control of any tactile actuator as long as the relation between a desired stimulus and the respective driving parameterization is sufficiently known. Given the presented hardware in chapter 2, this chapter focuses on the generation of tactile illusory sensations to transport textural surface properties by means of sparsely distributed tactile displays that implement vibro-tactile actuators.

3.1.3 Chapter Organization

This chapter is organized as follows: in section 3.2, the theory behind the psychophysical layer of human material perception, its importance for texture recognition, and its relation to the auto-compression of tactile sensor data are briefly explained. Section 3.3 elaborates on the proposed end-to-end tactile feedback loop for the projection of tactile sensor data into tactile actuator driving signals to emulate textural surface properties by means of vibro-tactile actuation patterns. Next, section 3.4 describes the experiments and user studies that were conducted to verify the proposed approach by deploying the GRU-encoder to control the first prototype of the

custom-made SMA-based tactile display module (refer to chapter 2) for the generation of micro-vibrations to emulate textural properties in accordance with the tactile sensor data. Then, section 3.5 reports and discusses the results. Finally, section 3.6 draws conclusion on the main findings and summarizes major limitations of the presented algorithm for end-to-end tactile texture projection.

3.2 Psychophysical Material Perception in Latent Space Coordinates

From previous literature studies [24] [111] on material perception, it is known that the sense of touch consists of several hierarchical layers, Fig. 3.1-A. While the upper layers increasingly involve individual judgement on the material properties, the psychophysical layer is defined as the primal layer of material perception in response to direct physical stimuli. This layer describes the human-perceivable properties of surfaces in terms of mutually independent physical quantities. They are therefore called psychophysical dimensions and numerically describe a material in terms of its hardness, temperature, friction, and roughness, Fig. 3.1-B. User responses on the evaluation of material probes, specifically their respective psychophysical property profile are therefore sets of ratings in these dimensions, Fig. 3.1-C. User evaluations on real texture probes were regarded as a common ground truth against which the performance of the tactile feedback loop was quantitatively measured during the user studies.

Given the definition of the psychophysical layer as the primal layer of material perception, a subset of only four fundamental physical properties that are sensed by the human cutaneous mechanoreceptors enable the perception of various surface properties. Therefore, it was assumed that the previously presented deep GRU-classifier [105] can be modified to auto-compress raw tactile sensor data into a latent space $\mathbf{Z}$ that encodes the most relevant tactile features for the discrimination of surface properties. Even though the auto-compression into latent space depends on the specific tactile sensor hardware, e.g the sensor's sensitivity, frequency response, and surface properties, the compressed representation of the tactile sensor data must allow for correlation with the psychophysical space, because the relevant tactile information are physical properties inherent to the material.

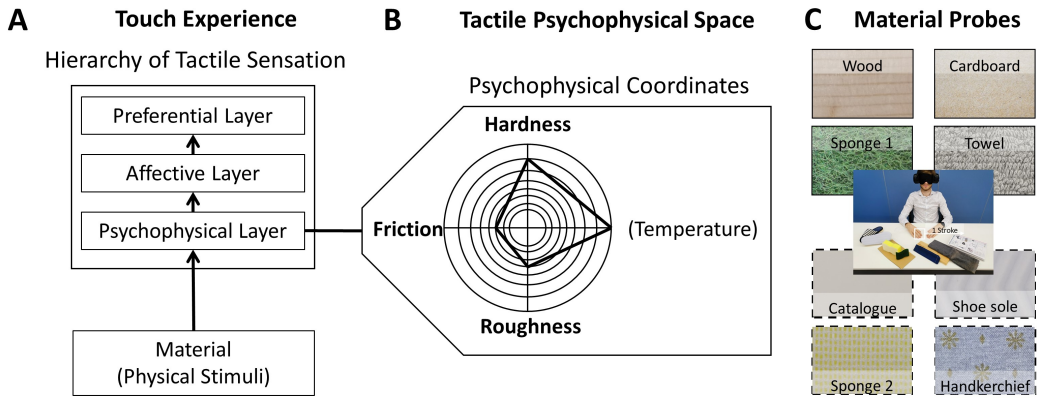

FIGURE 3.1: Layers of material perception [111] [50] (A), the definition of the psychophysical layer with its dimensions *Hardness*, *Temperature*, *Roughness*, *Friction*, and the material probes used for the experimental studies (C). Pictures are adopted from Geier *et al.* [112].

3.3 Control Scheme for End-to-end Tactile Texture Projection with Psychophysically-meaningful Latent Space Encodings

The control scheme aims at the end-to-end projection of the tactile input data into a tactile display control signal and allows for the generation of tactile stimuli that emulate textural properties of contact surfaces by means of sparse arrays of micro-vibrators. The concept of the end-to-end control of haptic or tactile devices by means of latent space encodings of tactile input data is, however, applicable to a broad set of tactile sensor - tactile actuator combinations.

Briefly, the tactile hardware comprised the *uSkin* tactile sensor module and the first prototype of the tactile display module with three sparsely distributed SMA-based micro-vibrators (cf. chapter 2). Furthermore, a deep GRU-AE [112] was deployed for the encoding of the tactile time-series data into latent space coordinates. The encoded tactile data was used for the parameterization of a control trial function. Given a meaningful relation between the latent space encodings and the free parameters of the control trial function, the tactile display can be driven in accordance with the tactile sensor raw input data.

The tactile sensor data was gathered during the active tactile texture exploration of several representative material probes with mutually

different surface properties [105]. This auto-compression of the raw tactile sensor data (Fig. 3.2-A) into coordinates of a latent space encoding $\boldsymbol{Z}$ was used to modulate the activation functions $\boldsymbol{A}$ by adjusting their free parameters in control space $\boldsymbol{C}$. As a result, the tactile display module generated micro-vibrations for the emulation of various textural surface properties from the tactile sensor data. A flow chart of the complete control scheme is depicted in Fig. 3.2. Note, the temperature dimension is not further considered, since the *uSkin* tactile sensor does not allow for determining heat fluxes.

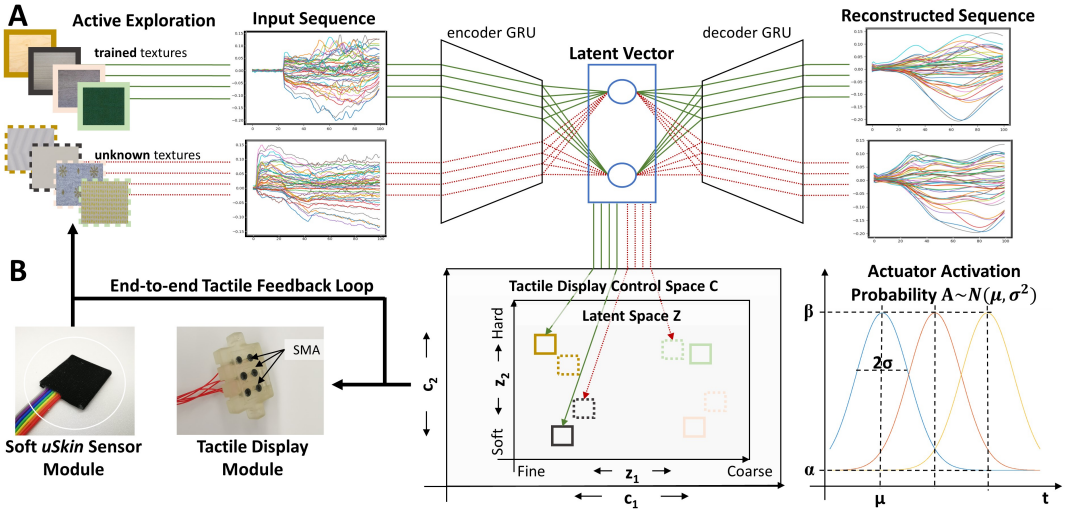

FIGURE 3.2: A deep GRU-based autoencoder was deployed to obtain an implicit representation of the *uSkin* tactile sensor data in latent space (A). The latent space variables $\boldsymbol{Z}$ were used to find the free parameters $\boldsymbol{C}$ that allow the controlled activation $\boldsymbol{A}$ of a SMA-based tactile display module (B). Pictures adopted from Geier *et al.* [112].

3.3.1 Gated Recurrent Unit-based Auto-compression for Implicit Tactile Texture Recognition

The GRU-AE addresses two major challenges: First, as reviewed in chapter 1, tactile sensors for the deployment to (anthropomorphic) robots [58] [66] [63], robot hands [50] [64] [44], and grippers [55] [46] are often soft or covered with compliant material to facilitate grasping and in-hand manipulation [58] [6] [10]. Specifically, the *uSkin* tactile sensor module is covered with a soft silicon layer which acts as a lowpass filter. Additionally, gripping tape covers the silicon layer to protect the silicone structure and to

increase the friction coefficient to facilitate in-hand manipulation. These layers of soft material limit the ability to sense fine vibrations and micro-geometric object features, which makes their direct extraction, or respectively sensing, for texture recognition difficult.

It was demonstrated, however, that the time-series tactile data may contain sufficient information for the discrimination of textural surface properties [72] [105]. By deploying a deep gated recurrent unit (GRU)-recurrent neural network, optimal filter banks that recognize abstract temporal features and thus allow for accurate texture recognition could be learned, as it has been shown in a preliminary study on active tactile texture multi-class classification [105].

Second, the network architecture of the GRU-AE implemented a bottleneck layer to perform a non-linear compression of the tactile input data into continuous latent space $\boldsymbol{Z}$. Precisely, the GRU-encoder comprised three stacked GRU layers each of which had 96 units to express the increasingly abstract temporal features of the tactile data as latent space encoding. The GRU-AE's encoder architecture resembled the aforementioned deep GRU-classifier presented in [105]. In contrast to the GRU-classifier that implemented the final dense-layer with soft-max activation for multi-class classification between only a limited number of textures, it implemented a GRU bottleneck layer with only three output units in order to compress the temporal feature sequences into an encoding in the latent space $Z \in \mathbb{R}^3$. Note that due to failure of one sensor element inside the module, the input feature number was $N_F = 45$.

In regard to the properties of the psychophysical layer (cf. section 3.2), the implicit representation of the tactile sensor data in latent space coordinates yields the potential to recognize and resemble an infinite number of texture property profiles, or micro-vibration patterns.

Although the use of the deep GRU-AE alleviates the aforementioned limitations of the *uSkin* tactile sensor to a certain extent, it is important to note that the lost information due to, e.g., a limited frequency response or sensitivity will generally limit the discrimination capacity of the overall system. The GRU units were implemented in their original version acc. to Cho *et al.* [113]. The GRU-AE architecture is depicted in Table 3.1.

The network's free parameters were optimized using Adam [114]. The learning rate was set to α=10^{-5}, the exponential decay rate for the first moment estimates to β_1=0.900, the exponential decay rate for the second

TABLE 3.1: Gated-Recurrent-Unit Autoencoder (GRU-AE) Architecture [112].

Layer	Type	Output Shape	Units	Remarks
0	Input	(_, _, 45)	/	
1	GRU	(_, _, 96)	96	returns tactile sequence
2	GRU	(_, _, 96)	96	returns tactile sequence
3	GRU	(_, _, 96)	96	returns tactile sequence
Encoding	GRU	(_, 3)	3	latent vector **z**
4	Repeat	(_, 100, 3)		
5	GRU	(_, 100, 3)	3	returns tactile sequence
6	GRU	(_, 100, 96)	96	returns tactile sequence
7	GRU	(_, 100, 96)	96	returns tactile sequence
8	GRU	(_, 100, 96)	96	returns tactile sequence
9	Dense	(_, 100, 45)	45	Linear Activation
Size: 299,106 trainable parameters.				

moment estimates to β_2=0.999, and the decay to δ= 0.0. The *mean squared error* between sequences of measured raw sensor data and their reconstructed counterpart served as loss function. Due to the low dimension of Z, explicit regularization was not implemented as the GRU-AE acted as undercomplete autoencoder.

As reported by the preliminary study on the GRU-classifier, the trained network was capable of accurately discriminating between a set of four objects of daily living with mutually different texture profile: a polishing *sponge1*, a cotton *towel*, a board of *wood*, and a piece of *cardboard*, Fig. 3.1-C. Therefore, the GRU-AE's encoder was assumed to find conclusive latent space encodings that would allow for driving the tactile display prototype by controlling the micro-vibrator activations $\boldsymbol{A}$ in accordance with the latent space encodings $\boldsymbol{Z}$.

Another four textures that were different from the training set, however, also exhibiting mutually different texture profiles were selected to validate the GRU-encoders ability to encode previously unseen texture samples: a softer *sponge2*, a *handkerchief*, a *catalogue* back cover, and a *shoe sole*. Note that this second set of texture probes was excluded from training and exclusively used for validation purposes.

Finally, the latent space encodings of the raw tactile data that was recorded during active tactile texture exploration of the entire sets of texture probes were compared to their psychophysical property profiles that were determined during a user studies.

3.3.2 Tactile Display Control with Psychophysically-meaningful Latent Space Encodings

As explained in chapter 2, the tactile display module deployed in the following experiments carries three linearly-arranged SMA-based micro-vibrators with mutual actuator distances of $6.5mm$, which is larger than the two-point-orientation threshold as defined by Tong and co-workers [22].

By choosing proper activation functions $A_n(t < T)$ [102] [27] that control the succession of activation and deactivation and thus the stimulus onset duration τ_d and inter-stimulus onset asynchrony τ_{SOA} across all the micro-vibrators, phantom tactile sensations [35] and apparent tactile movements [34] are combined to eventually trigger perceptions of moving textures with varying surface properties under the resting finger pad.

As a result, the stimuli control scheme enables the repetitive, vibratory stimulation of *Meissner* and *Pacinian* mechanoreceptors at the desired locations and allows for transmitting information on micro-geometric object properties by emulating generic textural surface properties.

The activation functions $A_n(t < T)$ are given by *Gaussian* trial functions defining the activation probabilities as normal distributions over a time interval T:

$$A_n(t < T) = \alpha + \beta e^{-(t-\mu)^2 / 2\sigma^2} \text{ for } n \in 1, ..., N_A, \tag{3.1}$$

where t is the time in ms, μ is the mean in ms, σ^2 is the variance in ms^2, α is the offset, β is the gain, and N_A is the total number of available actuators. Note that α and β are constants; moreover, $\alpha + \beta < 1$ must hold.

The micro-vibrators are arranged alongside a straight line with relative distances of $6.5mm$ for which reason μ_n and σ_n control the spatio-temporal density of the micro-vibrations. f_{PWM}, however, directly controls the frequency of the micro-vibrations. Hence, by defining the parameters μ_n, σ_n, and f_{PWM} in dependence on the target texture, the occurrence of pulsed current signals, thus, the occurrence of vibro-tactile stimuli is controlled such that the higher-level phantom tactile sensation and apparent tactile movement cause the perception of moving contact surfaces with varying textural properties.

Based on the results of prior user studies [102] [27] on the transmission of textural properties by means of SMA-based micro-vibrators, interval limits

of the control parameters $c_1 \in [\underline{\mu}, \overline{\mu}]$, $c_2 \in [\underline{\sigma}, \overline{\sigma}]$, and $c_3 \in [\underline{f}_{PWM}, \overline{f}_{PWM}]$ were assumed. Furthermore, a linear relation of a control parameter $c_i \in [\underline{c}_i, \overline{c}_i]$ to a coordinate of a latent space encoding $z_j \in [\underline{z}_j, \overline{z}_j]$ was assumed. Thus, the control parameters of the actuator driving signal $A_n(t < T)$ that enable the emulation of a desired textural property were obtained by

$$c_i = \frac{\underline{c}_i - \overline{c}_i}{\underline{z}_j - \overline{z}_j}(z_j - \overline{z}_j) + \overline{c}_i. \tag{3.2}$$

3.4 Experiments and User Studies

3.4.1 Data Acquisition and Training

To resemble the active exploration of arbitrary objects by a robotic manipulator, the tactile input data required for the training of the GRU-AE was collected using a flat *uSkin* tactile sensor module that was comparable to the modules implemented onto the *Allegro* robot hand (cf. chapter 2). The surfaces of two sets of four objects with mutually different surface properties (cf. section 3.2) was explored once at a time by moving the sensor module across the surface. The manual exploration resembled a linear motion pattern across the object surfaces.

The time limit of the data recording was set to T=2s, which comprised the complete motion pattern from initial impact on the object surface to the actual stroking motion across the surface. The GRU-AE was trained exclusively on the first set of textures: *sponge1*, *towel*, *wood*, and *cardboard*, depicted on the left-hand side in Fig. 3.3-A. Each of these four textures was explored 20 times and the tactile sensor data was recorded over 200 time steps. The second set of textures, depicted on the right-hand side in Fig. 3.3-A, were probed in the same manner, however, used for evaluation purposes only.

The input features to the GRU-AE, i.e., the x, y, z-tactile sensor raw readouts were scaled using their respective minimum and maximum values. The sequences of the tactile input data, which were fed to the GRU-AE and therefore had an impact on the real-time applicability, were chosen to have a length of S_L=100 and were offset with the negative of their initial values. The sequence length S_L=100 corresponded to a time window of approximately 1s real-time considering the *uSkin* tactile sensor's sampling frequency of approximately 100Hz. Given that the evaluation of textural surface properties by humans - solely from tactile feedback - is in

fact a challenging task, the time window of 1s should balance the requirements of a responsive texture recognition and sufficient data for the GRU-AE to compute the correct latent space encoding. Moreover, the training was conducted deploying a sliding window approach, which is beneficial during online deployment of the GRU-AE in conjunction with the tactile display. The dataset was partitioned into training (6335 sequences), test (1188 sequences), and cross-validation set (397 sequences). During the design process of the GRU-AE, the performance was evaluated in terms of the *mean squared error* signal between input and reconstructed sequences of test and cross-validation set.

The GRU-AE was implemented in KERAS[1] with Tensorflow[2] backend. The implicit texture recognition by the GRU-AE was run on the host machine: Intel(R) Core(TM) i7-8700K CPU @ 3.70GHz and 32.0GB RAM, GeForce GTX 1080 Ti with 11 GB frame buffer. The training comprised 500 epochs with a batch size of one.

3.4.2 User Study I

The first user study aimed at the quantification of the true psychophysical coordinates of the above-defined texture probes. Accordingly, the first user study required the subjects to actively touch the real texture probes and rate their property profile in terms of the aforementioned psychophysical coordinates. These user ratings of the psychophysical property profile served as a common ground truth, i.e., an objective numeric reference against which the performance of the end-to-end tactile texture projection for the emulation of textural property profiles was quantitatively measured.

Four healthy subjects (one female, three males, mean age 28.25yrs) were asked to stroke across the texture probe surfaces of all the objects mentioned in section 3.2 in a natural, linear motion as depicted in Fig. 3.3-A. To prevent any impact from auditory and visual sensory channels on the evaluation of the psychophysical property profile, all subjects were blindfolded and wearing soundproof earmuffs. At the end of each trial, the subjects were asked to rate the psychophysical property profile in a questionnaire with integer numbers ranging from 1 to 6, where 1 or 6 equaled, e.g., very smooth or very rough, respectively. Only one texture probe at a time was presented

[1] https://keras.io/
[2] https://www.tensorflow.org/

and all probes were shown in a random order for three times. The texture probe was removed before evaluation and previous evaluations were made unavailable to reduce the training effect.

During an introductory session before the user study, the participants were explained the meaning of the quantities *hardness*, *roughness*, and *friction*. Furthermore, before the very first trial, the subjects were presented pairs of texture probes exhibiting a very soft/ hard, a very rough/ smooth, and a very high/low-friction psychophysical property profile to ensure that even initial ratings during the actual user studies covered the full range of possible ratings.

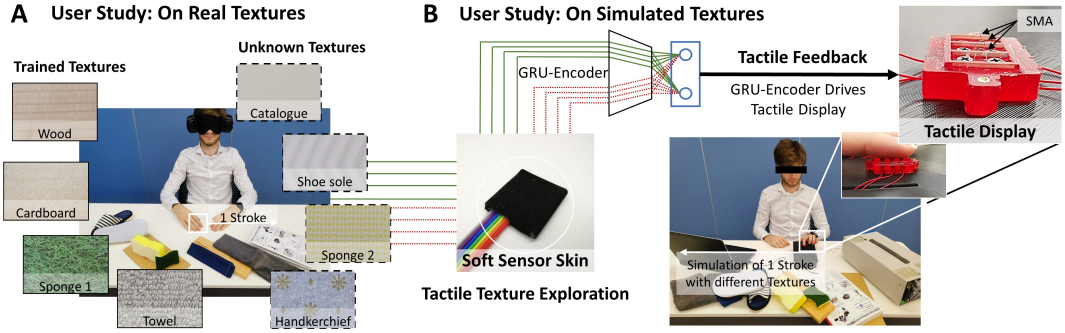

FIGURE 3.3: Experimental setup for the evaluation of the psychophysical property profile of the texture probes (A) and the proposed end-to-end tactile texture projection (B). Pictures adopted from Geier *et al.* [112].

3.4.3 User Study II

The second user study was identical to the first user study, however, the target psychophysical property profile was generated by the proposed end-to-end tactile texture projection algorithm. Thus, the second user study included the implementation of the above introduced control scheme (cf. section 3.3) and the tactile display module prototype from chapter 2, Fig. 3.3-B.

The subjects were instructed to rest their index finger on top of the tactile display module. Then, one target texture was chosen randomly from the cross-validation set (cf. Fig. 3.3, trained textures) or the unseen texture probes (cf. Fig. 3.3, unknown textures), upon which the corresponding raw data was propagated through the end-to-end tactile texture projection algorithm.

Similar to the first user study, the subjects were asked to rate the perceived property profile in terms of psychophysical coordinates.

However, the textures were emulated by the tactile display prototype that was controlled by the proposed end-to-end tactile texture projection algorithm, thus, generated micro-vibrations in accordance with the raw tactile sensor data that was collected during the active tactile exploration of the respective texture probe.

Finally, these user ratings were compared against the ratings of the real texture probes to draw conclusion on the performance of the end-to-end tactile texture projection. *Mann-Whitney-U* tests were performed on evaluation pairs of real and emulated textures. Statistically significant discrepancies between real and emulated tactile ratings were labelled accordingly.

3.5 Results and Discussion

3.5.1 Textures and their Psychophysical Property Profile

The user evaluations on the perceived psychophysical property profile are depicted in Fig. 3.4. Since the psychophysical property profile was measured in terms of user ratings and is therefore ordinal data, all results are shown as box plots.

The user evaluations exhibited a high to very high range indicating the increased difficulty of determining textural properties solely from a short stroke across an object's surface. This is in line with a previous study by Fukuyama *et al.* who investigated the explicit recognition of similar texture probes by human subjects [27]. A detailed analysis on individual user responses showed that the intra-subject evaluations for one texture over all the trials were relatively constant, i.e. deviations were typically within 1 rating. However, the inter-subject evaluations varied largely for which reason the results exhibited such a high variance. While the dimension hardness was rated rather consistently, the dimensions roughness and friction were rated less consistently between trials and subjects with friction having the largest variance among all the dimensions.

Friction is perceived as a quantity that relates to the counteracting force and the dynamic shear deformations that occur during finger motion. Friction thus depends on the sticky-slippery or the moist-dry factor levels of the skin in contact with an object [24]. Hence, particularly the subjects' individual moist-dry factor levels of the finger pad skin could have had an

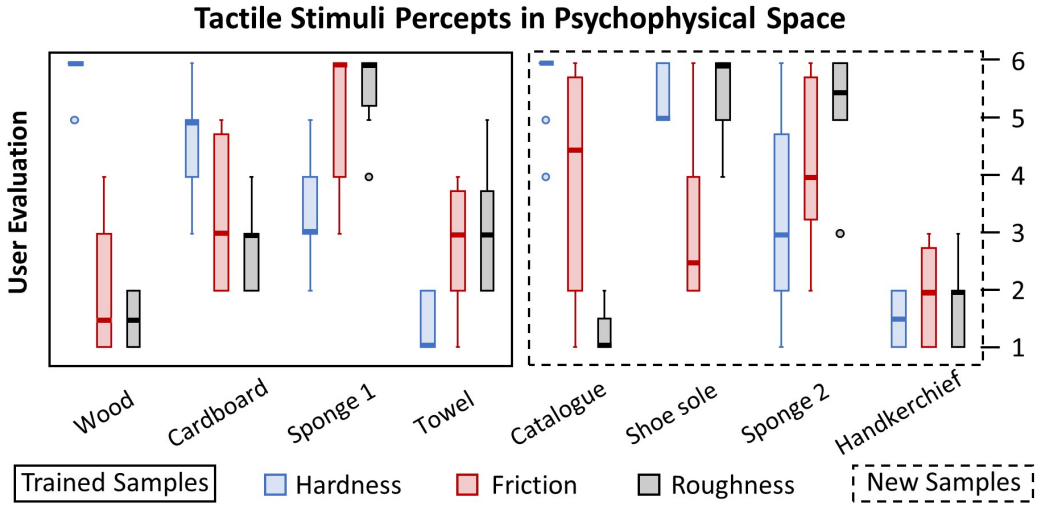

FIGURE 3.4: Results of the first user study showing the psychophysical property profile of all the texture probes. The median is depicted as bold horizontal bar, outliers are depicted as circles. Pictures adopted from Geier *et al.* [112]

impact on the perceived friction thereby causing the high inter-subject variances in the user evaluations.

Besides the high variance of the ratings for friction and roughness, both dimensions were frequently rated equal for one type of texture probe. Even though friction and roughness are independent psychophysical properties, these two dimensions are often thought of related [24]. In view of this fact, roughness seemed to have an impact on the perceived friction level as it likewise counteracts the finger motion. This effect may have contributed to the higher variance of the user evaluations of both the dimensions.

As it regards the textural property profile, the first set of texture probes that was used for the training of the GRU-AE featured enough variety for assessing the plausibility of the encodings in terms of the psychophysical properties. Considering the severe restriction on the reconstruction of the original sequence of tactile sensor input data from the low dimensional latent space as was imposed by the GRU-AE's bottleneck layer, it was assumed that the GRU-encoder was forced to learn a conclusive and physically meaningful representation of the tactile sensor data that coincided with the psychophysical property profile. Regarding the second set of texture probes, the textural property profile ratings were different enough from the first set and should allow for evaluating the generalization capabilities of the GRU-AE.

It would have been desirable, however, to sample the psychophysical

space systematically and exhaustively, e.g., by either increasing the number of texture probes until the space that is spanned by the psychophysical properties is saturated with user ratings or the direct metrological measurement of the psychophysical coordinates. Yet the set of psychophysical coordinates of a texture probe, if quantified in terms of user ratings, relies on subjective perception exhibiting a considerable variance. In regard to the evaluation of the tactile display, which eventually must involve user studies, the direct metrological evaluation can merely be a supplemental evaluation, because tactile perception is subjective.

3.5.2 Relation between Latent and Psychophysical Space

Fig. 3.5-A shows the latent space encodings of the tactile data of all the texture probes in comparison to the user ratings of the psychophysical property profiles (cf. Fig. 3.5-B). Regarding the hardness, the z_2-coordinates of the encodings coincided with the respective user ratings of the perceived hardness, i.e., the latent space encodings were in line with the reported median user percepts of the respective texture probe's hardness. Similarly, yet less consistently, the tactile sensor data of texture probes that received high user ratings in terms of the combined roughness and friction were encoded alongside the z_1-axis towards the right end of the latent space.

Fig. 3.5-A shows that all the latent space encodings had rather high variances, which most likely was due to the variances in the stroking patterns when collecting the tactile sensor data. As the stroking motion had an impact on the location of the encoding, the resulting actuator driving signal is likewise affected by the stroking motion. As it concerns the roughness, this effect seemed to be in line with observations that higher speeds of the explorative motion of the finger cause higher vibration frequencies resulting in a change of the perceived surface roughness [24], however, needs further experimental validation. As it concerns the hardness, the high variances alongside the z_2-axis may have been due to the dynamic contact when engaging with the texture probe, i.e., harder materials (cf. *wood*) exhibiting higher variances due to the quickly increasing reaction forces upon contact in contrast to softer materials being deformed (cf. *sponge1*).

The z_1, z_2-coordinates of the latent space encodings of the second set of texture probes, which were excluded from the training of the GRU-AE, were

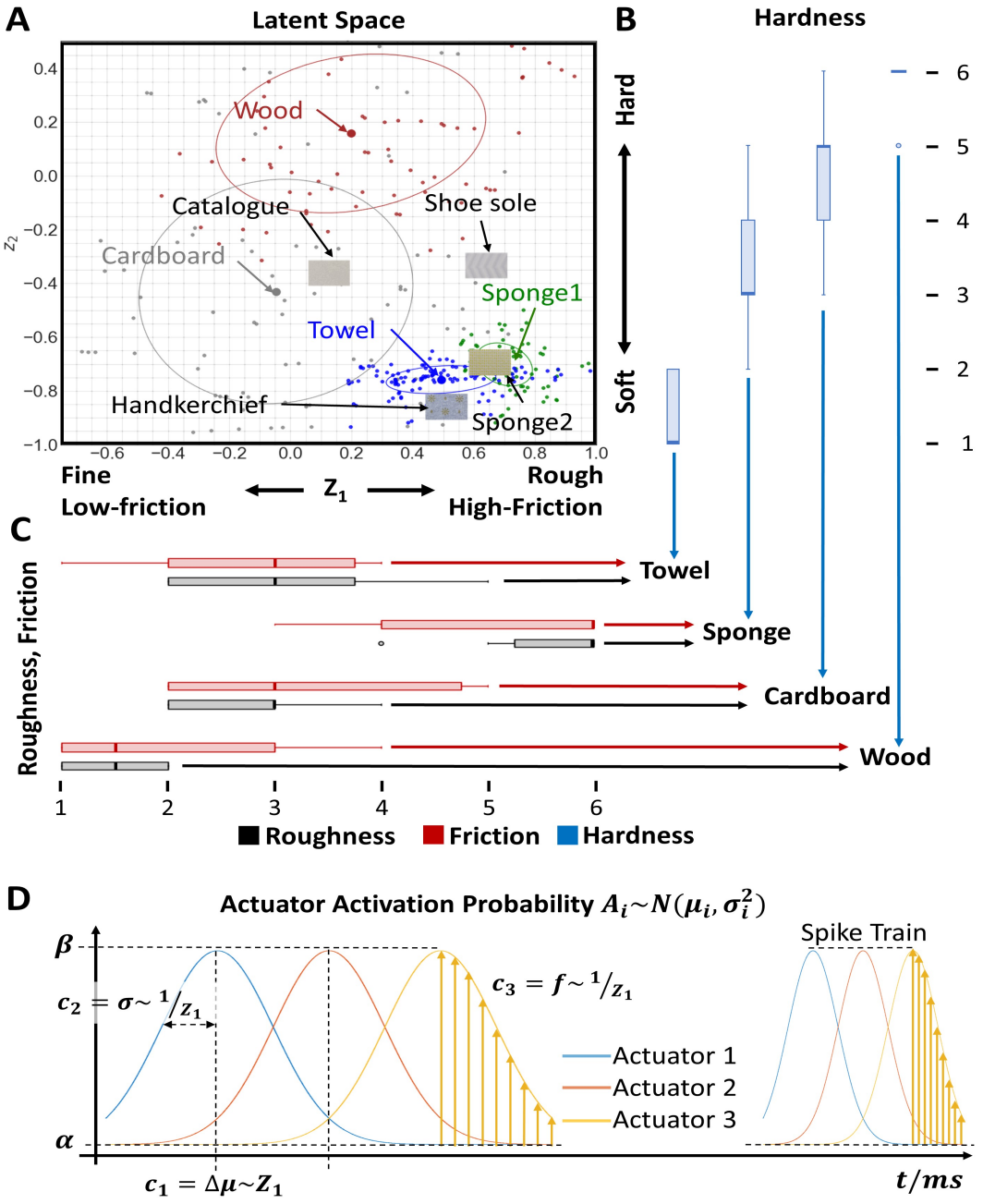

FIGURE 3.5: Shown are the latent space encodings after auto-compression by the trained GRU-AE (A), ellipses are 1σ-confidence ellipses. Additionally, the user ratings of the perceived psychophysical property profile are shown in relation to the latent space encodings (B) and (C). The latent space coordinate z_1 was selected to parameterize the actuator driving signal for tactile display control (D). Pictures adopted and modified from Geier *et al.* [112].

generally meaningful. Their respective location in latent space was in agreement to the locations of the first set of texture probes and their

respective psychophysical property ratings. For example, the z_2-coordinates of the probes *catalogue* and *shoe sole*, which were assumed to encode the hardness of these probes, were located between the z_2-coordinates of the probes *wood* and *cardboard*. The location of these encodings in the latent space were in agreement with the user-rated hardness and in meaningful relation to the encodings of the trained texture probes.

Similarly, the auto-compressed tactile data of the texture probes *catalogue*, *shoe sole*, and *sponge2* were encoded in agreement with the user-rated property profile and in agreement with the encodings of the trained textures. For example, the roughness of *shoe sole* was rated similarly to the roughness of *sponge1* and their z_1-coordinates coincided very well. Yet, *sponge1* received a much lower hardness rating which is in agreement with its comparatively lower z_2-coordinate.

Discrepancies were found for the encoding of the texture probe *handkerchief*, as the z_1-coordinate indicated a rather high surface friction or roughness. This is in contrast to the user-rated property profile of this texture probe. During the course of the experiments it was noted that the material pairing of the *handkerchief* and the *uSkin* sensor module's gripping tape exhibited an extremely high friction, which made the probing of this surface with the *uSkin* module very difficult. In contrast, the subjects could slide their fingers with ease across the *handkerchief*'s surface, for which reason it was rated as being smooth and having low friction. Consequently, the discrepancy between the mutual material pairings of finger pad skin, *uSkin* sensor module, and *handkerchief* negatively affected the latent space encoding, which inherently affects the emulation of the psychophysical properties of *handkerchief* by the proposed algorithm and the tactile display module in a negative manner.

Moreover, it must be noted that the correlation of the latent space encoding and the user-rated psychophysical property profile of a specific texture probe was not enforced, as it was assumed that the latent space describes the minimum feature space necessary to discriminate between textures and therefore naturally coincided with the physical properties of a texture's surface. It would be more desirable, however, to ensure the coincidence of the psychophysical property rating and the latent space encoding, e.g., by adopting the compounded loss function of variational autoencoders.

As it regards the tactile display control, the latent space encodings

alongside the z_1-axis were used to modify the parameters μ, σ, and f_{PWM} of the actuator activation function $A_n(t < T)$ in equation (3.1), i.e. were selected to control the friction and roughness of an emulated texture (Fig. 3.5-D). This allowed for driving the tactile display in accordance with the tactile sensor input data by, first, encoding a sequence of tactile sensor readings alongside the z_1-axis in latent space coordinates and, second, by computing the activation probabilities of the tactile display actuators via substituting the modulated control parameters μ, σ, and f_{PWM} into equation (3.1). Note, the dimension hardness was not considered further, because it requires the combination with proprioceptive feedback loops.

3.5.3 Evaluation of the End-to-end Tactile Texture Projection

Fig. 3.6 shows the ratings of the perceived psychophysical properties for the dimensions roughness and friction. The ratings of the emulated psychophysical properties as generated by the end-to-end tactile texture projection are depicted in comparison to the ratings of the real texture probes.

While the ratings exhibited rather large variances, the proposed approach on the end-to-end projection of textural properties seemed to generate meaningful tactile sensations in agreement with the corresponding real texture for both the sets of texture probes. The median ratings of the perceived psychophysical coordinates in response to the stimulation by the tactile display were roughly similar to the median ratings of the actual texture probe.

Particularly the emulated stimuli of textures that exhibited distinct physical properties, e.g. *sponge2*, were perceived in accordance with their real counterpart. Generally, the large variances in the results indicate the need for a larger cohort of subjects. Since the proposed approach focused solely on the cutaneous feedback without complementing kinesthetic feedback, a more extensive training of the subjects on the tactile display feedback would likely improve the discrimination ability.

However, the absence of important modalities of cutaneous feedback, specifically dynamic skin shear, and the absence of proprioceptive feedback generally limit the ability to project some physical quantities. For example, the driving signal for the emulation of friction, i.e. the resistance counteracting the finger motion when stroking across a surface, was

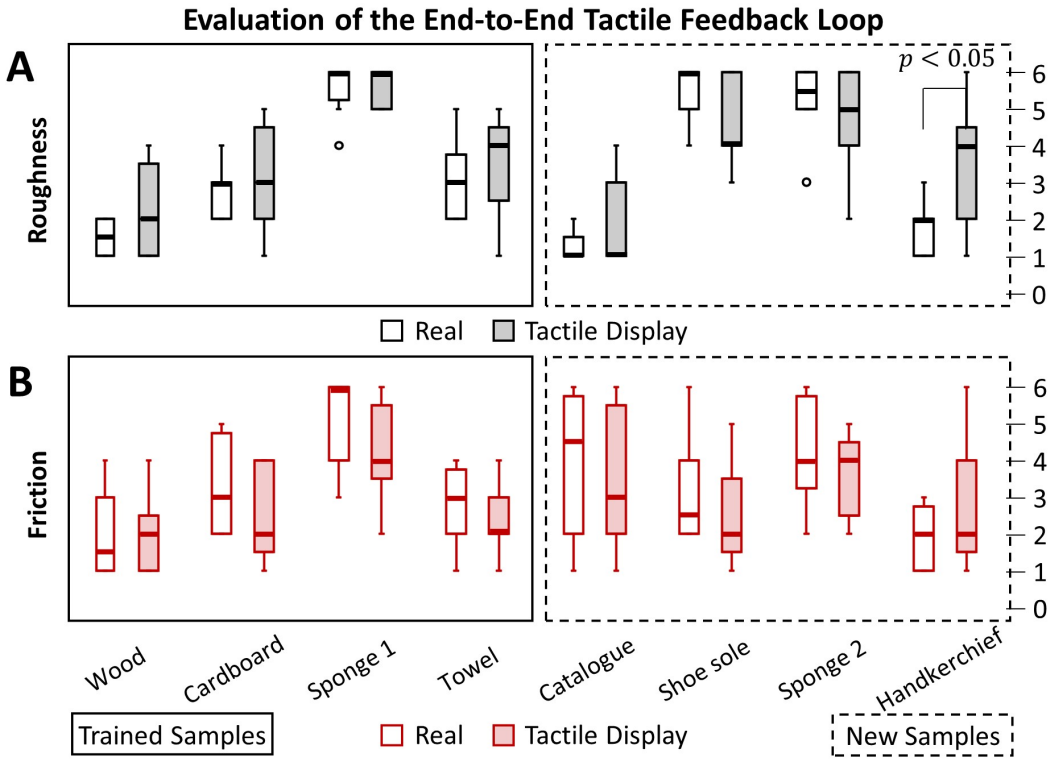

FIGURE 3.6: Evaluation of the end-to-end tactile texture projection for the psychophysical dimensions roughness (A) and friction (B). Note, a p-value<0.05 indicates a statistically significant difference (Mann-Whitney-U test). Pictures adopted from Geier *et al.* [112]

modulated by the relative difference $\Delta\mu$ (cf Fig. 3.5-D), which equaled a lower emulated speed of the moving texture and must be therefore regarded as mere surrogate for this physical quantity.

Moreover, the ranges of the user ratings were comparatively larger in the *Tactile Display*-group, Fig. 3.6-A. These higher ranges may indicate that the users experienced greater difficulty to rate the emulated textural properties in comparison to the actual textures.

A large disagreement was found between the *Real*- and the *Tactile Display*-group for the rating of the roughness and friction of the texture *handkerchief*: The stimuli resulting from the end-to-end tactile texture projection were often rated higher, i.e. exhibiting a higher roughness and friction. In regard to the above discussed influence of the relative material pairings (Fig. 3.5-A), this issue was most likely caused by the GRU-AE that encoded the tactile data of the *handkerchief* probe incorrectly, i.e. towards the far right in latent space causing the emulation of a rough texture. Since

roughness and friction are jointly encoded by the z_1-coordinate, this disagreement might have been caused by the comparably higher friction coefficient between the *uSkin* sensor gripper tape and the fabric of the *handkerchief*. The mismatch in the material properties between finger pad skin and *uSkin* tactile sensor was surely one reason for the biased projection of the physical properties. This would suggest that besides the tactile sensor's characteristics like frequency response and sensitivity, hardware specifications like the sensor's material properties can have a great impact on the projection of the physical properties, as it concerns the proposed approach in its current implementation.

3.6 Chapter Summary

The contribution of this chapter lies in the introduction of the algorithm *End-to-end Tactile Texture Projection with Psychophysically-meaningful Latent Space Encodings* that solves the unknown transformation from tactile sensor data into actuator driving signals and thus enables the control of tactile displays for the conveyance of cutaneous feedback from compliant and distributed tactile skin sensors.

The algorithm utilizes an autoencoder approach to compress potentially massive amounts of tactile sensor data into a low-dimensional, psychophysically meaningful latent space that allows for the modulation of the actuator driving signals in accordance with the tactile input data such that an object's psychophysical property profile is emulated.

The proposed algorithm was experimentally verified by executing two user studies on the perception of the psychophysical property profiles of eight texture probes: The first user study aimed at the quantification of the true psychophysical properties of all the texture probes by requesting the study participants to evaluate the textures by direct probing with the index finger. This first user study provided a ground truth against which the performance of the end-to-end tactile texture projection for the emulation of textural property profiles was quantitatively measured. The second user study thus deployed the tactile display prototype from chapter 2 in conjunction with the proposed algorithm to generate tactile stimuli from tactile sensor data that was collected by probing all the texture probes with a *uSkin* tactile sensor module.

The results indicated that the proposed algorithm enables the end-to-end control of tactile displays and the generation of psychophysically meaningful tactile perceptions from tactile sensor data in unstructured environments, due to the implicit encoding of previously unseen and thus untrained tactile sensor data. While this chapter focused exclusively on the development of the algorithm for the end-to-end projection of tactile sensor data into a control signal for tactile displays, the results clearly suggested that besides the tactile sensor's characteristics like frequency response and sensitivity, other hardware specifications like the sensor's material properties can have a great impact on the projection of the physical properties. This influence was seen in the case of the texture probe *handkerchief* that involved the emulation of inconsistent tactile feedback due to the mutual material mismatch of human skin and tactile skin sensor in combination with this texture probe.

Albeit the promising results, future research should, first, investigate how a modified loss function may enforce the coincidence of the psychophysical properties with the respective coordinates of the latent space encodings and, second, should aim for the technical realization of more modalities of tactile feedback. In fact, the absence of key modalities of cutaneous feedback, such as dynamic skin deformation, and the absence of proprioceptive feedback impose limitations on the projection of some physical quantities, e.g. friction, and stress the importance of the deployed tactile display hardware. Moreover, as experiments must involve user evaluations on the emulated tactile feedback, the deployed hardware has a significant impact on the experimental evaluation of the entire system. In this regard, the concept of the end-to-end control of haptic or tactile devices by means of latent space encodings of tactile input data yields an approach that is widely applicable to a broad set of tactile sensor - tactile actuator combinations, e.g. for the projection of hardness.

Chapter 4

Sequential Tactile Data Clustering for Tactile Image Compression to Enable Direct Adaptive Feedback

4.1 Problem Formulation and Solution Concept

4.1.1 Problem Formulation

As explained in section 1.2.2.1, major research is directed towards the large-scale implementation of tactile sensors into (anthropomorphic) robots [58] [66] [63], robot hands [50] [64] [44], and grippers [55] [46]. As it regards human-robot interaction or robot-teleoperation, a significant problem is the meaningful and intuitive representation of the massive raw sensor information to human operators [83] [84] [15] [4] [5]. In particular, the display of meaningful feedback via visual cues is a limitation in itself and, for technical reasons, tactile displays inherently suffer from a limited number of actuators and a limited output for optimal stimuli generation [24], [11] [2] [82].

Moreover, the sensor information that is relevant to a task is often obscured behind redundancy and sensory noise. Extracting and displaying meaningful and intuitive information from the massive amounts of sensor data poses challenges on both the software, which has to process the data in real-time to extract meaningful information, and the hardware, which has to display the extracted information to the user.

Note, contacts are defined as locations of cutaneous information exchange with the environment by means of forces, vibrations, and heat fluxes (cf. chapter 1). It is an open question how tactile compression techniques can preserve the physical meaning of massive tactile sensor data

in order to provide useful information to a human by means of rather compact tactile displays (cf. section 1.2.2.2).

4.1.2 Solution Concept

In this context, chapter 3 dealt with an end-to-end mapping from tactile sensor data to tactile actuator driving signal that deploys tactile illusory phenomena (PS and AM) to enable the efficient projection of textural properties from raw tactile sensor data. This chapter, however, addresses the mismatch between tactile sensor space and tactile display space to enable the compressed projection of independently moving contacts from the tactile sensor raw data and in accordance with the tactile display specifications, i.e. limitations in terms of energy and actuator density.

Precisely, the presented algorithm enables the compression of the tactile sensor raw data alongside a timely trajectory, i.e., it enables the projection of distributed contacts onto the skin of a human operator in a meaningful and intuitive manner. In fact, only after this compression, the deployment of tactile illusory phenomena becomes feasible, because the exact contact location has to be known in order to associate tactile actuators for the creation of phantom actuators. Moreover, sensory noise should not be projected to the skin, as it does not carry useful information, however, causes the actuators to consume energy.

Apart from the immense variety of compression techniques, *K*-means clustering [115] is due to its flexibility an often preferred choice over more complicated algorithms for clustering [116]. For example, *K*-means clustering uses physically meaningful *Euclidean* distance measures, furthermore, allows for the integration of domain knowledge while it does not require training.

The presented algorithm, termed *Sequential Tactile Data Clustering for Tactile Image Compression*, allows for an end-to-end projection of distributed contacts into a well-defined set of quantized stimuli locations and stimuli intensities that are necessary to construct moving contact patterns by means of illusory tactile sensations. The algorithm dynamically compresses the tactile sensor data into a number of discrete contact locations and stimuli intensities by deploying two stages of rapid *K*-means++ [117] clustering on the raw tactile sensor data at each time instant. In this manner, the compressed tactile data preserves its physical meaning, i.e. the tactile

information remains intuitive and direct, and sensory noise is removed. The algorithm does not depend on any specific hardware and enables direct adaptive feedback for a broad variety of tactile sensors and tactile displays. This dynamic compression is almost always beneficial, either due to technical limitations as mentioned above, or for reasons specific to the application, e.g. in prosthetics where the tactile sensation must be re-reproduced on another body part with different mechanoreceptor density [118].

4.1.3 Chapter Organization

This chapter is organized as follows: in section 4.2, the control scheme of the algorithm is presented in terms of a block diagram. Section 4.3 gives a detailed explanation of the algorithm, its building blocks, and its operational principle. Then, in section 4.4, the algorithm is extensively evaluated on experimental data that was collected using the *uSkin* tactile sensor modules in conjunction with the *Allegro* robot hand during various dynamic contact scenarios with objects of daily living. The results are discussed in section 4.5. Finally, section 4.6 summarizes the main findings and revisits the limitations of the presented algorithm.

4.2 Control Scheme for End-to-end Tactile Image Compression

The objective of the algorithm is to compress raw tactile sensor data into a specifiable number of contact points and stimulus intensities while enabling direct and adaptive feedback when dynamically interacting with arbitrary objects. The compression, however, should preserve the physical meaning to be intuitively understood by a human operator. Again, contacts are locations of cutaneous information exchange with the environment by means of forces, vibrations, and heat fluxes. The algorithm *Sequential Tactile Data Clustering for Tactile Image Compression* outputs a maximum number of desired contact locations, K_C^{max}, and stimulus intensities, K_I^{max}, which must be set in accordance with the tactile display specifications and may incorporate laws of psychophysics [119] [120] [34] [35], Fig. 4.2.

The **initializer** identifies non-operational sensors and identifies a contact threshold upon which contacts are detected. The **preprocessor** renders the

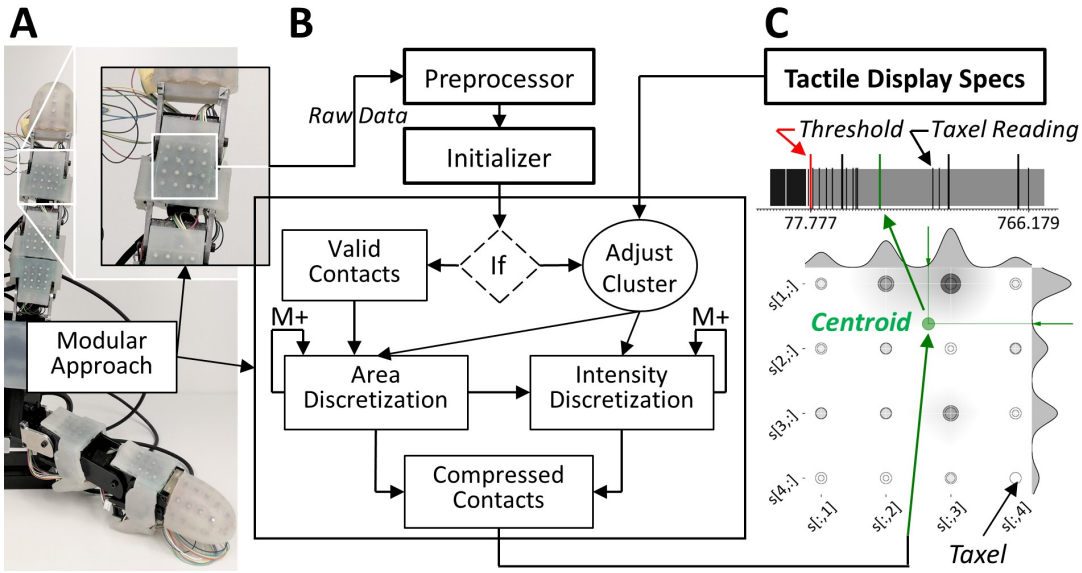

FIGURE 4.1: Control scheme for end-to-end tactile contact compression. The raw tactile sensor data, here from *uSkin* modules (A), is fed to the algorithm (B), which outputs compressed contacts, i.e. a specifiable number of contact locations and stimulus intensities (C).

tactile sensor data into *RGB*-like images, in which the channel dimension corresponds to the modality of the tactile input data, e.g. tri-axial x, y, z-sensor readouts in case of the *uSkin* tactile sensor module. The tactile image compression sequentially deploys two stages of K-means++ clustering: The first stage estimates the location of contact points in regard to the maximum simultaneously displayable contact locations, i.e. performs a **contact area discretization**. The second stage adaptively compresses the range of the measured sensor readouts into a set of stimulus clusters, i.e. performs a **stimulus intensity discretization**.

The compressed contact locations K_C and compressed stimulus intensities K_I are dynamic values, since the number of contacts needs to be dynamically adjusted in accordance with the contact scenario, e.g. different contact area sizes or no contact at all. Moreover, the algorithm keeps track of the previous cluster centroids for rapid convergence of the clustering process of the subsequent time instants. In this manner, the tactile sensor information available in the locations of contact is adaptively compressed, however, in a way that maintains or even enhances their psychophysical meaning.

As it regards the **stimulus intensity discretization**, note that the dynamic clustering of the sensor readouts into discrete intensity values

might lead to physical inconsistencies for the user, because the cluster centroids and thus their associated stimulus intensities as generated by the tactile display actuators change between time instants. Cluster centroids representative for the intended application may be pre-selected and fixed during run-time. The importance of the intensity clustering is discussed later in the light of psychophysics [119], [120] and energy conservation.

4.3 Sequential Tactile Data Clustering for Tactile Image Compression

4.3.1 Algorithm Description

K-means clustering is an iterative method of vector quantization [115] [117] [121][116]. It belongs to the unsupervised learning algorithms and partitions an N-dimensional data set into K distinguished clusters of equal size and shape in which each data point of arbitrary dimension belongs to the cluster with the shortest distance. For example, the *Euclidean distance*, i.e. the distance measured as the sum of the squared differences of the coordinates in each direction.

Briefly, the tactile data at each time instant t is denoted as $S_t = [s_1, ..., s_{N_S}]$, where each of the N_S coordinates s_{n_s} is a D-dimensional vector and can be assigned to exactly one of the clusters $k \in 1, ..., K$. The assignment of sensor data point s_{n_s} to cluster k is denoted by $a_n = k$ and permits the calculation of a cluster centroid μ_k. Within each iteration, the algorithm alternates between updating the cluster assignments a_n and updating the cluster centroids μ_k until a convergence criteria $\zeta_k \leq J(\mu_k)$ with some objective $J(\mu_k)$ is reached. This clustering can be performed on either the spatially distributed sensor array, i.e. resulting in a contact area compression, the sensor readouts, i.e. resulting in a contact stimulus intensity compression, or both.

K-means clustering is conceptually simple, its computational cost scales with the dimensionality and size of the data set, and it allows for the injection of domain knowledge [121] [116]. Note, *K*-means++ refers to a seeding method that improves the speed of the traditional *K*-means clustering dramatically, and was implemented here to speed up the algorithm [117]. Further relevant key features of *K*-means clustering are the assumption of an a-priorily fixed number of K clusters, an isotropic data

space, and usually a geometrically meaningful distance measure, which is typically fulfilled for the application of tactile sensor data.

K-means clustering can be deployed to alleviate the inherent hardware limitations of state-of-the-art tactile displays, namely, the need for **intensity discretization** addressing the limited range of force generation capacity and the need for **actuator discretization** addressing the limited number of actuators or limited number of displayable contact points.

Figure 4.2 summarizes the complete algorithm for *Sequential Tactile Data Clustering for Tactile Image Compression* in a flowchart. In the following, the algorithm is explained in regard to the *Allegro* robot hand equipped with 15 *uSkin* sensor modules, as introduced in chapter 2.

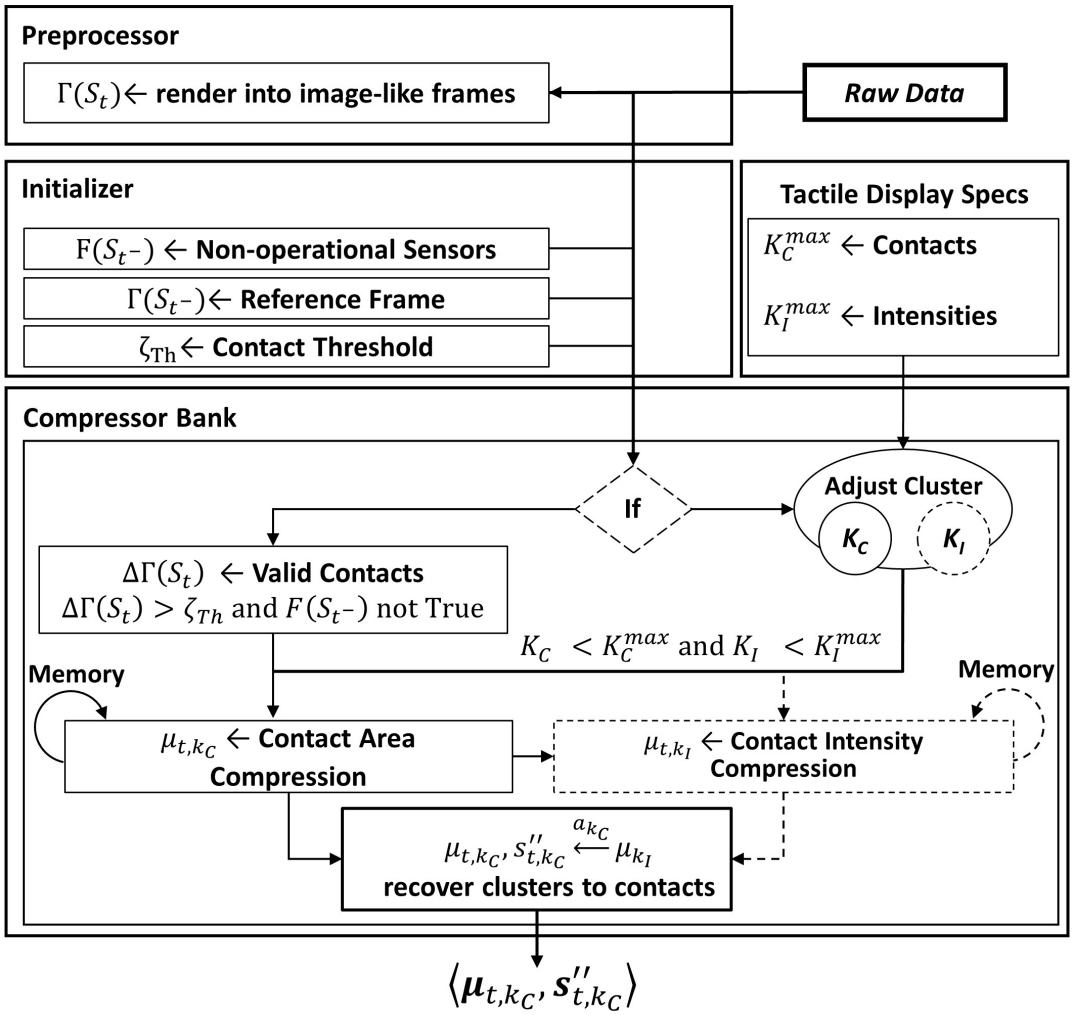

FIGURE 4.2: Flowchart of the algorithm for the sequential tactile data clustering for tactile image compression.

4.3.2 Preprocessing

As depicted in Fig. 4.2, the **preprocessor** renders the entirety of the raw sensor readouts for each of the 15 uSkin modules at each time instant t into an image-like input frame of the size $n_W \times n_H \times n_A$, where n_W refers to the width, n_H refers to the height, and n_A refers to the number of axes of the sensor array. Accordingly, the input frame contains the tactile sensor data with reference to their physical location on the *Allegro* robot hand and $\Gamma(S_t)$ holds these spatial attributes:

$$\Gamma(S_t) \in \mathbb{R}^{n_W \times n_H \times n_A}. \tag{4.1}$$

4.3.3 Initialization

The **initializer** receives image-like rendered input frames and performs three tasks before passing the tactile data to the compressor bank; it:

1. identifies and stores non-operational sensors in F_{n_S} to prevent unnecessary operations,
2. calculates a reference frame $\Gamma(S_{t<T=t^-})$, and
3. determines a contact threshold ζ_{Th} upon which exceedence a sensor readout is registered as valid contact.

The initialization procedures should be run after the implementation of the tactile sensors onto the robot and before contact with any object is made. If these conditions are met, an input frame is called initial frame $\Gamma(S_{t=0})$.

As it concerns the identification of faulty sensors, they are identified by statistically evaluating all sensor readings of the initial frame $\Gamma(S_{t=0})$. Within this work, a sensor is considered as faulty and excluded from further calculations, if one of the readings $s_{x,n_S}, s_{y,n_S}, s_{z,n_S}$ deviates from the arithmetic mean μ_x, μ_y, μ_z among all N_S sensor readings by a multiple of its standard deviation $\sigma_x, \sigma_y, \sigma_z$, respectively. Accordingly, a sensor s_{n_S} is assigned with the attribute $F_{n_S} = 1$, if faulty and $F_{n_S} = 0$, if operational. Then, a relative tactile frame $\Delta\Gamma(S_t)$ is calculated as the absolute difference between the average sensor readouts of a number of initial frames $\Gamma(S_{t<T=t^-})$ and any following frame $\Gamma(S_{t\geq T=t})$

$$\Delta\Gamma_t = \Gamma(\Delta S_t) = |\Gamma(S_t) - \Gamma(\bar{S}_{t^-})|, \tag{4.2}$$

where $\Gamma(\bar{S}_{t^-})$ summarizes the rendered tactile data without contact over the time span $t < T$, thus serves as a set of reference values.

Lastly, the threshold ζ_{Th}, upon which exceedence a contact is registered, is defined as the maximum value:

$$\zeta_{Th} = \max(\Delta\Gamma_{t=1}). \tag{4.3}$$

Once the contact threshold is defined, the parts of the *Allegro* robot hand covered with the *uSkin* sensor modules can detect contact points.

4.3.4 Tactile Compressor: Contact Area Compression

The actuator discretization precedes the intensity discretization and addresses the limitation of a finite, usually smaller number of tactile display actuators (or conveyable contact points) compared to the number of tactile sensors. Moreover, the projection of illusory tactile sensations requires to carefully match the number of detected contacts with the number of available actuators to project these contacts, e.g. by means of spatio-temporally controlled vibro-tactile stimuli alongside a timely trajectory [20] [39].

In case a number of valid contacts N_C is identified at time instant t, the actuator discretization compresses the tactile frame $\Delta\Gamma_t(S_{n_C})$ by performing a K-means cluster compression across the tactile frame to compress the number of contact locations in order to match the number of desired contacts K_C^{max}. If $N_C \leq K_C^{max}$, i.e., the number of contact points is initially lower or equal to the number of desired contact points, a further compression is not required. Then, $\Delta\Gamma_t(S_{n_C})$ translates directly to the output of the actuator discretization, and K_I is set to N_C. In contrast, if K_C is exceeded by N_C, the compression must be performed. Using K-means, the initial centroids μ_{K_C} are rapidly initialized to a set of mutually far spread contact locations by using the K-means++ cluster seeding procedure [117] that samples all N_C contact locations and returns K_C seeds.

$$\mu_{k_C} \xleftarrow{K++} \Delta\Gamma_t(S_{n_C}). \tag{4.4}$$

Subsequently, the algorithm has to alternate between only a very limited number of points to compute the *Euclidean* distance between the n_C-*th*

contact point and cluster centroid μ_{i,k_C} at every iteration i

$$d_{n_C,k_C} = \|\Delta\Gamma_t(S_{n_C}) - \mu_{i,k_C}\|_2 \tag{4.5}$$

and to find the cluster assignments a_{n_C} that represent the physical centroid of the contact area

$$a_{n_C} = \arg\min_{k_C \in 1,\ldots,K_C} (d_{n_C,k_C}). \tag{4.6}$$

The cluster centroids μ_{k_C} are updated by averaging over the cluster members

$$\mu_{k_C} = \frac{1}{N_{k_C}} \sum_{n:a_{n_C}=k_C}^{N_{k_C}} \|s_{t,n_C}\|_l^p \times \Delta\Gamma_t(s_{n_C}) \text{ for } k_C \in 1,\ldots,K_C, \tag{4.7}$$

where $\|s_{t,n_C}\|_l^p$ is the *l-th* vector norm of s_{t,n_C} and p is an exponent, which allow for the introduction of a weighted update rule for improved stability and smoothness. This update terminates, when

$$\zeta_C \leq J(\mu_{k_C}) = \frac{1}{2} \sum^{K_C} \left\|\Delta\mu_{k_C}\right\|_2 . \tag{4.8}$$

The compressed contact locations are the terminal cluster centroids $\mu_{t,k_C} = \mu_{k_C}$ from equation (4.7) and the new contact intensities s'_{t,k_C} at the compressed locations μ_{t,k_C} are found by simple interpolation:

$$s'_{t,k_C} = \mathbf{I}(\Delta\Gamma_t(s_{n_C}), \mu_{t,k_C}). \tag{4.9}$$

4.3.5 Tactile Compressor: Contact Intensity Compression

The stimulus discretization refers to the compressed representation of the contact intensities while dynamically interacting with an object. The relevant information arising from this interaction is often obscured behind redundancy and sensory noise, which may be accounted for by deploying another K-means clustering that compresses the sensor readouts into K_I intensity clusters. As this compression succeeds the contact area compression, only $K_I \leq K_C$ intensities must be considered, which makes this compression far less computationally expensive. In fact, the

compression of the contact intensities is somewhat comparable to the compression of the color depth in *RGB*-images.

Again, using *K*-means, the initial centroids μ_{K_I} are initialized to a set of mutually far spread contact intensities by using the *K*-means++ cluster seeding procedure [117] that samples from K_C contact intensities $S'_t = [s'_{t,1}, ..., s'_{t,K_C}]$ and returns K_I seeds:

$$\mu_{k_I} \xleftarrow{K++} S'_{t,k_C}\,, \tag{4.10}$$

i.e., the preceding compression into K_C contact locations limits the maximum number of intensity clusters to K_C. Subsequently, the algorithm calculates the *Euclidean* distance between sensor readout s'_{k_C} and the current intensity centroid μ_{i,k_I} for iteration i:

$$d_{k_C,k_I} = \|s'_{t,k_C} - \mu_{i,k_I}\|_2. \tag{4.11}$$

Then the algorithm alternates between updating the intensity cluster assignments a_{k_C}:

$$a_{k_C} = \arg\min_{k_I \in 1,...,K_I} (d_{k_C,k_I}) \tag{4.12}$$

and updating the cluster centroids in a *K*-means typical manner

$$\mu_{k_I} = \frac{1}{N_{k_I}} \sum_{n:a_{k_C}=k_I}^{N_{k_I}} s'_{t,k_C} \text{ for } k_I \in 1, ..., K_I \tag{4.13}$$

until the convergence criteria is reached:

$$\zeta_I \leq J(\mu_{k_I}) = \frac{1}{2} \sum^{K_I} \left\|\Delta\mu_{k_I}\right\|_2. \tag{4.14}$$

Eventually, the final contact intensities are obtained by

$$s''_{t,k_C} = \mu_{k_I=a_{k_C}} \text{ for } k_C \in 1, ..., K_C, \tag{4.15}$$

where s''_{t,k_C} is a compressed sensor reading that fulfills the conditions of a contact and μ_{t,k_C} is its corresponding compressed contact location of the original input frame $\Gamma(S_t)$ that rendered the tactile sensor readouts S_t.

4.3.6 Implementational Notes

1. Importantly, if the intensity centroids μ_{k_I} are updated at each time instant, one and the same sensor reading may be represented differently between time instants. This is desirable for finely resolving the tactile feedback over the full range of the tactile display's actuator output range, however, may require the superposition of kinesthetic feedback to provide continuity to the human operator. Otherwise, it could lead to inconsistencies in the representation of physical stimuli. To prevent this problem, the intensity compression might be run on a dataset that is representative for an entire application scenario (e.g. rolling a ball in ones hand) to find a static compression via fixed intensity cluster centroids $\mu^*_{k_I}$. Then, the online intensity compression exclusively assigns the sensor readings to the predefined cluster centroids $\mu^*_{k_I}$ by using equations 4.11 & 4.12, thereby, considerably speeds up the entire algorithm.

2. Another important consideration is the initialization between the time instants t. To speed up the initialization and improve the representation of the original dataset $\Gamma(S_t), S_t$, the K-means++ initialization procedure according to Arthur *et al.* [117] was chosen. However, it is beneficial to keep track of the previous compressions μ_{t,k_C}, s''_{t,k_C}, as depicted in Fig. 4.2. Since physical stimuli change continuously, the previous cluster centroids most likely provide a very good starting point for the current K-means update procedure. Hence, K-means++ might be run only after loss of contact.

4.4 Evaluation Studies

4.4.1 uSkin Tactile Sensor Module

For the evaluation of the algorithm, the dynamically moving contact of a Styrofoam^{TM} sphere ($Ø19.45mm$, $0.28g$) rolling across the *uSkin* tactile sensor module's surface was exemplarily analyzed, Fig. 4.3. More precisely, the Styrofoam^{TM} sphere was rolled across the surface from the bottom edge to the top edge of the sensor module with varying degrees of contact pressure.

For each time instant, the algorithm was run on the rendered tactile $(4 \times 4 \times 3)$-image frame to output the contact locations and contact intensities after compression. The maximum number of desired contact locations, K_C^{max}, and stimulus intensities, K_I^{max}, were set to $K_C^{max} \in 1, 2, 4, 8, (4 \times 4)$ and $K_I^{max} = 10$. Since kinesthetic feedback was not investigated in this thesis, the intensity centroids $\mu_{k_I}^*$ were set to static, and were identified via K-means intensity clustering on the complete dataset.

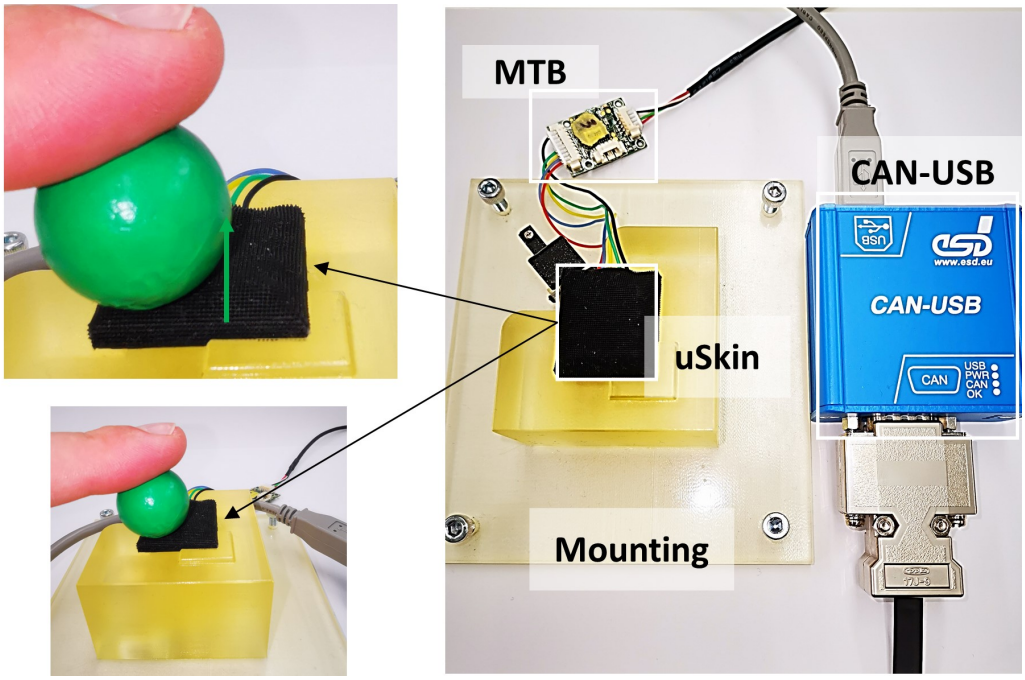

FIGURE 4.3: Tactile image compression experiment with the *uSkin* tactile sensor module and a rolling Styrofoam^{TM} sphere.

As a reference, each sensor readout was recorded and the contact pressure distribution was calculated over the entire sensor module surface, which allowed for comparison of the uncompressed and compressed tactile data as well as the estimation of the actual contact area. The algorithm was verified by analyzing the compressed tactile image in comparison to the raw tactile sensor data.

Moreover, the algorithm was evaluated in terms of its capacity to estimate the location of the contact points and in terms of how the sensor readings at the contact point were efficiently represented after intensity quantization. For the sake of simplicity, however, each of the N_S vector entries in $\Gamma_t(S_{n_S})$ was summarized to its corresponding vector magnitude $s_{n_S} \leftarrow \|\mathbf{s}_{n_S}\|_2$.

The maximum sampling frequency of the data collection that could be achieved with the *uSkin* tactile sensor module was approx. $100Hz$, referred

to as *uSkin* sampling frequency. Finally, a parameter study was implemented that demonstrated the estimation of the contact imprint area and the corresponding speed of the algorithm for different numbers of displayable contacts.

4.4.2 Scalability to Robotic Hands with Massive Tactile Data

In order to analyze the algorithm under realistic conditions and evaluate its scalability, tactile sensor data was gathered during the active tactile exploration of representative objects of daily living using the *Allegro* robot hand that was covered with 15 uSkin sensor modules that provided 240 tri-axial force vector measurements at each time instant [107][45], Fig. 4.4.

Thus, in complementation to the above study on the compression of the tactile data, this evaluation study investigated the scalability towards massive amounts of tactile sensor data and different tactile display specifications. For a detailed explanation of the *Allegro* robot hand, the reader is also referred to section 2.1.1.

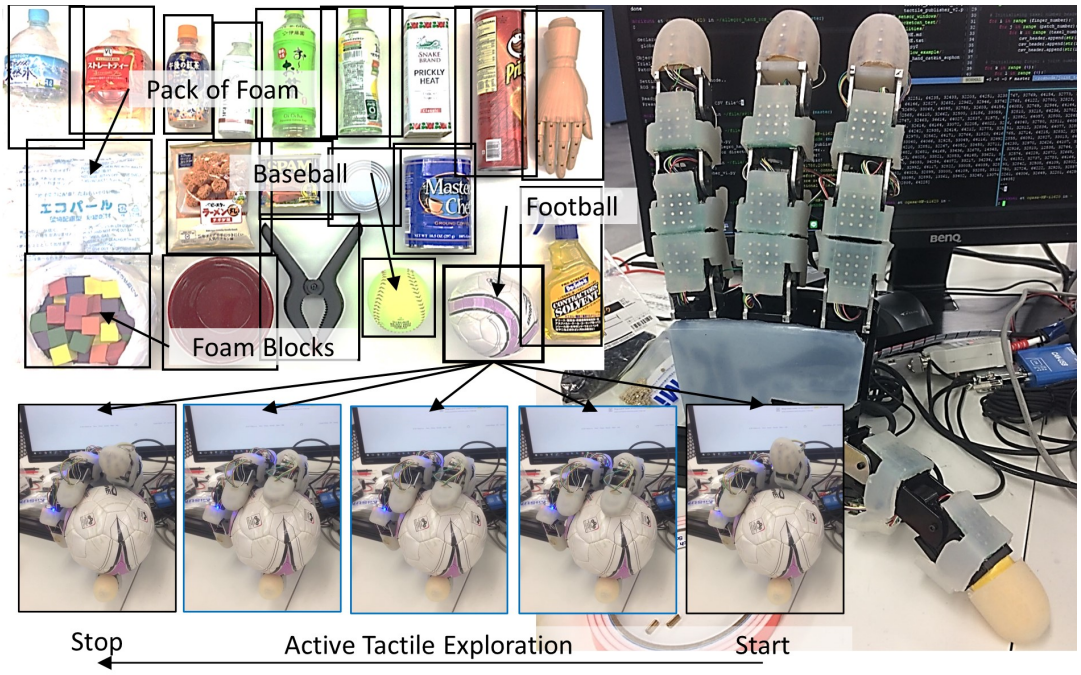

FIGURE 4.4: Active tactile object exploration using the *Allegro* robot hand on the Yale-CMU-Berkeley object model set.

Briefly, the *Allegro* robot hand was mounted on a sturdy aluminum profile with the fingers pointing upwards. A grasping motion that dynamically moved all four fingers was pre-recorded to actively explore a

set of objects. The data collection sequence started with all fingers in a fully open state. Then, one out of 20 everyday objects from the YCB object model set (Yale-CMU-Berkeley[1]) were placed into the *Allegro* robot hand and the pre-recorded motion sequence together with the data logging software that streamed the *uSkin* sensor readings and the 16 servo motors' joint angles into a *.csv* (comma separated value)-file were triggered. Accordingly, one data set consisted of 720 tactile sensor and 16 joint angle readouts. Note that, however, the joint angle information was not used, since it is not relevant to the tactile display.

As a result, the algorithm compressed 720 tactile sensor readings at each time instant, as available across the finger phalanges and fingertips of the *Allegro* robot hand, into the specified number of contact locations K_C and stimulus intensities K_I. Similarly to the above test conditions, the maximum number of desired contact locations, K_C^{max}, and stimulus intensities, K_I^{max}, were set to $K_C^{max} \in 1, 2, 4, 8, (4 \times 4)$ and $K_I^{max} = 10$ per sensor module; and the intensity centroids $\mu_{k_I}^*$ were identified via K-means intensity clustering on the complete dataset of an object. Note that the phalanx of the thumb carries only three *uSkin* modules for which reason the missing sensor readings were treated similarly to faulty sensor readings.

The maximum sampling frequency of the data collection that could be achieved with the *Allegro* robot hand was approx. $30Hz$, referred to as *Allegro* sampling frequency. The results were evaluated with the focus on the algorithm speed, since the compression of the tactile data has been analyzed in depth in the previous section. All calculations were run on an off-the-shelf PC with Intel(R) Core(TM) i7-8700K CPU @ 3.70GHz and 32.0GB RAM on one core.

4.5 Results and Discussion

4.5.1 uSkin Tactile Sensor Module

Figure 4.5 shows the results of the tactile image compression experiment with the *uSkin* tactile sensor module. The compressed contact locations and the contact pressure distribution across the entire sensor module were superposed for all tactile images, Fig. 4.5-A. Figure 4.5-B depicts the entirety of tactile sensor readouts as rug plot, in which the left-hand side black area

[1] http://www.ycbbenchmarks.com/

contains the inactive sensor readouts that were not registered as valid contacts and the right-hand side grey area contains all active sensor readouts. Finally, Figure 4.5-C shows the raw tactile data as a reference: time step $t = 102$ marks the initial contact and time step $t = 210$ marks the tactile image frame with the highest number of tactile sensing points registered as contact.

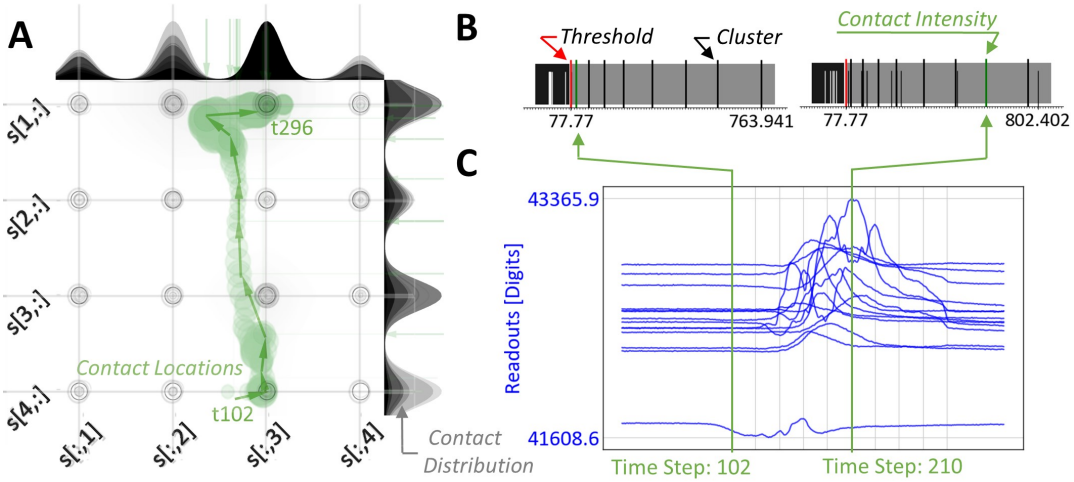

FIGURE 4.5: The compressed contact locations and the contact pressure distribution across the entire sensor module are shown (A). A rug plot shows the entirety of sensor readouts and the intensity clusters (B). The entirety of raw tactile sensor readout magnitudes are shown in (C).

It can be seen that the centroid location that is an estimate of the contact location coincided very well with the relative contact pressure distribution depicted at the top and right-hand side of the graph in Fig.4.5-A, therefore indicating an accurate estimation of the centroid location. The contact path was very smooth, which can be attributed to the compression algorithm that estimates the contact location from a group of associated cluster members, therefore efficiently mitigates sensor noise. From the intensity rug plot in Fig. 4.5-B, it can be seen that as soon as a sensor readout was registered as valid contact, it was assigned to the first intensity centroid $\mu_{k_I=1}$. Note that the intensity clusters do not change between time steps, which guarantees physically consistent stimuli. The timely trajectory of discrete contact locations and their corresponding intensities are well suited as input data for tactile illusory algorithms as proposed in [20] [39] [21].

Figure 4.6 shows detailed results of the tactile image compression experiment $K_C^{max} \in 1, 2, 4, 8, (4 \times 4)$ at time step $t = 210$, where the maximum number of $N_C = 12$ contacts were registered. Despite the rather

small contact of the spherical Styrofoam^{TM} probe with the flat sensor module, the registration of $N_C = 12$ out of 16 sensing points was surprisingly high. This might be attributed to the crosstalk among the sensing points that is introduced by the gripping tape (cf. section 2.1.2) and should be addressed in future version of the sensor module.

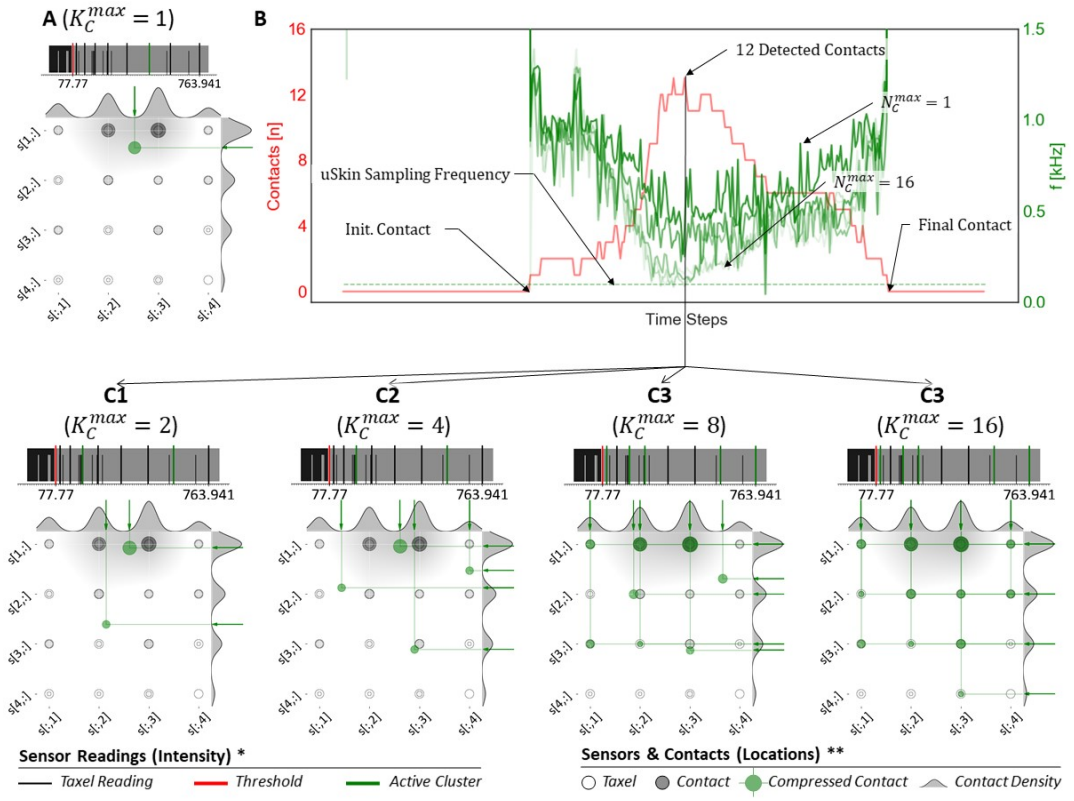

FIGURE 4.6: The compression of the time instant with the maximum number of registered contacts $N_C = 12$ (A) was analysed in detail in terms of algorithm speed (B) and contact area discretization (C) for a varying number of desired contact clusters $K_C^{max} \in 1, 2, 4, 8, (4 \times 4)$.

Figure 4.6-A shows that the actual point of contact was located at the top border of the sensor module. Due the dependency of K-means on the number of points N, clusters K, and the data point dimensionality D ($O(NKD)$), Figures 4.6-B and C illustrate the algorithm's speed and the distribution of cluster centroids for higher numbers of desired contact clusters K_C^{max}. While the algorithm speed decreased with an increasing number of registered contacts, it did never fall below the *uSkin* sampling frequency, except for $K_C^{max} = 16$. This was, however, a rather theoretical value, since $K_C^{max} = n_W \times n_H$, which effectively means that no compression was performed and the algorithm has no impact on the tactile sensor data.

Following a modular approach and considering the small size of the *uSkin* tactile sensor module, a maximum $K_C^{max} = 4$ contact point estimates per sensor module should be sufficient for most applications with tactile displays. With increasing K_C^{max} the true contact area was increasingly covered with discrete contact point estimates until for $K_C^{max} = 16$ the algorithm stopped increasing this number, since all unique contact points were represented and the compression coincided with the actual contact area. Note that the estimation of continuous contact areas is always bound to discrete sensing points.

4.5.2 Scalability to Robotic Hands with Massive Tactile Data

Figure 4.7 shows the results of the tactile image compression experiment during the active tactile object exploration of several representative objects of the YCB object model set.

Several points were noteworthy: For example the compressed intensity profiles (A-D, top) were mutually different between the different objects, which most likely was due to their different shapes and hardnesses. This was interesting, because the pre-set cluster reflected the complete motion scenario and would cause notable differences in conjunction with a tactile display alone from the distribution of intensity values.

Due to the active engagement of the *Allegro* robot hand with the differently shaped and sized objects, the number of contacts N_C was considerably higher and oscillated within one motion cycle of active engagement between 75 and 125. While the algorithm speed decreased with an increasing number of registered contacts, it did rarely fall below the *Allegro* sampling frequency, except for $K_C^{max} = 16$. Again, $K_C^{max} = 16$ effectively means no compression, since for each sensor module $K_C^{max} = n_W \times n_H$, and the algorithm should not be deployed.

4.6 Chapter Summary

The importance of this chapter lies in the introduction of the algorithm termed *Sequential Tactile Data Clustering for Tactile Image Compression to Enable Direct Adaptive Feedback* that allows for the dynamic compression of tactile sensor data for its representation by tactile displays that suffer from a limited number of actuators (or displayable contacts) and high energy

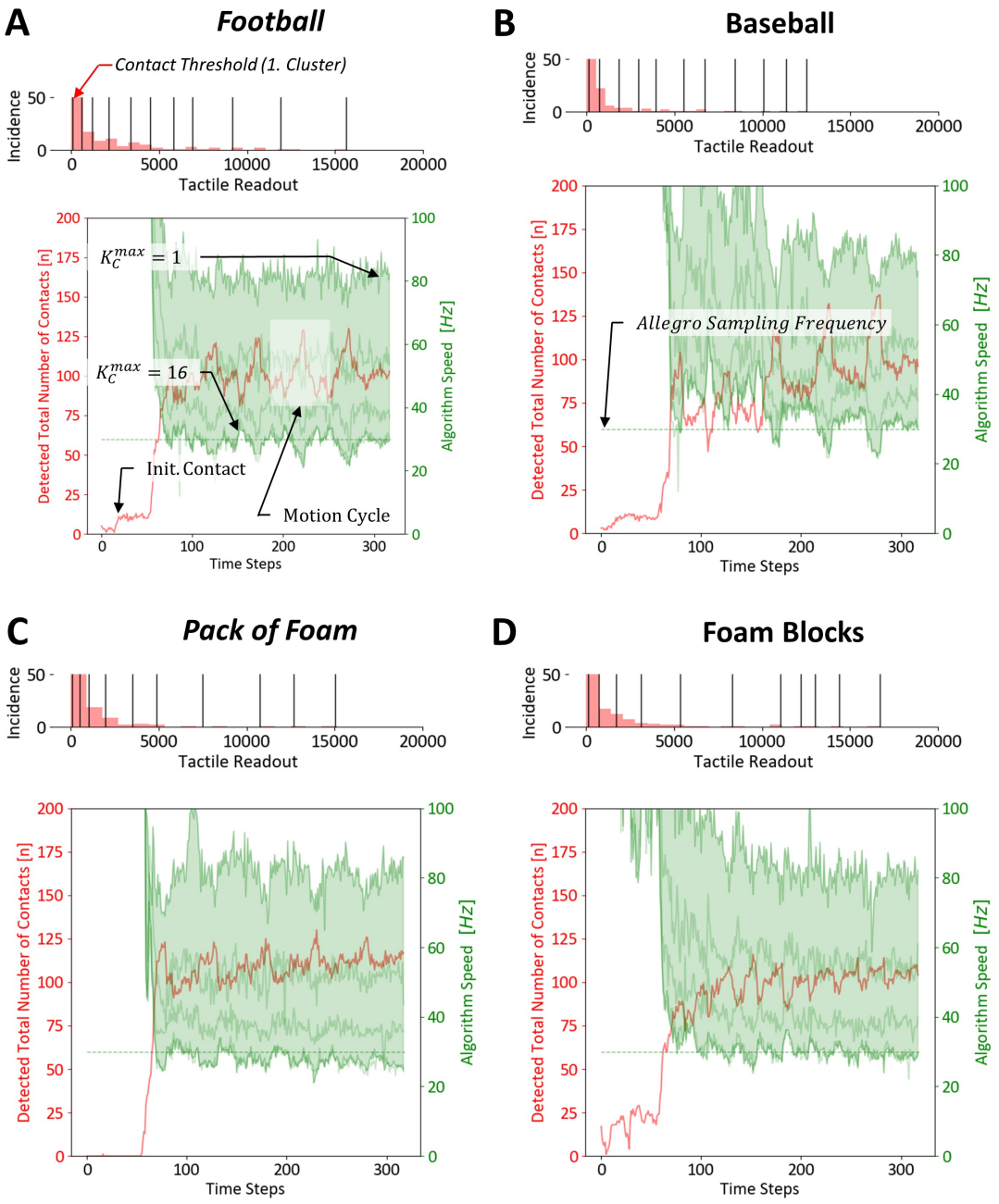

FIGURE 4.7: Results of the tactile image compression during the active tactile object exploration experiment are shown for representative objects of different size and hardness: football (A), baseball (B), a pack of foam (C), and foam blocks (D). The respective top graph shows the incidence of individual sensor readouts as histogram (24 bars) and the pre-set intensity clusters as rug plots. The respective bottom graph shows the number of registered contacts and the corresponding algorithm speed. Note that K_C^{max}, K_I^{max} are per sensor module.

consumption. The algorithm resolves the dimensional mismatch between tactile sensor space and tactile display space by performing two stages of

unsupervised *K*-means++ clustering on the raw tactile sensor data at each time instant.

The capabilities of the algorithm have been experimentally verified by compressing the massive tactile information that was captured by *uSkin* sensor modules mounted onto an anthropomorphic *Allegro* robot hand that actively explored a representative selection of objects of everyday living. The rendering of 240 tri-axial sensor readings of the *uSkin* tactile sensor module into image-like frames allowed for the sequential clustering for tactile image compression. In this manner, the location of the contact point could be precisely estimated and, moreover, the tactile information stored in the contact point could be optimized for the representation via tactile displays while removing sensor noise and therefore smoothing the contact point trajectory.

The results suggest that the algorithm is capable of dynamically compressing the tactile sensor readings into the tactile display space, in a way that maintains their physical meaning, scales to the capacities of the respective tactile display, and enables direct adaptive feedback with (varying intensity cluster μ_{k_I}) or without (representative intensity cluster $\mu_{k_I^*}$) the complementation by kinesthetic feedback.

These characteristics yield a promising potential for important applications like human-robot interaction, e.g. teleoperation and prosthetics, all of which would require the tactile display to resemble the physical meaning of tactile information in real-time. In this regard, the results also suggested that the algorithm, as tested in conjunction with the *Allegro* robot hand and *uSkin* sensor module, is very fast; it well exceeded the respective sampling frequencies of *Allegro* robot hand and *uSkin* sensor module.

Following a modular paradigm, however, future versions of the algorithm should include implementational improvements, e.g. the multiprocessing of several tactile sensor modules on distributed CPU-cores in order to maintain the algorithm's speed even for very high resolving tactile sensors, e.g camera-based tactile sensors like the *DIGIT* [47], and very large-scale implementations across large surfaces of humanoid robots, e.g the *iCub* with 2000 force sensors [66] or the *H1* robot with 1260 *Hex-O-Skin*-sensors [67].

The current implementation of the algorithm assumes geometrically simple contact imprints that are approximated by a varying number of

contact location centroids (linear *Euclidean* distance kernel). Tactile sensors with very high resolutions, e.g. camera-based sensors (cf. *GelSlim* [55]), however, are capable of sensing fine micro-geometric surface details. Those complex contact imprints that are caused by the detailed features of an object's surface would most likely require modifications to the algorithm and, as of now, would pose severe challenges on their efficient projection by means of tactile illusions [20] [28]. Since the proposed algorithm produces discrete contact locations with varying contact intensity, it could be, however, combined with the algorithm from chapter 3 to give independently moving contact points generic surface properties.

Another interesting direction of future research would be the incorporation of psychophysical domain knowledge into the intensity compression. In fact, the consideration of the principle of *Just Noticeable Differences* [119] [120], i.e. the minimum amount by which the stimulus intensity must be changed in order to produce a noticeable variation in sensory experience, is akin to the meaningful compression of intensity values. Next to the contact location compression, this could further contribute to the tactile display's energy conservation, since the output of stimulus intensities that are higher, but not noticeable can be assigned to lower clusters μ_{k_I}, i.e. actuator outputs with lower energy consumption.

Chapter 5

System Integration into a Wearable Tactile Display Fingertip Module

5.1 Problem Formulation and Solution Concept

5.1.1 Problem Formulation

As initially explained in chapter 1, the overall goal is to develop and implement a vastly applicable end-to-end tactile feedback loop that uses the raw data from tactile skin sensors to transmit physical contact information by means of tactile displays for the application in telerobotics and human-robot interaction. The large majority of tactile displays is designed for the application in virtual reality settings [99] [97] [20] [39] [2] [1] [82] [21] which constitutes a well defined environment, or other specific applications, e.g. *Braille* information displays [98].

To the author's best knowledge, there is no wearable tactile feedback system that uses sparse actuator distributions to encounter energy and space restrictions in tactile displays in combination with tactile illusory phenomena to transmit meaningful tactile information from massive amounts of raw tactile sensor data for the application in unstructured environments [11] [2] [82].

Moreover, due to the multi-modal nature of the sense of touch, the tactile display module should implement ultra-compact and energy-dense actuators to allow for being scaled in accordance with the intended application and eventually for being complemented with further actuators for multi-modal haptic feedback. Another vital requirement are networking capabilities, i.e. the wireless connectivity to accompanying systems, to allow for the system integration into robotic application scenarios.

5.1.2 Solution Concept

In addressing these challenges, chapters 3 and 4 developed the required software that enables end-to-end tactile sensor data projections for the construction of psychophysical tactile illusory phenomena and thus allows for the transmission of physical contact information, i.e. micro-geometric surface properties and contact locations, onto the skin of a human user by means of tactile displays.

This chapter is therefore concerned with the integration of the system architecture, as introduced in chapter 2, into a compact and wearable tactile display fingertip module. The following sections present the implementation of a scalable tactile display fingertip module with a sparsely distributed 3D-array of ultra-compact SMA-based micro-vibrators together with a modular WiFi- and I^2C-enabled driver unit.

In combination with the in chapters 3 and 4 developed software, this tactile display fingertip module realizes a novel data-driven tactile feedback framework that deploys end-to-end tactile sensor data projections to provide tactile feedback from massive tactile sensor data by means of compact tactile displays with sparse actuator distributions for its use in robot-teleoperation and human-robot interaction.

5.1.3 Chapter Organization

This chapter is organized as follows: in section 5.2, both the system architecture and the tactile display fingertip module with sparse actuator array are explained in detail. Next, section 5.3 describes the control strategy that deploys the presented hardware in combination with the in chapter 4 introduced algorithm *sequential tactile data compression* to identify and enable the projection of compressed contacts on the skin of a human operator by means of psychophysical tactile illusions. Section 5.4 describes the experimental setup and the user studies that were conducted to verify the proposed tactile feedback system, i.e., the transmission of arbitrary contact trajectories from raw tactile sensor data to a human user by means of the tactile display fingertip module. The results are presented and discussed in section 5.5. Finally, section 5.6 summarizes the main findings and limitations of the presented tactile feedback system.

5.2 Implementation of a Wearable Tactile Display Fingertip Module

5.2.1 System Architecture and Networking

Fig. 5.1 summarizes the entire system architecture in the form of a block diagram depicting the components and the information flow, Fig. 5.1. Referring back to the system architecture and system components as introduced in chapter 2 (Fig. 2.1), the tactile display fingertip module comprises the latest tactile display fingertip prototype (Fig. 5.1-A) with eight SMA-based micro-vibrators as well as the driver unit. A driver unit consists of a set of custom-made driver boards with I²C-enabled pulse-width modulation (PWM) driver and eight current amplifying units as well as a WiFi-enabled MCU that stacks on top of the driver boards (Fig. 5.1-B).

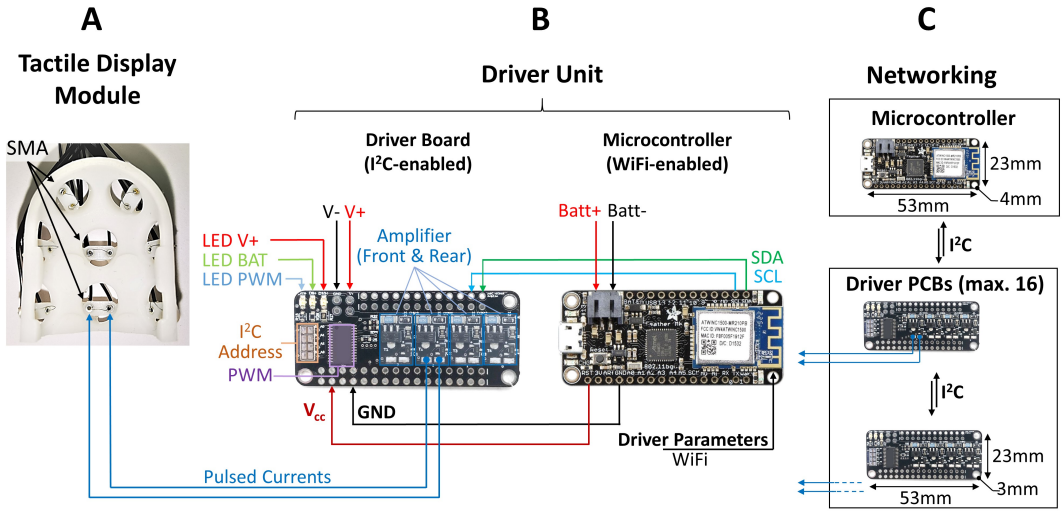

FIGURE 5.1: The tactile display fingertip module implements eight SMA-based micro-vibrators in a 3D-array covering all sides of the fingertip (A). The MCU is stacked on top of custom-made driver boards each of which comprising a pulse-width modulation (PWM) driver and eight current amplifying units (B). Each driver unit is associated with a tactile display module, up to 16 driver boards connect with one WiFi-enabled MCU (C).

The tactile display fingertip prototype connects via 16 AWG30 copper wires (two wires per micro-vibrator) to the driver boards, which then connects via I²C to the MCU. Each driver board connects with a tactile display unit and up to 16 driver boards can be conveniently stacked onto

one MCU. Finally, the MCU connects via WiFi (or USB) to the host PC executing the algorithms for the actuator driving parameter computation.

The MCU manages the time-critical actuation of the micro-vibrators in order to generate spatio-temporal actuation patterns that elicit illusory tactile sensations. For this reason, each driver board implements not only current amplifiers but also a PWM driver with built-in, i.e., autonomous oscillator. In this manner, a single MCU can be connected to up to 16 daisy-chained driver boards of which each of them drives one tactile display unit independently, thus, enables scalable design and control in a compact form factor, Fig. 5.1-C. Note, in its current implementation, the module furthermore requires to be connected to an external power source (here: Kikusui PWR800L, Regulated Power Supply).

5.2.2 SMA-based Tactile Display Fingertip Module

The tactile display fingertip module prototype utilizes bare SMA wires ($Ø75\mu m$, L$5mm$, R1.9Ω) to generate micro-vibrations and project tactile stimuli directly onto the skin, Fig. 5.2-A. The SMA wires are implemented into a small 3D-printed package covering all the sides and the front of the fingertip.

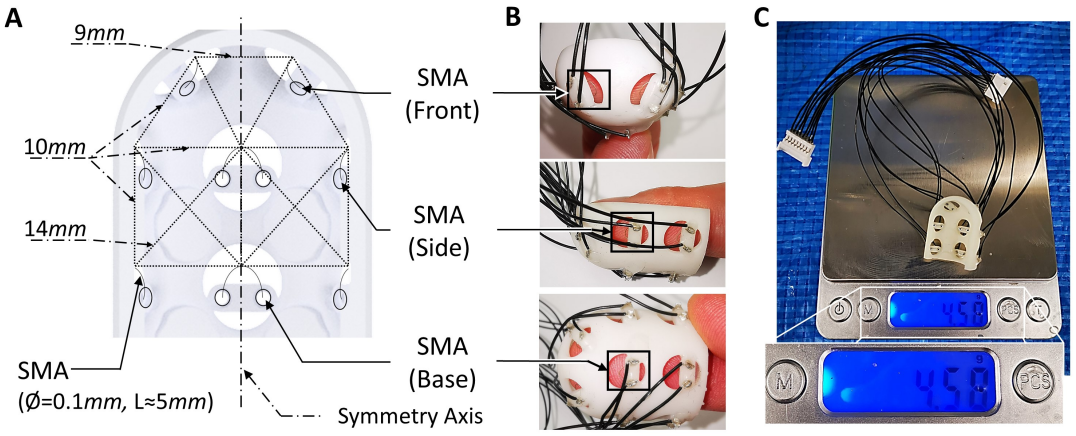

FIGURE 5.2: The tactile display fingertip module implements eight SMA-based micro-vibrators within a 3D-array covering the front and all sides of the finger (A). At room temperature, the SMA-based micro-vibrators rest loosely against the skin without being compressed (B). The tactile display prototype including all wires and connectors had a weight of $4.58g$ (C).

As explained in chapter 1, the two-point-orientation discrimination threshold of the fingertips is around $5mm$ [22]: In realizing a sparse actuator

distribution, the actuator array of the new prototype has mutual actuator distances of $9mm$ to $14mm$, which is larger than the discrimination threshold and enables discretely perceivable signals for the generation of illusory tactile stimuli [34], [35]. The SMA wire-carrying bar is similar to the structure in the first prototype, however, is set $1mm$ into the fingertip module and surrounded by a notch to allow for free vibration and proper cooling of the SMA wire. In the low-temperature state (no current flow), the SMA wire is barely noticeable and rests loosely against the skin of the fingertip.

In order to maintain the smallest possible form factor, the SMA wires are threaded through flanged eyelets ($Ø_o 760\mu m$, $Ø_i 530\mu m$, L$2.41mm$) that are crimped around the SMA wire and soldered to the current supplying cables, Fig. 5.2-B. Compared to the first fingertip prototype, the manufacturing of this fingertip module is simpler and the SMA-based micro-vibrator itself requires less space allowing for a more flexible and less intrusive design.

The tactile display unit including all the wires and connectors had a total weight of approx. $4.58g$, Fig. 5.2-C. The combined weight of I^2C-driver PCB ($5.77g$) and MCU ($6.39g$) was $12.16g$, resulting in a total weight of $16.74g$ for one tactile display fingertip module. Every additional tactile display unit increases the weight by only $10.35g$.

5.3 Control Scheme for Quasi-dynamic Contact Trajectory Projection

For the tactile transmission of an arbitrary contact trajectory that results from the free interaction of a moving object in contact with a tactile sensor module, it is necessary to construct discrete contact points that can be well projected onto the skin of a human user using illusory tactile sensations. Since it is difficult to assume any prior information on the interaction, such as duration, speed or direction, the tactile sensor data must be continuously sampled and the identified contact trajectory must be projected on-the-fly in a dynamic fashion. Note, the variable t thus refers to the time instants at which the tactile sensor data is sampled.

The subsequently explained control scheme aims at the quasi-dynamic projection of contacts, i.e., the identification of contact centroids from raw tactile sensor data and their immediate projection at each time instant t

using a set of neighbouring micro-vibrators for the generation of an apparently moving phantom tactile illusion.

Accordingly, the stimuli duration τ_d, i.e. the duration that stimuli are presented, and the SOA τ_{SOA}, i.e. the delay between subsequent stimulus onsets, are well-defined constants that enable the perception of a moving contact point [20] [21]. Note that τ_{SOA} refers to the duration between time instants t, not however, to the delay between stimulus onsets within the same time instant. This is because for the generation of phantom tactile illusion, this duration must be negligibly small [35]. For more information on the theory of these parameters, the reader is referred to chapter 1 and the therein recommended literature. The calculation of the parameters τ_d and τ_{SOA} is described by Israr [20] and Baik *et al.* [21]. A flow chart of the complete control scheme is depicted in Fig. 5.3.

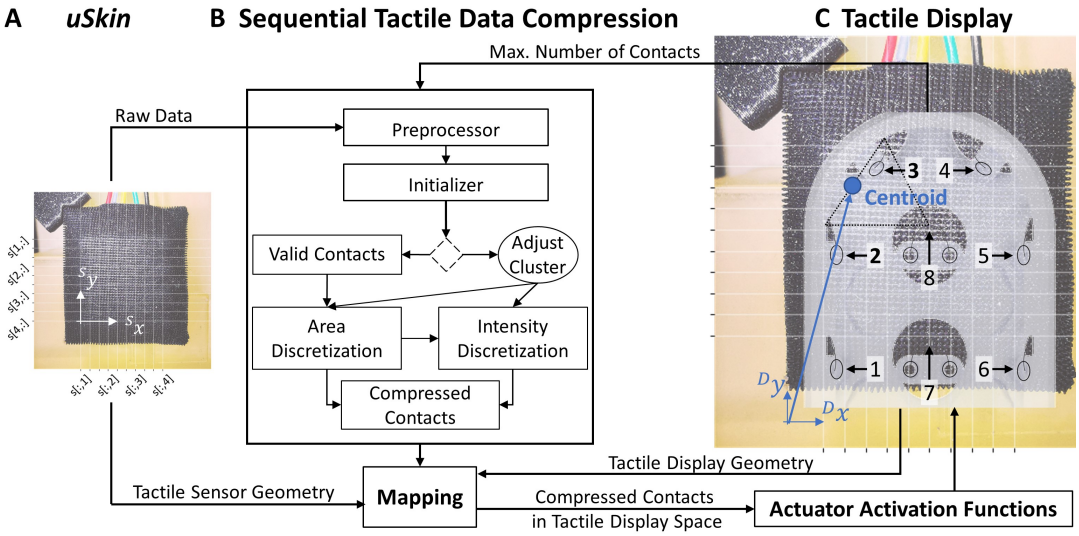

FIGURE 5.3: For the quasi-dynamic contact trajectory projection, firstly, the raw tactile sensor data from the *uSkin* module (A) is fed to the algorithm for *sequential tactile data compression* (B). Then, the contact centroid location is mapped into tactile display space. Finally, the micro-vibrators of the tactile display module are activated such that the perceived stimulus location corresponds with the contact location on the tactile sensor module. This is achieved using local actuator activation functions for the generation of tactile illusions [20] [38] [21] (C).

At each time instant t, the algorithm for *sequential tactile data compression* receives the tactile sensor raw data to compress the detected contacts and to identify the centroid location in tactile sensor space ${}^{S}(x,y)_C$, Fig. 5.3-B. With the knowledge on the geometries of the *uSkin* tactile sensor and the tactile

fingertip display modules, the centroid location ${}^{S}(x,y)_C$ can be mapped into tactile display space ${}^{D}(x,y)_C$, such that the tactile display space is entirely contained inside the tactile sensor space, Fig. 5.3-C.

The respective micro-vibrators that are relevant for the generation of the phantom tactile illusion at time instant t are simultaneously activated for the stimuli duration τ_d and their relative vibration intensities are regulated in accordance with the location of the contact location in tactile display space ${}^{D}(x,y)_C$. For this reason, all actuators are assigned local activation functions $A_n({}^{D}x_C, {}^{D}y_C)$ of the form:

$$A_n({}^{D}x_C, {}^{D}y_C) = \alpha + \beta \times a_n({}^{D}x_C, {}^{D}y_C) \text{ for } n \in 1, ..., N_A, \tag{5.1}$$

where α is the PWM duty offset that increases/ decreases the absolute micro-vibrator intensity in accordance with the individual's sensation level [20], β is the PWM duty ratio that scales the variation of the micro-vibrator intensity, a_n is the activation ratio to control the generation of phantom tactile illusions, and N_A is the total number of available actuators. Note that $a_n \leq 1$.

The activation ratio $a_n(t)$ is a logarithmic function. This definition goes back to the research of Alles [35], Lee [38] and Park [30], however, has been adopted and modified for the use in this thesis. Precisely, the modifications restrict the functions to local activity in a larger actuator array such that only the surrounding actuators exhibit activity. For example, in case the locations of the contact centroid and one actuator coincided, the respective actuator was fully activated ($a_n = 1$), while the others were fully deactivated.

As a result, the actuator activation, i.e. the vibration intensity that is controlled by the PWM duty cycle ratio, and therefore the stimulus intensity is scaled depending on the location of the centroid ${}^{D}(x,y)_C$ in relation to the location of the surrounding actuators ${}^{D}(x,y)_{A_n}$ inside the actuator array:

$$\begin{aligned} a_n({}^{D}x_C, {}^{D}y_C) = \mathbf{max}\left[1 - \left(\frac{\log_2(|{}^{D}x_C - {}^{D}x_{A_n}| + 1)}{\log_2({}^{D}d_x + 1)}\right)^{s_x}, 0\right] \\ \times \mathbf{max}\left[1 - \left(\frac{\log_2(|{}^{D}y_C - {}^{D}y_{A_n}| + 1)}{\log_2({}^{D}d_y + 1)}\right)^{s_y}, 0\right]. \end{aligned} \tag{5.2}$$

The parameters s_x, s_y are the shape factors of the activation function and d_x, d_y are the relative actuator distances. These parameters are constants and control the shape of the activation function depending on the geometry of the tactile display in x- and y-direction, respectively.

5.4 Experiments and User Studies

For the experimental evaluation, the control scheme implemented the *uSkin* tactile sensor module for collecting raw tactile sensor data, the in chapter 4 introduced algorithm *sequential tactile data compression* for the identification of well-defined contact centroids, and the tactile display fingertip module for the generation of micro-vibrations in accordance with the tactile input data. The overall system as described in the previous sections was deployed in a preliminary user study.

Briefly, users were asked to wear the tactile fingertip display on the index finger and to evaluate the perceived stimuli that were generated by the end-to-end projection in response to the incoming tactile sensor raw data. Figure 5.4 shows the experimental setup and an exemplary user evaluation.

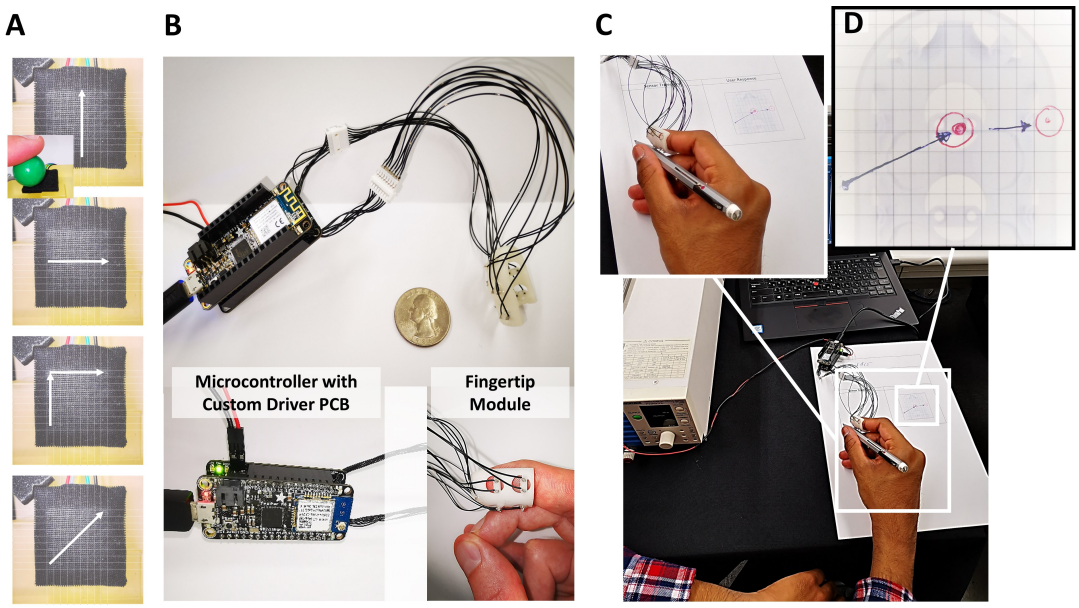

FIGURE 5.4: For the evaluation of the overall system, a Styrofoam™ sphere was rolled across the *uSkin* tactile sensor module resembling four representative contact trajectories (A). These contact trajectories were identified using the algorithm from chapter 4 and projected onto the skin of a human user using the tactile display fingertip module (B). The tactile display module was evaluated by asking the users to reproduce the perceived contact trajectory on an image of the fingertip module; red annotations mark perceived discontinuities (C, D).

To generate the tactile sensor input data, a small Styrofoam™ sphere ($Ø19.45mm$, $0.28g$) was manually moved across the *uSkin* tactile sensor module resembling four dynamic contact scenarios, Fig. 5.4-A. It was

assumed that the arbitrary rolling/slipping of the Styrofoam^{TM} sphere on the tactile sensor module is a meaningful model case for fine in-hand manipulation of a small object with index finger and thumb. The sampling frequency of the data collection was approx. $100Hz$, referred to as *uSkin* sampling frequency. The in chapter 4 introduced algorithm *sequential tactile data compression* was deployed to identify one contact centroid $K_C^{max} = 1$ with the coordinates ${}^{S}(x,y)_C(t)$ from the tactile sensor raw data at each time instant t, which enabled the sequential projection of these dynamic contact locations that sampled the true path of the Styrofoam^{TM} sphere on the sensor module.

The identified contact centroid coordinates ${}^{S}(x,y)_C(t)$ were linearly mapped into tactile display space coordinates ${}^{D}(x,y)_C(t)$. An activation function $A_n({}^{D}x_C, {}^{D}y_C)$ was defined for each of the eight SMA-based micro-vibrators (Eq. 5.1) to generate the quasi-dynamic phantom tactile illusions.

As it concerns the actuation of the tactile display module, the PWM-driver of the tactile display module was set to $f = 200Hz$ around which the sensitivity of the *Meissner* and *Pacinian* mechanoreceptors to vibratory signals is very high [24], [3]. The stimulus duration was set to $\tau_d = 35mSec$ and the inter-stimulus onset asynchrony τ_{SOA} was calculated to $58.5mSec$ [20] [21]. The tactile display actuators were driven at a PWM duty ratio of $\beta = 2.44\%$ resulting in a power consumption of approx. $180mW$ per actuator; in case fully activated.

Finally, the users were handed a sheet of grid paper depicting a top-view image of the tactile display fingertip prototype. Then, they were asked to draw a line that best described the perceived contact trajectory, Fig. 5.3. The users were also asked to annotate the direction of the moving contact and to mark any discontinuities on the same sheet of paper. Each dynamic contact trajectory was evaluated five times and presented in random order to two healthy users (male, mean age $29.5yrs$) amounting to 40 trials in total.

In a brief training session before the experiment, participants were made familiar with the experimental setup and procedure. Furthermore, it was assured that the fingertip module was worn correctly so that the users could perceive stimuli from all actuators. All the user responses were digitized, i.e., saved in terms of x- and y-coordinates to a *.csv*-file to allow for proper evaluation of the perceived contact trajectories.

5.5 Results and Discussion

Figures 5.5 shows the results of the real-time tactile image compression to a trajectory of contact centroids (A), the compression algorithm's performance (B), and the user evaluations of the perceived contact locations (C) for all the trajectories and over all trials. Columns refer to the above defined contact scenarios, i.e. the motion trajectory of the Styrofoam^{TM} sphere across the *uSkin* tactile sensor module's surface.

In detail, Figs. 5.5-A1 to A4 show the sequences of compressed contact locations ${}^{S}(x,y)_C(t)$ alongside their respective trajectory for each of the above defined contact scenarios (green markers). These contact centroid trajectories are the result of the sequential tactile contact area compression by means of the algorithm from chapter 4, which rendered the complete tactile sensor data as tactile image and compressed it into $K_C = 1$ contact centroid in real-time at each time instant t. The contact centroid trajectories are shown in comparison to the raw tactile sensor data over the complete time horizon.

Even though the tactile imprint, i.e. the contact area, of the Styrofoam^{TM} sphere was small, the data in Fig. 5.5-B1 to B4 reveals that up to 12 sensing points of the *uSkin* tactile sensor module were activated simultaneously at a single time instant, which amounts to 75% of the entire module's surface and was likely a result of the cross-talk between the sensing points. Thus, only after the compression of the tactile raw data into a discrete contact centroid with a well-specified location ${}^{S}(x,y)_C(t)$, the generation of phantom tactile illusion at a specified target location ${}^{D}(x,y)_C(t)$ in tactile display space became possible.

For the sake of completeness, Fig. 5.5-B depicts the performance of the algorithm throughout all the contact scenarios. Fig. 5.5-B emphasizes the need for compression of the raw data before the projection via tactile displays, as the number of sensor readouts that exceeded the contact threshold upon contact with an object increased quickly. Denser tactile sensor arrays would exacerbate this problem, as the contact area would cover a greater number of sensing points. In case of $K_C^{max} = 1$, the algorithm essentially performs a weighted center of mass computation to identify the sequence of contact locations for which reason the computation performance (CPU-bound) was very high and well above the *uSkin* sampling frequency.

Generally speaking, depending on the tactile sensor's resolution and

sensitivity, macro-geometric and micro-geometric object features are approximated by a number of sensing points of a tactile sensor module. In regard to the *uSkin*'s resolution and sensitivity (cf. chapter 1), only macro-geometric object features, i.e., rough contact imprints can be approximated by the array of sensing points (4×4-array, center-to-center distances are $4.7mm$). More complex contact features, i.e. detailed tactile imprints due to micro-geometric surface features, would require an even denser sensor array and modifications to the algorithm as mentioned in chapter 4. The algorithm *sequential tactile data compression*, however, generated an accurate and smooth contact trajectory as a sequence of compressed contact locations, which enabled the generation of phantom tactile illusion and, thus, the projection of contacts onto the skin of the human users by means of sparse actuator arrays.

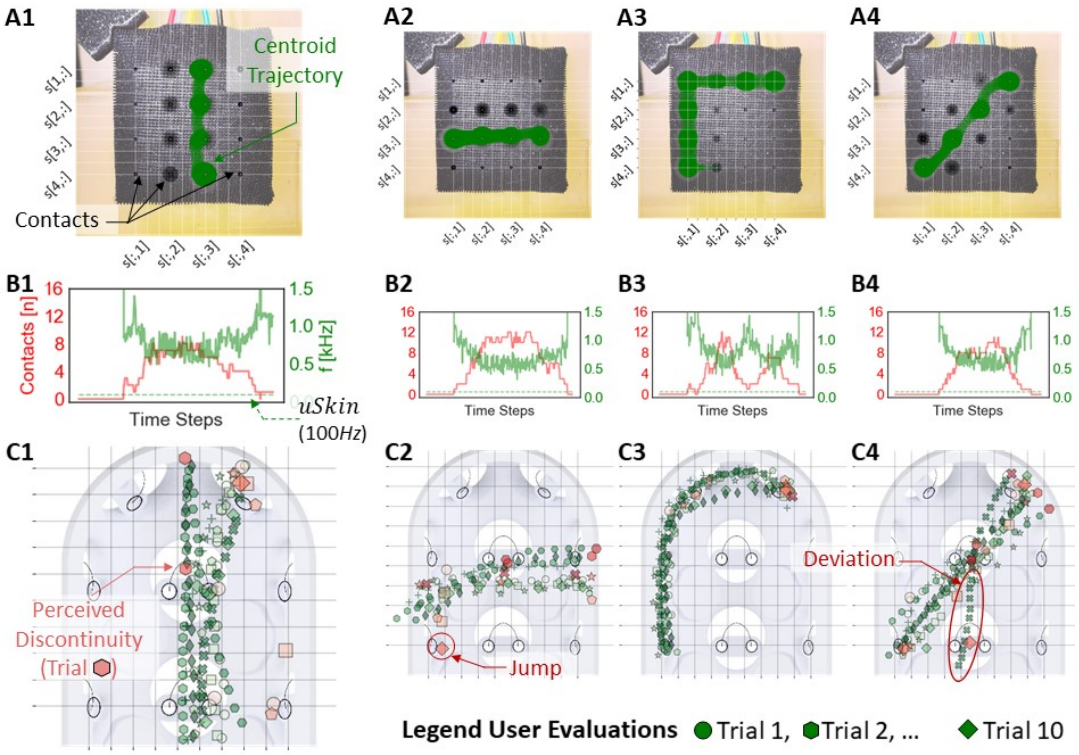

FIGURE 5.5: The contact trajectories were identified using the algorithm from chapter 4 for $K_C^{max} = 1$ (A1-A4). The total number of contacts and the algorithm speed of compressing the tactile data into a succession of compressed contact centroids are shown in comparison to the *uSkin* tactile sensor module sampling frequency for evaluation purposes (B1-B4). The user evaluations on the perceived contact locations are depicted (C1-C4), where each marker type represents one trial and red markers annotate discontinuities.

Finally, Fig. 5.5-C shows the digitized user responses on the perceived contact trajectories. The user responses show that the successions of compressed contact centroids were perceived as quasi-dynamic contact trajectories. Moreover, the perceived contact trajectories were in good agreement with the actual contact trajectories of the rolling Styrofoam^{TM} sphere on the *uSkin* tactile sensor module in most of the cases (Fig. 5.5-A).

Yet, the projection of contact trajectories *A2* and *A4* exhibited partially considerable *deviations* from the true contact trajectory, Fig. 5.5-C2 and C4. It is assumed that these deviations originated from the irregular skin contact of the actuator that could vary dynamically when moving the finger inside the module, thus, could have caused the curved contact trajectory projection in Fig. 5.5-C1. This effect is also believed to have caused *jumps* in the contact projection, i.e. temporary irregularities in the projection of the tactile phantom due to the wiggling of the fingertip inside the module back and forth causing a brief change in contact intensity.

The perceived *discontinuities* (annotated in red), however, mark the temporary destruction of the phantom tactile illusion and occurred at the actuator locations (Fig. 5.5-C2) and around the center between actuators (Fig. 5.5-C4). While this might be caused by the relative motion between fingertip skin and tactile actuator, it is more likely that the actuator locations ${}^{D}(x,y)_{A_n}$ in combination with the assigned local activation functions $A_n({}^{D}x_C, {}^{D}y_C)$ caused a decrease of the vibration intensity below the sensation level; specifically when the contact centroid approached the center between actuators followed by a sudden increase above the sensation level when the contact centroid approached the vicinity of an actuator. This effect is exacerbated by the very restricted actuator output range of the SMA-based micro-vibrator, since it prevents from driving the display well beyond the sensation level [20], thus making the generation of phantom tactile illusions less accurate and robust.

Albeit the conducted user study comprised only two different users and must be regarded as preliminary with limited conclusiveness, the results were sufficient to identify technical limitations of the presented tactile display module and were in agreement with recent studies on the control of tactile displays implementing sparse actuator arrays for the use in virtual reality applications [38], [30], [31]. Hence, before conducting larger user studies, the identified limitations are worth addressing in future prototype versions.

Concretely, the foremost important limitation revealed to be the mechanical design of the fingertip module as a rigid 3D-printed module. A compliant silicone structure carrying separated micro-vibrator modules would allow for a widely regular contact between fingertip skin and SMA wire, therefore would alleviate the above mentioned problem of irregular skin contact of the actuators that was associated with the perceived deviations, discontinuities, and jumps in the phantom tactile illusion.

In this regard, equidistant spaces in the actuator array or the selective activation of a set of three actuators surrounding the contact centroid location may increase the accuracy of the projected phantom illusion [28] [21]. This is in contrast to the overall activation across all local activation functions that might cause discontinuities in the resulting hyperplane that describes the activation across the entire actuator array.

Another important limitation was the rather narrow actuator output range of the SMA-based micro-vibrator that limits the generation of variable, yet perceivable vibration stimuli for the projection of phantom tactile illusions. This issue might be addressed by controlling the peak current flowing through the SMA wire instead of the PWM duty ratio, because the impulse against the skin that is generated when the SMA wire heats up and shrinks depends directly on the amount of the injected electrical power [99].

Despite the above discussed limitations, the user responses suggest that the momentaneous contact location and eventually the complete contact trajectory could be effectively projected with an overall good level of accuracy and robustness in real-time and with a very compact device design. Due to the sparsity of the actuator array, the power consumption and space requirements are lower compared to a dense implementation of actuators of the same type, which was achieved by quasi-dynamic phantom tactile sensations that enable tactile feedback on the object's location and its trajectory across the fingertip with relative actuator distances beyond the two-point-orientation threshold [22].

Apart from the distortions of the phantom tactile illusion due to the above mentioned effects, recent research [20] [28] [40] [29] [31] [32] [21] and the obtained results clearly advocate the proposed approach that uses end-to-end projection of tactile data to enable tactile feedback by means of tactile illusions for the use in human-robot interaction applications.

In this regard, the exact positioning of a virtual phantom actuator,

therefore the exact projection of a contact location is theoretically possible, but the achievable accuracy will ultimately depend on practical factors, such as the density of tactile display actuators, their stimuli production range, and the relative contact between the user's skin and the actuators. For this reason, the design of the tactile display actuator array must be a compromise between the desired application performance, the availability of space and energy, and the body site [41].

Using a sparse actuator array in combination with tactile illusions poses limitations on the instantaneous projection of detailed, micro-geometric surface features, e.g. the tactile imprint of a thread of a screw (cf. [55]). This is because tactile illusions require the timely succession of spatially distributed tactile stimuli, which restricts the achievable complexity of the simultaneous projection of an object's micro-geometric surface features. However, bearing the biological limits of the human touch in mind [23] [24] [3], the two-point-orientation threshold [22] seems a good candidate for the lower limit of the actuator implementation density.

For the efficient projection of micro-geometric surface features, future research should be directed towards the incorporation of the algorithm from chapter 3, which yields the prospect of realizing projected contact trajectories that exhibit textural properties.

5.6 Chapter Summary

This chapter implemented the initially outlined thesis objectives 1.3 of a compact and wearable tactile display into a fingertip module that uses end-to-end tactile data projections and tactile illusory phenomena to project contact information onto the skin of a human user. The module integrates eight energy-dense SMA micro-vibrators into a 3D-printed package with relative actuator distances of approx. 9-14mm, i.e. a very sparse actuator distribution. For this reason and due to the optimization for the use of tactile illusions, it is compared to the in chapter 1 reviewed tactile displays very space (0.35×0.25 cm per actuator) and energy (approx. $180mW$/actuator) conserving.

The tactile fingertip display module prototype was successfully tested in a preliminary user study: Several representative contact trajectories of an object that moved across a *uSkin* tactile sensor module were transmitted to human users by deploying the algorithm from chapter 4 that enabled the

quasi-dynamic, consecutive projection of compressed contact locations by means of tactile illusions. Hence, the proposed human-machine interface solves the unknown transformation from tactile sensor space to tactile actuator space and utilizes tactile illusions to mitigate limitations of tactile display actuators in terms of energy consumption and actuator density.

In this respect, the developed fingertip module exhibits similar limitations as described in the previous chapters: The projection of tactile stimuli using SMA-based micro-vibrators is limited to a subset of perceivable tactile stimuli, excluding static protrusion, shear, and heat flux. Moreover, the generation of accurate and robust tactile illusions is still a matter of research: The experiments on the feedback of moving contact patterns revealed inconsistencies in the perceived stimuli with respect to the desired contact trajectory due to the SMA-based actuator's limited range of producible stimulus intensities and relative movements between finger pad and display module that caused irregular contacts, and in turn, the degradation of the tactile illusions.

However, the experiments on both the hard- and software components have shown that the proposed data-driven tactile feedback system effectively utilizes end-to-end tactile data projections to efficiently convey physical contact information in real-time from tactile sensor data.

Future research should address improvements on the accuracy and robustness of tactile illusions by the use of compliant actuator arrays for uniform and steady skin contact and by increasing the perceivable output range of the SMA-based micro-vibrators, e.g. by implementing a controller that regulates the current amplification. The incorporation of the algorithm from chapter 3 yields the prospect of the combined projection of textural properties in addition to the contact location projection for richer tactile feedback.

Chapter 6

Conclusion

The sense of touch enables humans to perform a great variety of exploration and manipulation tasks in the real world [1] [2] [3] [4] [5]. Tactile information therefore constitutes a key sensory channel that is especially important in unstructured environments. Thus, tactile sensor skin has been widely adopted in robot design and control [9] [6] [10] [7]. The integration of distributed tactile sensors enables information-rich feedback from the robot's environment and makes robot manipulators increasingly capable of dexterous object manipulation and even active (tactile) exploration. For this reason, not only modern industrial robots but especially emerging robot applications like social and service robots benefit from the deployment of anthropomorphic, dexterous robot hands, because they exhibit higher manipulation capabilities, a higher flexibility, and in turn, possess a tremendous potential for versatile, human-like interaction with the physical world [58] [59] [60] [57] [61] [62].

However, in human-centered applications, e.g., robot-teleoperation or human-robot interaction, this massive sensor data must be projected to the skin of a human operator in order to create meaningful, yet efficient tactile feedback that allows either for highly-efficient teleoperation of the robot or for tactile immersion while using the robot [92] [83] [84] [15] [16] [4] [5].

This final chapter revisits the major milestones in the hard- and software development of a data-driven tactile display module that implements end-to-end sensor data projections and addresses the establishment of the tactile information flow from massive tactile sensor data to wearable human-machine interfaces with respect to the design and transduction principles of the deployed tactile sensors and tactile actuators as integral part of any technical tactile feedback loop.

The presented algorithms for the implicit or compressed representation of tactile sensor data allow for the generation of carefully orchestrated

spatio-temporal actuation patterns that allow for mapping from the tactile sensor space to the actuator driving space for efficient, yet intuitive end-to-end tactile stimuli generation, i.e. the conveyance of macro-geometric (locations of contact) and micro-geometric (properties of surface) contact information. Finally, this chapter outlines directions of future research to address the current limitations of the proposed tactile feedback framework.

6.1 Contributions and Limitations

Chapter 1 laid the groundwork to this thesis: First, insight into the mechanisms of tactile stimuli perception and an extensive overview over tactile technologies and the application to (anthropomorphic) robot manipulators were provided. Secondly, the benefits and drawbacks of existing tactile feedback systems with the focus on tactile sensors, tactile displays and tactile recognition algorithms in the domain of anthropomorphic robots were summarized and evaluated. The end of chapter 1 outlined the objectives of the development of a novel data-driven tactile display module that used end-to-end tactile data projections and illusory tactile sensations to mitigate space and energy restrictions of the tactile display hardware that implemented shape memory alloy (SMA)-based actuators.

Chapter 2 introduced the complete system architecture for the experimental design and evaluation of the proposed data-driven tactile feedback system together with the associated software algorithms for end-to-end tactile data projection. The system architecture involved the anthropomorphic *Allegro* robot hand covered with *uSkin* tactile sensor modules, a host PC running resource-intensive algorithms on the tactile data, a compact WiFi-enabled microcontroller unit that calculated resulting spatio-temporal actuation patterns, an I^2C-enabled custom-made tactile display driver circuit for the generation of pulsed current signals, and shape memory alloy-based tactile display prototypes to create vibro-mechanical stimuli on the human skin. Even though soft- and hardware developments evolved throughout the experimental trials, Chapter 2 also reviewed fundamental design and operational principles and thereby characterized the potential applications and inherent limitations of the proposed tactile feedback system. An important *a priori* limitation in using SMA-based

micro-vibrators is the restriction to dynamic vibrations, i.e. only a subset of required tactile stimulus modes to resemble the sense of touch, and the absence of proprioceptive feedback, i.e. stimuli that inform the brain on dynamic positioning/loading of articulated body segments. The SMA-based micro-vibrator could generate mechanical vibrations perceived by the *Meissner* and *Pacinian* corpuscles and therefore could convey information on the textural properties of distributed contacts that is majorly important for in-hand manipulation. The realization of sustained pressure (*Merkel*), skin shear (*Ruffini*) or proprioceptive feedback, however, would necessitate a different embodiment of the actuator or the complementation with a different actuator as discussed in chapters 1 and 2.

Chapter 3 described the algorithm of *end-to-end tactile texture projection* in psycho-physically meaningful latent space coordinates. This algorithm deployed a deep gated recurrent unit-based autoencoder (GRU-AE) to capture the perceptual dimensions of tactile textures in latent space coordinates that coincided with the psychophysical layer of human material perception. The auto-compression of tactile sensor data enabled an end-to-end mapping from tactile sensor data to tactile actuator driving signal by modulating the tactile display actuator driving signal in accordance with the latent space coordinates. The approach was experimentally verified by evaluating the prediction performance of the GRU-AE on seen and unseen tactile data that were gathered during active tactile exploration of objects commonly encountered in daily living using a *uSkin* tactile sensor module. Additionally, a user study on a custom-made tactile display was conducted in which real tactile perceptions in response to active tactile object exploration were compared to the emulated tactile feedback using the proposed GRU-AE approach. The algorithm was able to drive the first prototype of a custom-made tactile display module and generated convincing tactile stimuli even for new, unseen textures alone from the *uSkin* tactile sensor readouts. The results suggested that the GRU-AE, or AE approaches in general, may allow for finding an end-to-end mapping between tactile sensor and tactile display space over a wide range of tactile sensor and actuator combinations. However, the specifics of tactile sensor and tactile display must be accounted for, because their respective hardware limitations in capturing and projecting relevant surface features immediately impact the quality and integrity of the tactile perception. Finally, another important limitation was the pre-definition of the moving

contact pattern in order to emulate the sensation of moving object surfaces with a variety of different textural properties.

Chapter 4 introduced *Sequential Tactile Data Clustering for Tactile Image Compression*, which resolved the dimensional mismatch between tactile sensor space and tactile display space by performing two stages of *K*-means++ clustering on the raw tactile sensor data at each time instant. This dynamic compression is almost always necessary, either due to technical limitations of the deployed tactile display, or for reasons specific to the application, e.g. in prosthetics where the tactile sensation must be reproduced on another body part with different mechanoreceptor density. The algorithm compresses the tactile sensor data into a number of discrete contact locations and stimuli intensities to match the tactile display specifications. In this manner, the compressed tactile data preserves its physical meaning and enables direct adaptive feedback by means of tactile illusions. The algorithm was experimentally verified within an extensive parameter study by evaluating the original and compressed tactile data that was gathered during the active tactile exploration of several objects of daily living by the *Allegro* robot hand that was covered with 15 *uSkin* tactile sensor modules providing 240 x, y, z-axis force vector measurements at each time instant. Since *K*-means++ clustering is an iterative algorithm, chapter 4 also discussed multiprocessing-implementations to alleviate the speed problem that may become problematic in very large-scale applications due to the iterative nature of the algorithm. *Sequential Tactile Data Clustering for Tactile Image Compression* allows for the direct feedback from massive tactile sensor data for a broad variety of tactile sensors and tactile displays, thereby, enables the compressed yet intuitive representation of massive tactile sensor information for real-time applications. Furthermore, the algorithm produces discrete contact points of varying intensity, which could be combined with the algorithm from chapter 3 to give contact points textural properties.

Chapter 5 was concerned with the integration of the system architecture as introduced in chapter 2, 3, and 4 into a compact and wearable human-machine interface. Chapter 5 was therefore more application-oriented and described the mechanical (wearable fingertip module) and electronic (compact PCB of the I^2C-enabled driver circuit) implementation of the system components with optimized wiring into a compact, ergonomic fingertip module. As a result, chapter 5 arrived at a novel, scalable tactile fingertip module that successfully implements the in

chapters 1 and 2 initially outlined design paradigms. The proposed human-machine interface solves the unknown transformation from tactile sensor space to tactile actuator space and utilizes tactile illusions to mitigate limitations of tactile display actuators in terms of energy consumption and actuator density. In this respect, the developed fingertip module exhibits similar limitations as described in the previous chapters, i.e., the projection of tactile stimuli using SMA-based micro-vibrators is limited to a subset of perceivable tactile stimuli, excluding static protrusion, shear, and heat flux. Moreover, the generation of robust tactile illusions in wearable devices is still a matter of research and, indeed, the results of the user experiments confirmed partial integrity losses of the perceived stimuli yielding the need for further design improvements. However, the experiments on both the hard- and software components have shown that the proposed data-driven tactile feedback system utilizes end-to-end tactile data projections effectively to convey locations of contact and micro-geometric surface properties; which undoubtedly is very useful for teleoperation and human-robot interaction.

6.2 Future Work

The contribution of this thesis lies in the introduction of a novel data-driven tactile feedback system that uses generally applicable end-to-end tactile data projections and illusory tactile sensations to mitigate space and energy restrictions and therefore exhibits highest scalability in a compact form factor. The tactile feedback system was implemented into a compact, wearable fingertip module with WiFi- and I^2C-interface and was experimentally verified in user studies that confirmed the capability of generating convincing tactile stimuli of moving contact points with varying textural properties from raw tactile sensor data in an end-to-end manner.

For a greater coverage of perceivable stimulus modalities, the deployment of merely one type of actuator (embodiment) is not sufficient. Further developments should be directed towards the integration of heat flux feedback and the complementation of the cutaneous feedback with kinesthetic feedback, i.e., the implementation of actuators that target the proprioceptive receptors in the joints and muscles of articulating body segments. As it concerns the former, the developments of the presented tactile feedback module have been accompanied by the development of a

data-driven thermoelectric actuator for heat flux generation [122]. This thermoelectric actuator uses a custom control circuit to generate PWM-signals that drive a compact *Peltier* element for the generation of positive or negative heat fluxes. Since the developments of both the tactile display modules have been coordinated and carried out together, they allow for the rapid integration into the existing fingertip module from chapter 5.

The implementation of kinesthetic feedback, on the other side, requires actuators with greater power output in order to resemble the sensations of variable resistances when statically holding or dynamically moving objects. The implementation of kinesthetic feedback into the presented wearable system would overall benefit from the small form factor and low energy consumption (approx. $180mW$/actuator) of the SMA-based tactile display and is ultimately required to increase the range of achievable tactile stimuli. One conceivable solution would be a parallel-link manipulator that moves the presented tactile display module relative to the finger pad and thereby creates mechanical protrusion and shear forces. Recently, Lim *et al.* [101] have demonstrated that SMA-based actuators could be deployed to enable such a combined design.

Due to the need for extensive experimental testing and debugging, the algorithms that enabled the data projections were run on a host PC (Intel(R) Core(TM) i7-8700K CPU @ 3.70GHz and 32.0GB RAM) with GPU (GeForce GTX 1080 Ti with 11 GB frame buffer). In this respect, another rather practical step, should be the migration of the algorithms to mobile, embedded computing boards with GPU, e.g. the *Nvidia Jetson Family*, which is currently in progress. In this context, the overall system integration with the *Cyberglove* and the *Allegro* robot hand for closed-loop robot-teleoperation and extensive field testing poses the next logical challenge. Due to the compactness and modularity of the developed hard- and software, several fingertip modules, e.g. four tactile display modules matching the four fingertips of the *Allegro* robot hand, could be integrated into a glove like wearable device that covers the finger tips of an operator and thus allows for being simultaneously worn with the *Cyberglove*.

Bibliography

[1] C. Pacchierotti, *Cutaneous Haptic Feedback in Robotic Teleoperation*. Jan. 2015, ISBN: 978-3-319-25457-9. DOI: 10.1007/978-3-319-25457-9.

[2] H. Culbertson, S. Schorr, and A. Okamura, "Haptics: The present and future of artificial touch sensation", *Annual Review of Control, Robotics, and Autonomous Systems*, vol. 1, no. 1, pp. 385–409, 2018. DOI: 10.1146/annurev-control-060117-105043.

[3] M. Park, B.-G. Bok, J.-H. Ahn, and M.-S. Kim, "Recent advances in tactile sensing technology", *Micromachines*, vol. 9, no. 7, 2018, ISSN: 2072-666X. DOI: 10.3390/mi9070321. [Online]. Available: https://www.mdpi.com/2072-666X/9/7/321.

[4] I. E. Rassi and J.-M. E. Rassi, "A review of haptic feedback in tele-operated robotic surgery", *Journal of Medical Engineering & Technology*, vol. 44, no. 5, pp. 247–254, 2020, PMID: 32573288. DOI: 10.1080/03091902.2020.1772391. eprint: https://doi.org/10.1080/03091902.2020.1772391. [Online]. Available: https://doi.org/10.1080/03091902.2020.1772391.

[5] C. Huang, Q. Wang, M. Zhao, C. Chen, S. Pan, and M. Yuan, "Tactile perception technologies and their applications in minimally invasive surgery: A review", *Frontiers in Physiology*, vol. 11, p. 1601, 2020, ISSN: 1664-042X. DOI: 10.3389/fphys.2020.611596. [Online]. Available: https://www.frontiersin.org/article/10.3389/fphys.2020.611596.

[6] Z. Kappassov, J. A. Corrales, and V. Perdereau, "Tactile sensing in dexterous robot hands -— review", *Robotics and Autonomous Systems*, vol. 74, pp. 195–220, 2015.

[7] Q. Li, O. Kroemer, Z. Su, F. F. Veiga, M. Kaboli, and H. J. Ritter, "A review of tactile information: Perception and action through touch", *IEEE Transactions on Robotics*, vol. 36, no. 6, pp. 1619–1634, 2020. DOI: 10.1109/TRO.2020.3003230.

[8] G. Westling and R. Johansson, "Factors influencing the force control during precision grip", *Experimental brain research. Experimentelle Hirnforschung. Expérimentation cérébrale*, vol. 53, pp. 277–84, Feb. 1984. DOI: 10.1007/BF00238156.

[9] R. S. Dahiya, G. Metta, M. Valle, and G. Sandini, "Tactile sensing—from humans to humanoids", *IEEE Transactions on Robotics*, vol. 26, no. 1, pp. 1–20, 2010.

[10] C. Piazza, G. Grioli, M. Catalano, and A. Bicchi, "A century of robotic hands", *Annual Review of Control, Robotics, and Autonomous Systems*, vol. 2, no. 1, pp. 1–32, 2019. DOI: 10.1146/annurev-control-060117-105003.

[11] C. Pacchierotti, S. Sinclair, M. Solazzi, A. Frisoli, V. Hayward, and D. Prattichizzo, "Wearable haptic systems for the fingertip and the hand: Taxonomy, review, and perspectives", *IEEE Transactions on Haptics*, vol. 10, no. 4, pp. 580–600, Oct. 2017, ISSN: 1939-1412. DOI: 10.1109/TOH.2017.2689006.

[12] C. Pacchierotti, D. Prattichizzo, and K. J. Kuchenbecker, "Displaying sensed tactile cues with a fingertip haptic device", *IEEE Transactions on Haptics*, vol. 8, no. 4, pp. 384–396, 2015. DOI: 10.1109/TOH.2015.2445770.

[13] T. Sheridan, "Telerobotics", *Automatica*, vol. 25, no. 4, pp. 487 –507, 1989, ISSN: 0005-1098. DOI: https://doi.org/10.1016/0005-1098(89)90093-9. [Online]. Available: http://www.sciencedirect.com/science/article/pii/0005109889900939.

[14] W. McMahan, J. Gewirtz, D. Standish, P. Martin, J. A. Kunkel, M. Lilavois, A. Wedmid, D. I. Lee, and K. J. Kuchenbecker, "Tool contact acceleration feedback for telerobotic surgery", *IEEE Transactions on Haptics*, vol. 4, no. 3, pp. 210–220, 2011. DOI: 10.1109/TOH.2011.31.

[15] Z. Quek, W. Provancher, and A. Okamura, "Evaluation of skin deformation tactile feedback for teleoperated surgical tasks", *IEEE Transactions on Haptics*, vol. PP, pp. 1–1, Oct. 2018. DOI: 10.1109/TOH.2018.2873398.

[16] A. Abiri, J. Pensa, A. Tao, J. Ma, Y. Juo, S. J. Askari, J. Bisley, J. E. Rosen, E. P. Dutson, and W. S. Grundfest, "Multi-modal haptic feedback for grip force reduction in robotic surgery", *Sci Rep*, vol. 9, pp. 1–1, Oct. 2019. DOI: 10.1038/s41598-019-40821-1.

[17] C. Pacchierotti, E. M. Young, and K. J. Kuchenbecker, "Task-driven pca-based design optimization of wearable cutaneous devices", *IEEE Robotics and Automation Letters*, vol. 3, no. 3, pp. 2214–2221, 2018. DOI: 10.1109/LRA.2018.2810953.

[18] C. Pacchierotti, D. Prattichizzo, and K. Kuchenbecker, "Cutaneous feedback of fingertip deformation and vibration for palpation in robotic surgery", *IEEE transactions on bio-medical engineering*, vol. 63, Jul. 2015. DOI: 10.1109/TBME.2015.2455932.

[19] G. Huisman, A. Darriba Frederiks, B. van Dijk, B. Krose, and D. Heylen, "Self touch to touch others: Designing the tactile sleeve for social touch", in *TEI 13: Seventh International Conference on Tangible, Embedded and Embodied Interaction*, ser. 5, Universitat Pompeu Fabra, vol. 4, Barcelona, Spain, Feb. 2017, p. 213.

[20] A. Israr and I. Poupyrev, "Tactile brush: Drawing on skin with a tactile grid display", in *Proceedings of the SIGCHI Conference on Human Factors in Computing Systems*, ser. CHI '11, Association for Computing Machinery, 2011, 2019–2028, ISBN: 9781450302289. DOI: 10.1145/1978942.1979235. [Online]. Available: https://doi.org/10.1145/1978942.1979235.

[21] S. Baik, I. Han, J. Park, and J. Park, "Multi-fingertip vibrotactile array interface for 3d virtual interaction", in *2020 IEEE Haptics Symposium (HAPTICS)*, 2020, pp. 898–903. DOI: 10.1109/HAPTICS45997.2020.ras.HAP20.5.08241ef4.

[22] J. Tong, O. Mao, and D. Goldreich, "Two-point orientation discrimination versus the traditional two-point test for tactile spatial acuity assessment", *Frontiers in human neuroscience*, vol. 7, p. 579, Sep. 2013. DOI: 10.3389/fnhum.2013.00579.

[23] A. Zimmerman, L. Bai, and D. Ginty, "The gentle touch receptors of mammalian skin", *Science (New York, N.Y.)*, vol. 346, pp. 950–4, Nov. 2014. DOI: 10.1126/science.1254229.

[24] H. Kajimoto, M. Konyo, and S. Saga, *Pervasive haptics: Science, design, and application*. Springer, Jan. 2016, pp. 1–306. DOI: 10.1007/978-4-431-55772-2.

[25] S. Carl, "The psychology of touch", in. Psychology Press, 1991, ch. Vibrotactile Pattern Perception: Some Findings and Applications.

[26] R. Klatzky, S. Lederman, C. Hamilton, M. Grindley, and R. Swendsen, "Feeling textures through a probe: Effects of probe and surface geometry and exploratory factors", *Perception & psychophysics*, vol. 65, pp. 613–31, Jun. 2003. DOI: 10.3758/BF03194587.

[27] K. Fukuyama, N. Takahashi, F. Zhao, and H. Sawada, "Tactile display using the vibration of sma wires and the evaluation of perceived sensations", in *2009 2nd Conference on Human System Interactions*, May 2009, pp. 685–690. DOI: 10.1109/HSI.2009.5091060.

[28] J. Park, J. Kim, Y. Oh, and H. Z. Tan, "Rendering moving tactile stroke on the palm using a sparse 2d array", in *Haptics: Perception, Devices, Control, and Applications*, F. Bello, H. Kajimoto, and Y. Visell, Eds., Cham: Springer International Publishing, 2016, pp. 47–56, ISBN: 978-3-319-42321-0.

[29] J. V. Salazar Luces, K. Okabe, Y. Murao, and Y. Hirata, "A phantom-sensation based paradigm for continuous vibrotactile wrist guidance in two-dimensional space", *IEEE Robotics and Automation Letters*, vol. 3, no. 1, pp. 163–170, 2018. DOI: 10.1109/LRA.2017.2737480.

[30] G. Park and S. Choi, "Tactile information transmission by 2d stationary phantom sensations", Apr. 2018, pp. 1–12. DOI: 10.1145/3173574.3173832.

[31] G. Yun, S. Oh, and S. Choi, "Seamless phantom sensation moving across a wide range of body", in *2019 IEEE World Haptics Conference (WHC)*, 2019, pp. 616–621. DOI: 10.1109/WHC.2019.8816104.

[32] B. Dandu, Y. Shao, A. Stanley, and Y. Visell, "Spatiotemporal haptic effects from a single actuator via spectral control of cutaneous wave propagation", in *2019 IEEE World Haptics Conference (WHC)*, 2019, pp. 425–430. DOI: 10.1109/WHC.2019.8816149.

[33] H. E. Burtt, "Tactual illusions of movement", *Journal of Experimental Psychology*, vol. 2, no. 5, pp. 371–385, 1917. DOI: 10.1037/h0074614.

[34] G. v. Békésy, "Sensations on the skin similar to directional hearing, beats, and harmonics of the ear", *The Journal of the Acoustical Society of America*, vol. 29, no. 4, pp. 489–501, 1957. DOI: 10.1121/1.1908938.

[35] D. S. Alles, "Information transmission by phantom sensations", *IEEE Transactions on Man-Machine Systems*, vol. 11, no. 1, pp. 85–91, Mar. 1970, ISSN: 2168-2860. DOI: 10.1109/TMMS.1970.299967.

[36] J. H. Kirman, "Tactile apparent movement: The effects of interstimulus onset interval and stimulus duration.", *Perception and Psychophysics*, vol. 15, pp. 1–6, 1974. DOI: 10.3758/BF03205819.

[37] C. Sherrick and R. Rogers, "Apparent haptic movement.", *Perception and Psychophysics*, vol. 1, pp. 175–180, 1966.

[38] J. Lee, Y. Kim, and G. Jounghyun Kim, "Rich pinch: Perception of object movement with tactile illusion", *IEEE Transactions on Haptics*, vol. 9, no. 1, pp. 80–89, 2016. DOI: 10.1109/TOH.2015.2475271.

[39] J. Kim, Y. Oh, and J. Park, "Adaptive vibrotactile flow rendering of 2.5d surface features on touch screen with multiple fingertip interfaces", in *2017 IEEE World Haptics Conference (WHC)*, 2017, pp. 316–321. DOI: 10.1109/WHC.2017.7989921.

[40] S. Zhao, A. Israr, M. Fenner, and R. L. Klatzky, "Intermanual apparent tactile motion and its extension to 3d interactions", *IEEE Transactions on Haptics*, vol. 10, no. 4, pp. 555–566, 2017. DOI: 10.1109/TOH.2017.2678502.

[41] H. Elsayed, M. Weigel, F. Müller, M. Schmitz, K. Marky, S. Günther, J. Riemann, and M. Mühlhäuser, "Vibromap: Understanding the spacing of vibrotactile actuators across the body", *Proc. ACM Interact. Mob. Wearable Ubiquitous Technol.*, vol. 4, no. 4, Dec. 2020. DOI: 10.1145/3432189. [Online]. Available: https://doi.org/10.1145/3432189.

[42] J. Fishel and G .Loeb, "Bayesian exploration for intelligent identification of textures", *Frontiers in Neurorobotics*, vol. 6, p. 4, 2012, ISSN: 1662-5218. DOI: 10.3389/fnbot.2012.00004. [Online]. Available: https://www.frontiersin.org/article/10.3389/fnbot.2012.00004.

[43] *Shadow Robot Company Shadow Dexterous Hand^{TM}*. https://www.shadowrobot.com/products/dexterous-hand, Accessed: 2020-06-19.

[44] T. P. Tomo, M. Regoli, A. Schmitz, L. Natale, H. Kristanto, S. Somlor, L. Jamone, G. Metta, and S. Sugano, "A new silicone structure for uskin—a soft, distributed, digital 3-axis skin sensor and its integration on the humanoid robot icub", *IEEE Robotics and Automation Letters*, vol. 3, no. 3, pp. 2584–2591, 2018. DOI: 10.1109/LRA.2018.2812915.

[45] A. Geier, G. Yan, T. P. Tomo, S. Ogasa, S. Somlor, A. Schmitz, and S. Sugano, "Sequential clustering for tactile image compression to enable direct adaptive feedback", in *2019 IEEE/RSJ International Conference on Intelligent Robots and Systems (IROS)*, 2019, pp. 8117–8124. DOI: 10.1109/IROS40897.2019.8968493.

[46] D. Ma, E. Donlon, S. Dong, and A. Rodriguez, "Dense tactile force estimation using gelslim and inverse fem", May 2019, pp. 5418–5424. DOI: 10.1109/ICRA.2019.8794113.

[47] M. Lambeta, P.-W. Chou, S. Tian, B. Yang, B. Maloon, V. R. Most, D. Stroud, R. Santos, A. Byagowi, G. Kammerer, and et al., "Digit: A novel design for a low-cost compact high-resolution tactile sensor with application to in-hand manipulation", *IEEE Robotics and Automation Letters*, vol. 5, no. 3, 3838–3845, Jul. 2020, ISSN: 2377-3774. DOI: 10.1109/lra.2020.2977257. [Online]. Available: http://dx.doi.org/10.1109/LRA.2020.2977257.

[48] *SynTouch Inc. Resource & Download*, https://syntouchinc.com/wp-content/uploads/2017/01/BioTac-Brochure.pdf, Accessed: 2020-06-19.

[49] N. Wettels and G. E. Loeb, "Haptic feature extraction from a biomimetic tactile sensor: Force, contact location and curvature", in *2011 IEEE International Conference on Robotics and Biomimetics*, 2011, pp. 2471–2478. DOI: 10.1109/ROBIO.2011.6181676.

[50] M. Kaboli, R. Walker, and G. Cheng, "Re-using prior tactile experience by robotic hands to discriminate in-hand objects via texture properties", May 2016, pp. 2242–2247. DOI: 10.1109/ICRA.2016.7487372.

[51] *Barrett^{TM} Advanced Robotics BarrettHand^{TM}*, https://advanced.barrett.com/barretthand, Accessed: 2020-06-19.

[52] *Wonik Robotics Allegro Hand*, http://www.simlab.co.kr/Allegro-Hand.htm, Accessed: 2020-06-19.

[53] T. P. Tomo, A. Schmitz, W. K. Wong, H. Kristanto, S. Somlor, J. Hwang, L. Jamone, and S. Sugano, "Covering a robot fingertip with uskin: A soft electronic skin with distributed 3-axis force sensitive elements for robot hands", *IEEE Robotics and Automation Letters*, vol. 3, no. 1, pp. 124–131, 2018. DOI: 10.1109/LRA.2017.2734965.

[54] S. Funabashi, G. Yan, A. Geier, A. Schmitz, T. Ogata, and S. Sugano, "Morphology-specific convolutional neural networks for tactile object recognition with a multi-fingered hand", in *2019 International Conference on Robotics and Automation (ICRA)*, 2019, pp. 57–63.

[55] E. Donlon, S. Dong, M. Liu, J. Li, E. Adelson, and A. Rodriguez, "Gelslim: A high-resolution, compact, robust, and calibrated tactile-sensing finger", in *2018 IEEE/RSJ International Conference on Intelligent Robots and Systems (IROS)*, Oct. 2018, pp. 1927–1934. DOI: 10.1109/IROS.2018.8593661.

[56] A. Padmanabha, F. Ebert, S. Tian, R. Calandra, C. Finn, and S. Levine, *Omnitact: A multi-directional high resolution touch sensor*, 2020. arXiv: 2003.06965 [cs.RO].

[57] N. F. Lepora, K. Aquilina, and L. Cramphorn, "Exploratory tactile servoing with active touch", *IEEE Robotics and Automation Letters*, vol. 2, no. 2, pp. 1156–1163, Apr. 2017, ISSN: 2377-3766. DOI: 10.1109/LRA.2017.2662071.

[58] H. Iwata and S. Sugano, "Design of human symbiotic robot twendy-one", in *2009 IEEE International Conference on Robotics and Automation*, 2009, pp. 580–586.

[59] H. van Hoof, T. Hermans, G. Neumann, and J. Peters, "Learning robot in-hand manipulation with tactile features", in *2015 IEEE-RAS 15th International Conference on Humanoid Robots (Humanoids)*, 2015, pp. 121–127. DOI: 10.1109/HUMANOIDS.2015.7363524.

[60] H. van Hoof, N. Chen, M. Karl, P. van der Smagt, and J. Peters, "Stable reinforcement learning with autoencoders for tactile and visual data", in *2016 IEEE/RSJ International Conference on Intelligent Robots and Systems (IROS)*, 2016, pp. 3928–3934. DOI: 10.1109/IROS.2016.7759578.

[61] A. Garcia-Garcia, B. S. Zapata-Impata, S. Orts-Escolano, P. Gil, and J. Garcia-Rodriguez, "Tactilegcn: A graph convolutional network for predicting grasp stability with tactile sensors", in *2019 International Joint Conference on Neural Networks (IJCNN)*, 2019, pp. 1–8. DOI: 10.1109/IJCNN.2019.8851984.

[62] OpenAI, M. Andrychowicz, B. Baker, M. Chociej, R. Jozefowicz, B. McGrew, J. Pachocki, A. Petron, M. Plappert, G. Powell, A. Ray, J. Schneider, S. Sidor, J. Tobin, P. Welinder, L. Weng, and W. Zaremba, *Learning dexterous in-hand manipulation*, 2019. arXiv: 1808.00177 [cs.LG].

[63] G. Cheng, E. Dean-Leon, F. Bergner, J. Rogelio Guadarrama Olvera, Q. Leboutet, and P. Mittendorfer, "A comprehensive realization of robot skin: Sensors, sensing, control, and applications", *Proceedings of the IEEE*, vol. 107, no. 10, pp. 2034–2051, 2019. DOI: 10.1109/JPROC.2019.2933348.

[64] M. Kaboli and G. Cheng, "Robust tactile descriptors for discriminating objects from textural properties via artificial robotic skin", *IEEE Transactions on Robotics*, vol. PP, pp. 1–19, Jul. 2018. DOI: 10.1109/TRO.2018.2830364.

[65] P. Mittendorfer and G. Cheng, "Humanoid multimodal tactile-sensing modules", *IEEE Transactions on robotics*, vol. 27, no. 3, pp. 401–410, 2011.

[66] A. Schmitz, P. Maiolino, M. Maggiali, L. Natale, G. Cannata, and G. Metta, "Methods and technologies for the implementation of large-scale robot tactile sensors", *IEEE Transactions on Robotics*, vol. 27, no. 3, pp. 389–400, 2011. DOI: 10.1109/TRO.2011.2132930.

[67] F. Bergner, E. Dean-Leon, J. R. Guadarrama-Olvera, and G. Cheng, "Evaluation of a large scale event driven robot skin", *IEEE Robotics and Automation Letters*, vol. 4, no. 4, pp. 4247–4254, 2019. DOI: 10.1109/LRA.2019.2930493.

[68] J. M. Romano, T. Yoshioka, and K. J. Kuchenbecker, "Automatic filter design for synthesis of haptic textures from recorded acceleration data", in *2010 IEEE International Conference on Robotics and Automation*, 2010, pp. 1815–1821. DOI: 10.1109/ROBOT.2010.5509853.

[69] H. Culbertson, J. Unwin, and K. J. Kuchenbecker, "Modeling and rendering realistic textures from unconstrained tool-surface interactions", *IEEE Transactions on Haptics*, vol. 7, no. 3, pp. 381–393, 2014. DOI: 10.1109/TOH.2014.2316797.

[70] Y. Massalim, Z. Kappassov, and A. Varol, "Deep vibro-tactile perception for simultaneous texture identification, slip detection, and speed estimation", *Sensors*, vol. 20, p. 4121, Jul. 2020. DOI: 10.3390/s20154121.

[71] D. S. Chathuranga, Z. Wang, V. A. Ho, A. Mitani, and S. Hirai, "A biomimetic soft fingertip applicable to haptic feedback systems for texture identification", in *2013 IEEE International Symposium on Haptic Audio Visual Environments and Games (HAVE)*, 2013, pp. 29–33.

[72] K. Takahashi and J. Tan, "Deep visuo-tactile learning: Estimation of material properties from images", *CoRR*, vol. abs/1803.03435, 2018. arXiv: 1803.03435. [Online]. Available: http://arxiv.org/abs/1803.03435.

[73] M. Polic, I. Krajacic, N. Lepora, and M. Orsag, "Convolutional autoencoder for feature extraction in tactile sensing", *IEEE Robotics and Automation Letters*, vol. 4, no. 4, pp. 3671–3678, Oct. 2019, ISSN: 2377-3774. DOI: 10.1109/LRA.2019.2927950.

[74] J. Abello, P. M. Pardalos, and M. G. Resende, *Handbook of massive data sets*. Springer, 2013, vol. 4.

[75] K. Sayood, *Introduction to data compression*. Morgan Kaufmann, 2017.

[76] B. Hollis, S. Patterson, and J. Trinkle, "Compressed sensing for tactile skins", in *2016 IEEE International Conference on Robotics and Automation (ICRA)*, 2016, pp. 150–157. DOI: 10.1109/ICRA.2016.7487128.

[77] ——, "Compressed learning for tactile object recognition", *IEEE Robotics and Automation Letters*, vol. 3, no. 3, pp. 1616–1623, Jul. 2018, ISSN: 2377-3766. DOI: 10.1109/LRA.2018.2800791.

[78] C. Liu, W. Huang, F. Sun, M. Luo, and C. Tan, "Lds-fcm: A linear dynamical system based fuzzy c-means method for tactile recognition", *IEEE Transactions on Fuzzy Systems*, vol. 27, no. 1, pp. 72–83, 2019. DOI: 10.1109/TFUZZ.2018.2859184.

[79] H. Liu, J. Greco, X. Song, J. Bimbo, L. Seneviratne, and K. Althoefer, "Tactile image based contact shape recognition using neural network", in *2012 IEEE International Conference on Multisensor Fusion and Integration for Intelligent Systems (MFI)*, Sep. 2012, pp. 138–143. DOI: 10.1109/MFI.2012.6343036.

[80] C.-H. Lin, J. A. Fishel, and G. Loeb, "Estimating point of contact , force and torque in a biomimetic tactile sensor with deformable skin", 2013.

[81] M. Graña, M. Alonso, and A. Izaguirre, "A panoramic survey on grasping research trends and topics", *Cybernetics and Systems*, vol. 50, no. 1, pp. 40–57, 2019. DOI: 10.1080/01969722.2018.1558013. [Online]. Available: https://doi.org/10.1080/01969722.2018.1558013.

[82] D. Prattichizzo, M. Otaduy, H. Kajimoto, and C. Pacchierotti, "Wearable and hand-held haptics", *IEEE Transactions on Haptics*, vol. 12, no. 3, pp. 227–231, 2019. DOI: 10.1109/TOH.2019.2936736.

[83] C. Pacchierotti, L. Meli, F. Chinello, M. Malvezzi, and D. Prattichizzo, "Cutaneous haptic feedback to ensure the stability of robotic teleoperation systems", *International Journal of Robotics Research. In Press*, vol. 34, Oct. 2015. DOI: 10.1177/0278364915603135.

[84] C. Pacchierotti, F. Ongaro, F. van den Brink, C. Yoon, D. Prattichizzo, D. H. Gracias, and S. Misra, "Steering and control of miniaturized untethered soft magnetic grippers with haptic assistance", *IEEE Transactions on Automation Science and Engineering*, vol. 15, no. 1, pp. 290–306, 2018. DOI: 10.1109/TASE.2016.2635106.

[85] S. J. Biggs and M. A. Srinivasan, "Haptic interfaces", in *Human factors and ergonomics. Handbook of virtual environments: Design, implementation, and applications*, Lawrence Erlbaum Associates Publishers, 2002, pp. 93–115.

[86] S. Kim, C. Kim, G. Yang, T. Yang, B. Han, S. Kang, and D. Kwon, "Small and lightweight tactile display(salt) and its application", in *World Haptics 2009 - Third Joint EuroHaptics conference and Symposium on Haptic Interfaces for Virtual Environment and Teleoperator Systems*, 2009, pp. 69–74. DOI: 10.1109/WHC.2009.4810820.

[87] M. Gabardi, M. Solazzi, D. Leonardis, and A. Frisoli, "A new wearable fingertip haptic interface for the rendering of virtual shapes and surface features", in *2016 IEEE Haptics Symposium (HAPTICS)*, 2016, pp. 140–146. DOI: 10.1109/HAPTICS.2016.7463168.

[88] S. Mun, S. Yun, S. Nam, S. K. Park, S. Park, B. J. Park, J. M. Lim, and K. Kyung, "Electro-active polymer based soft tactile interface for wearable devices", *IEEE Transactions on Haptics*, vol. 11, no. 1, pp. 15–21, 2018.

[89] S. B. Schorr and A. M. Okamura, "Three-dimensional skin deformation as force substitution: Wearable device design and performance during haptic exploration of virtual environments", *IEEE Transactions on Haptics*, vol. 10, no. 3, pp. 418–430, 2017. DOI: 10.1109/TOH.2017.2672969.

[90] M. Rahimi, F. Jiang, C. Ye, and Y. Shen, "Dynamic spatiotemporal pattern identification and analysis using a fingertip-based electro-tactile display array", in *2019 IEEE/RSJ International Conference on Intelligent Robots and Systems (IROS)*, 2019, pp. 8132–8137. DOI: 10.1109/IROS40897.2019.8967906.

[91] E. M. Young and K. J. Kuchenbecker, "Implementation of a 6-dof parallel continuum manipulator for delivering fingertip tactile cues", *IEEE Transactions on Haptics*, vol. 12, no. 3, pp. 295–306, 2019.

[92] A. M. Murray, R. L. Klatzky, and P. K. Khosla, "Psychophysical characterization and testbed validation of a wearable vibrotactile glove for telemanipulation", *Presence*, vol. 12, no. 2, pp. 156–182, 2003. DOI: 10.1162/105474603321640923.

[93] H. Kajimoto, M. Suzuki, and Y. Kanno, "Hamsatouch: Tactile vision substitution with smartphone and electro-tactile display", in *Proceedings of the extended abstracts of the 32nd annual ACM conference on Human factors in computing systems*, ACM, 2014, pp. 1273–1278.

[94] M. Rahimi, F. Jiang, and Y. Shen, "Non-linearity of skin properties in electrotactile applications: Identification and mitigation", *IEEE Access*, vol. 7, pp. 169 844–169 852, 2019. DOI: 10.1109/ACCESS.2019.2955648.

[95] R. D. Howe, D. A. Kontarinis, and W. J. Peine, "Shape memory alloy actuator controller design for tactile displays", in *Proceedings of 1995 34th IEEE Conference on Decision and Control*, vol. 4, 1995, 3540–3544 vol.4. DOI: 10.1109/CDC.1995.479133.

[96] P. S. Wellman, W. J. Peine, G. Favalora, and R. D. Howe, "Mechanical design and control of a high-bandwidth shape memory alloy tactile display", in *Experimental Robotics V*, A. Casals and A. T. de Almeida, Eds., Berlin, Heidelberg: Springer Berlin Heidelberg, 1998, pp. 56–66, ISBN: 978-3-540-40920-5.

[97] S. Okumoto, F. Zhao, and H. Sawada, "Tactoglove presenting tactile sensations for intuitive gestural interaction", in *2012 IEEE International Symposium on Industrial Electronics*, 2012, pp. 1680–1685. DOI: 10.1109/ISIE.2012.6237343.

[98] N. Aiemsetthee and H. Sawada, "Presenting braille information on two fingers using vibratory patterns from an array of shape-memory alloys", in *2020 13th International Conference on Human System Interaction (HSI)*, 2020, pp. 322–327.

[99] R. Scheibe, M. Moehring, and B. Froehlich, "Tactile feedback at the finger tips for improved direct interaction in immersive environments", in *2007 IEEE Symposium on 3D User Interfaces*, 2007. DOI: 10.1109/3DUI.2007.340784.

[100] D. Hwang, J. Lee, and K. Kim, "On the design of a miniature haptic ring for cutaneous force feedback using shape memory alloy actuators", *Smart Materials and Structures*, vol. 26, no. 10, p. 105 002, Sep. 2017. DOI: 10.1088/1361-665x/aa860d. [Online]. Available: https://doi.org/10.1088%2F1361-665x%2Faa860d.

[101] B. Lim, K. Kim, S. Oh, and D. Hwang, "Hapticube: A compact 5-dof finger-wearable tactile interface*", in *2019 IEEE/RSJ International Conference on Intelligent Robots and Systems (IROS)*, 2019, pp. 5094–5100. DOI: 10.1109/IROS40897.2019.8967773.

[102] Y. Mizukami and H. Sawada, "Tactile information transmission by apparent movement phenomenon using shape-memory alloy device", English, *International Journal on Disability and Human Development*, vol. 5, no. 3, pp. 277–284, Jan. 2006, ISSN: 2191-1231. DOI: 10.1515/IJDHD.2006.5.3.277.

[103] F. Chinello, M. Malvezzi, D. Prattichizzo, and C. Pacchierotti, "A modular wearable finger interface for cutaneous and kinesthetic interaction: Control and evaluation", *IEEE Transactions on Industrial Electronics*, vol. 67, no. 1, pp. 706–716, 2020. DOI: 10.1109/TIE.2019.2899551.

[104] G. Cannata, M. Maggiali, G. Metta, and G. Sandini, "An embedded artificial skin for humanoid robots", in *Multisensor Fusion and Integration for Intelligent Systems, 2008. MFI 2008. IEEE International Conference on*, IEEE, 2008, pp. 434–438.

[105] A. Geier, G. Yan, T. Pradhono Tito, S. Somlor, and S. Sugano, "Deep gru-ensembles for active tactile texture recognition with soft, distributed skin sensors in dynamic contact scenarios", in *2020 IEEE/SICE International Symposium on System Integrations*, IEEE, 2020.

[106] S. Funabashi, S. Ogasa, T. Isobe, T. Ogata, A. Schmitz, T. Tomo, and S. Sugano, "Variable in-hand manipulations for tactile-driven robot hand via cnn-lstm", in *2020 IEEE/RSJ International Conference on Intelligent Robots and Systems (IROS)*, 2020, pp. 9472–9479.

[107] S. Funabashi, S. Morikuni, A. Geier, A. Schmitz, S. Ogasa, T. P. Torno, S. Somlor, and S. Sugano, "Object recognition through active sensing using a multi-fingered robot hand with 3d tactile sensors", in *2018 IEEE/RSJ International Conference on Intelligent Robots and Systems (IROS)*, 2018, pp. 2589–2595. DOI: 10.1109/IROS.2018.8594159.

[108] T. P. Tomo, W. K. Wong, A. Schmitz, H. Kristanto, A. Sarazin, L. Jamone, S. Somlor, and S. Sugano, "A modular, distributed, soft, 3-axis sensor system for robot hands", in *2016 IEEE-RAS 16th International Conference on Humanoid Robots (Humanoids)*, 2016, pp. 454–460.

[109] T. P. Tomo, "Development of a compact, soft, distributed 3 - axis hall effect-based skin sensor: Uskin", PhD thesis, Waseda University, Tokyo, Japan, Feb. 2019.

[110] H. Sawada, "Micro-vibration actuators driven by shape-memory alloy wires and its application to tactile displays", in *2017 International Symposium on Micro-NanoMechatronics and Human Science (MHS)*, Dec. 2017, pp. 1–5. DOI: 10.1109/MHS.2017.8305184.

[111] S. Okamoto, H. Nagano, and Y. Yamada, "Psychophysical dimensions of tactile perception of textures", *IEEE Transactions on Haptics*, vol. 6, no. 1, pp. 81–93, 2013.

[112] A. Geier, R. Tucker, S. Somlor, H. Sawada, and S. Sugano, "End-to-end tactile feedback loop: From soft sensor skin over deep gru-autoencoders to tactile stimulation", *IEEE Robotics and Automation Letters*, vol. 5, no. 4, pp. 6467–6474, 2020. DOI: 10.1109/LRA.2020.3012951.

[113] K. Cho, B. van Merrienboer, C. Gulcehre, F. Bougares, H. Schwenk, and Y. Bengio, "Learning phrase representations using RNN encoder-decoder for statistical machine translation", *CoRR*, vol. abs/1406.1078, 2014. arXiv: 1406.1078. [Online]. Available: http://arxiv.org/abs/1406.1078.

[114] D. Kingma and J. Ba, "Adam: A method for stochastic optimization", *International Conference on Learning Representations*, Dec. 2014.

[115] S. Lloyd, "Least squares quantization in pcm", *IEEE Trans. Inf. Theor.*, vol. 28, no. 2, pp. 129–137, Sep. 2006, ISSN: 0018-9448. DOI: 10.1109/TIT.1982.1056489. [Online]. Available: http://dx.doi.org/10.1109/TIT.1982.1056489.

[116] Y. Raykov, A. Boukouvalas, F. Baig, and M. Little, "What to do when k-means clustering fails: A simple yet principled alternative algorithm", *PLOS ONE*, vol. 11, e0162259, Sep. 2016. DOI: 10.1371/journal.pone.0162259.

[117] D. Arthur and S. Vassilvitskii, "K-means++: The advantages of careful seeding", in *Proceedings of the Eighteenth Annual ACM-SIAM Symposium on Discrete Algorithms*, ser. SODA '07, Society for Industrial and Applied Mathematics, 2007, pp. 1027–1035, ISBN: 978-0-898716-24-5. [Online]. Available: http://dl.acm.org/citation.cfm?id=1283383.1283494.

[118] W. Taube Navaraj, C. García Núñez, D. Shakthivel, V. Vinciguerra, F. Labeau, D. H. Gregory, and R. Dahiya, "Nanowire fet based neural element for robotic tactile sensing skin", *Frontiers in Neuroscience*, vol. 11, p. 501, 2017, ISSN: 1662-453X. DOI: 10.3389/fnins.2017.00501. [Online]. Available: https://www.frontiersin.org/article/10.3389/fnins.2017.00501.

[119] G. T. Fechner, "Elemente der psychophysik", in *Elements of psychophysics*, E. G. Howes D H; Boring, Ed. New York: Holt, Rinehart and Winston, 1966.

[120] D. B. JUDD, "Chromaticity sensibility to stimulus differences", *J. Opt. Soc. Am.*, vol. 22, no. 2, pp. 72–72, Feb. 1932. DOI: 10.1364/JOSA.22.000072. [Online]. Available: http://www.osapublishing.org/abstract.cfm?URI=josa-22-2-72.

[121] G. Hamerly and J. Drake, "Accelerating lloyd's algorithm for k-means clustering", in *Partitional Clustering Algorithms*, M. E. Celebi, Ed. Cham: Springer International Publishing, 2015, pp. 41–78, ISBN: 978-3-319-09259-1. DOI: 10.1007/978-3-319-09259-1_2. [Online]. Available: https://doi.org/10.1007/978-3-319-09259-1_2.

[122] R. Tucker, "Development of an ai-driven thermo-electric actuator for heat flux generation in tactile displays", Master's thesis, Waseda University, Tokyo, Japan, Sep. 2020.

List of Publications

Thesis Publications

1. **A. Geier**, R. Tucker, S. Somlor, H.Sawada, and S. Sugano, "End-to-end Tactile Feedback Loop: From Soft Sensor Skin over Deep GRU-Autoencoders to Tactile Stimulation," in IEEE Robotics and Automation Letters, vol. 5, no. 4, pp. 6467-6474, Oct. 2020, doi: 10.1109/LRA.2020.3012951.

2. **A. Geier**, G. Yan, T. P. Tomo, S. Somlor, and S. Sugano, "Deep GRU-ensembles for active tactile texture recognition with soft, distributed skin sensors in dynamic contact scenarios," 2020 IEEE/SICE International Symposium on System Integration (SII), Honolulu, HI, USA, 2020, pp. 127-132, doi: 10.1109/SII46433.2020.9025993.

3. **A. Geier**, G. Yan, T. P. Tomo, S. Ogasa, S. Somlor, A. Schmitz, and S. Sugano, "Sequential clustering for tactile image compression to enable direct adaptive feedback," 2019 IEEE/RSJ International Conference on Intelligent Robots and Systems (IROS), Macau, China, 2019, pp. 8117-8124, doi: 10.1109/IROS40897.2019.8968493.

Others

1. S. Funabashi, G. Yan, **A. Geier**, A. Schmitz, T. Ogata, and S. Sugano, "Morphology-Specific Convolutional Neural Networks for Tactile Object Recognition with a Multi-Fingered Hand," 2019 International Conference on Robotics and Automation (ICRA), Montreal, QC, Canada, 2019, pp. 57-63, doi: 10.1109/ICRA.2019.8793901.

2. S. Funabashi, S. Morikuni, **A. Geier**, A. Schmitz, S. Ogasa, T. P. Tomo, S. Somlor, and S. Sugano, "Object Recognition Through Active Sensing Using a Multi-Fingered Robot Hand with 3D Tactile Sensors," 2018 IEEE/RSJ International Conference on Intelligent Robots and Systems (IROS), Madrid, 2018, pp. 2589-2595, doi: 10.1109/IROS.2018.8594159.